Dissertation zur Erlangung des Doktorgrades

der Fakultät für Chemie und Pharmazie

der Ludwig-Maximilians-Universität München

Structural and Biochemical Characterization of Cell Shaping Proteins

1. Microtubule Binding Protein p150$^{\text{glued}}$ and

2. Intraflagellar Transport Protein 172

Qianmin Wang

aus

Weinan, Shaanxi Proviz, P.R.China

2017

Erklärung

Diese Dissertation wurde im Sinne von § 7 der Promotionsordnung vom 28. November 2011 von Frau Prof. Dr. Elena Conti betreut.

Eidesstattliche Versicherung

Diese Dissertation wurde eigenständig und ohne unerlaubte Hilfe erarbeitet.

München, den 03.12.2017

....

Qianmin Wang

Dissertation eingereicht am 13.10.2017

1. Gutachter: Prof. Dr. Elena Conti

2. Gutachter: Prof. Dr. Karl-Peter Hopfner

Mündliche Prüfung am 28.11.2017

Contents

Summary

Microtubules are cytoskeletal filaments in eukaryotic cells where they are required for cell morphogenesis, cell division and intracellular trafficking. Microtubules are highly dynamically assembled from α-/β-tubulin heterodimers. The dynamic instability of microtubules is regulated by several highly conserved microtubule associated proteins (MAPs). In particular, a spatially specialized group of MAPs that accumulate at growing microtubule ends, the plus-end binding proteins (+TIPs), is important to modulate microtubule dynamics in cells. p150^{glued} is one of these +TIPs and is the largest subunit of the dynactin complex. Previous studies of p150^{glued} demonstrated that it functions in recruiting and binding endosomes and dynein to microtubules for initiating retrograde transport. p150^{glued} has two microtubule-binding domains at its N-terminus: a cytoskeleton associated proteins glycine-rich (CAP-Gly) domain, followed by a serine-rich basic domain. To understand how the p150^{glued} CAP-Gly domain and the basic extensions interact with microtubule, cyro-electron microscopic structures of p150^{glued} (1-105)-microtubule complex (CAP-Gly core with its N-terminal basic patch) and p150^{glued} (25-144)-microtubule (CAP-Gly core with its C-terminal basic patch) complex were determined at 9.7 Å and 10.2 Å resolution, respectively. These structures revealed that the CAP-Gly domain binds to the flexible C-terminus of the tubulin (known as E-hook) instead of the core of microtubules. Comparison of the p150^{glued} (1-105)-microtubule reconstruction and p150^{glued} (25-144)-microtubule reconstruction revealed that CAP-Gly interacts with microtubules very flexibly. In addition, the basic extensions of CAP-Gly core was found to induce microtubule lateral association by neutralization of the negatively charged tubulin C-terminus, which acts as an electrostatic shield to avoid the interaction between individual microtubules. Interestingly, p150^{glued} CAP-Gly together with the basic extensions could induce longitudinal interaction of tubulin for forming curved tubulin oligomers at low temperature, and this process happens in a GTP independent manner. Taken together, p150^{glued} CAP-Gly plus its adjacent basic patches interact with the acidic C-terminus of tubulin and promote tubulin polymerization in two directions, by inducing tubulin longitudinal association at low temperature and lateral interaction once temperature change to physiological condition. Our study about p150^{glued} explained how +TIPs regulate microtubule dynamics from a structure point of view.

Cilia are rod-like microtubule based structures protruding from most eukaryotic cells. Cilia are assembled and maintained through a bidirectional transport system called intraflagellar transport (IFT) mediated by IFT complexes and molecular motors moving along axonemal microtubules. The IFT complex is composed of at least 22 polypeptides organized into two complexes named IFT-A and IFT-B. The IFT-B complex is further divided into IFT-B1 and IFT-B2. IFT172, one of the IFT-B2 subunits, is the IFT protein with the highest molecular weight. *Chlamydomonas* IFT172 is a 1755-amino-acid protein that is encoded by *FLA11* gene. The N-terminus of IFT172 contains a WD40 domain, which folds into β-propellers structure while its C-terminus shows tetratricopeptide repeats (TPRs) predicted to form α-helical secondary structure. The domain architecture of IFT172 is highly similar to vesicles coat proteins like COPI and clathrin-adaptor subunits. To characterize IFT172, *Chlamydomonas* IFT172 was expressed from insect cell and further purified. Surprisingly, IFT172 showed lipid association during the purification and the purification products showed round oligomers containing both IFT172 and membrane. To obtain IFT172 in monomer form instead of the oligomers with lipid, n-Dodecyl β-D-maltoside (DDM) was used and by negative-stain electron microscope observation, the IFT172 monomer was found to adopt two conformations: a globular conformation and a rod-shape conformation. Furthermore, giant unilamellar vesicle (GUV) binding assay was employed to assess the interaction of membrane with IFT172. IFT172 showed high membrane binding affinity and clusters on the membrane surface. To investigate the effect of IFT172 on membrane surface closely, IFT172 with Folch fraction I was investigated under the electron microscope. Vesiculation of 18 nm-diameter small vesicles from the large unilamellar vesicle membrane surface was observed. Further studies revealed that the membrane binding property of IFT172 is mediated by its N-terminal β-propellers, but not C-terminal TPRs. Moreover, I demonstrated that IFT57, the direct binding partner of IFT172 within IFT proteins, competes with membrane for IFT172 binding. These results provided the first evidence that IFT172 binds to membrane through its N-terminal WD40 domains directly and it remodels membrane surface *in vitro*. Investigation of the functions of IFT172 *in vivo* is needed to address these issues in the future.

Preface

This thesis presents my PhD projects that I did in the lab of Dr. Naoko Mizuno at the Max Planck Institute of Biochemistry for the last four years in a cumulative style. I have worked on two projects during the time: 1, Structural and biochemical characterization of microtubule binding CAP-Gly domain of p150^{glued}; 2, Characterization of intraflagellar transport protein 172 (IFT172) shows that it associates with and remodels membrane *in vitro*. The introduction in the first part shows a broad overview about the microtubule dynamic regulations by microtubule plus end binding proteins and posttranslational modifications of tubulin, followed with a description of cilia, the microtubule-based organelle, and the building of cilia by intraflagellar transport. The Chapter I in the result part shows the published research article for the first topic about p150^{glued}. An extended discussion after Chapter I integrates the new insights from recent functional studies about p150^{glued} with results presenting in my article. The Chapter II presents a manuscript of the second topic about IFT172, which is under finalizing for submission. There is an extended discussion about function exploration of IFT172. Finally, there is a brief outlook pointing out some of the questions that remain to be addressed in the future.

Publications and Contributions

1), **Wang Q**, Crevenna A H, Kunze I, Mizuno N. Structural basis for the extended CAP-Gly domains of p150^{glued} binding to microtubules and the implication for tubulin dynamics. Proceedings of the National Academy of Sciences, 2014, 111(31): 11347-11352.

2), **Wang Q**, Taschner M, Ganzinger K, Schwille P, Lorentzen E, Mizuno N. Membrane association and remodeling by intraflagellar transport protein IFT172
 [In preparation]

The following experiments were performed by collaborators:

1), Fluorescence microscopy observation of p150^{glued} with microtubules and dissociation constants measurements:
   Dr. Alvaro H. Crevenna

2), Fluorescence microscopy binding assay of IFT172 with giant unilamellar vesicles:
   Dr. Kristina Ganzinger

1. Introduction

1.1 Microtubules and microtubule dynamics

Microtubules are fibrillar structures found in all dividing eukaryotic cells and in most differentiated cell types. Microtubules, together with actin filaments, and intermediate filaments, provide shape and strength to the cytoplasm, and they are the major structures in the cytoskeleton. Microtubules play essential roles in many important cellular activities, like cell division, organization and motility. Microtubules are assembled by polymerization of α-/β-tubulin heterodimers. The α-tubulin has a non-exchangeable site filled with GTP, while the β-tubulin contains an exchangeable site, which is exposed at the dimer surface and can bind to GTP (Hyman et al., 1992). α-/β-tubulin heterodimers are aligned in a polar head-to-tail fashion to form protofilaments, which associate laterally to form microtubule. In cells, the minus end of microtubule is typically anchored on the microtubule-organization center (MTOC) and MTOC is linked to the centrosome. Microtubule minus ends are relatively stable, whereas microtubule plus ends are highly dynamic. Cryo-electron microscopy studies reveal that growing microtubule plus end show slightly curved, flattened and tapered-sheet-like structures, while depolymerizing plus end exhibit strongly curved, 'peeling' protofilaments (Mandelkow et al., 1991).

Microtubule ends undergo continuous cycles of polymerization (growth) and depolymerization (shrinkage), with periods of pauses, a process referred to as 'dynamic instability' (Mitchison and Kirschner, 1984). The transition between growth and shrinkage is defined as 'catastrophe', and 'rescue' is defined as the switch from shortening to growth. Microtubule instability is intrinsically driven by hydrolysis of GTP-bound-β-tubulin, which occurs with a delay after a tubulin dimer has been incorporated into the microtubule plus end. Due to the delay in GTP hydrolysis, a cap of GTP-tubulin is formed at the end of the growing microtubule and is believed to protect the microtubule from depolymerization. A catastrophe occurs once the GTP-cap disappears and GDP-tubulin is exposed at the end of the microtubules. This so-called 'GTP-cap model' is a standard to explain microtubule dynamic instability (Figure 1) (Desai and Mitchison, 1997). The dynamic instability is important for

microtubule functions, such as the connections between various cellular components, exploration of the cytosol, and segregation of chromosomes towards cell poles during mitosis.
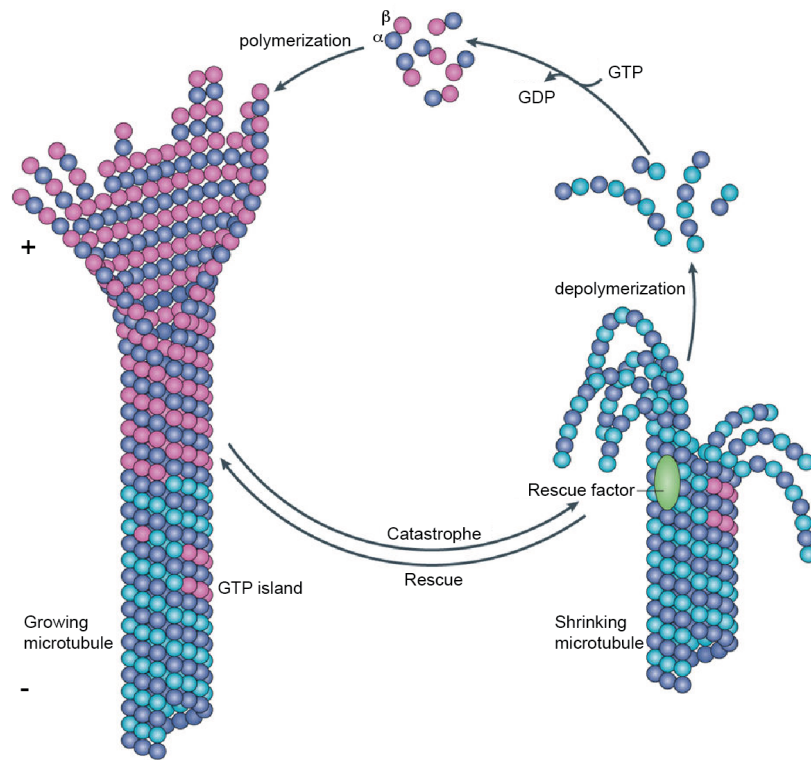
Figure 1. Dynamic instability of microtubules. Polymerization of microtubules is initiated from a pool of GTP-loaded tubulin dimers. Hydrolysis of the GTP-bound-β-tubulin enables microtubules to switch between catastrophe and rescues. Transition from growth to shrinkage is termed catastrophe; transition from shortening to growth is called rescue. Rescues might be induced by local lattice features that can halt microtubule disassembly, such as 'GTP island'. Scheme is adapted from (Akhmanova and Steinmetz, 2015).

1.1.1 Microtubule dynamics regulators - Microtubule plus-end tracking proteins

The microtubule dynamic instability is regulated by numerous factors spatially and temporally, which can be classified into molecular motors and microtubule-associated proteins (MAPs) (Jiang and Akhmanova, 2011). A subgroup of MAPs is characterized by their ability to accumulate at microtubule ends. Plus-end tracking proteins (+TIPs) recognize and bind to the plus-end of microtubules, and potentially modulate microtubules assembly dynamics and interactions between plus ends of microtubules and subcellular targets. Based on prominent structural element enable them to interact with microtubules and other +TIPs, +TIPs can be can be categorized into several groups.

1.1.1.1 End-binding family proteins

The end-binding proteins (EBs) are considered as master regulators of microtubule plus-end tracking proteins. There are three different EBs (EB1, EB2 and EB3) expressed in mammalian cells. EBs are proteins of about 300 amino-acid (a.a.) residues organized into an N-terminal calponin homology (CH) domain, responsible for binding to microtubule, a less conserved flexible linker region, and a C-terminal coiled-coil dimerization domain. The C-terminal 20-30 a.a. tails are flexible, sharing a conserved very C-terminus sequence of EEY/F.

Several studies revealed that EB proteins bind the nucleotide-sensitive cap at the microtubule ends, based on the observation that EB proteins bind stronger to the microtubule lattice in presence of GMPCPP, a GTP analogue, than to the GDP microtubule lattice. High-resolution cryo-EM studies showed that CH domain of EB1 bridges protofilaments at the corner of four tubulin subunits, which makes it ideally positioned to sense microtubule conformational changes induced by GTP hydrolysis

(Zanic et al., 2009, Maurer et al., 2012). Both *in vivo* and *in vitro* fluorescence microscopy studies showed that a large number of EB proteins bind to a region of microtubule plus ends, forming a comet-like distribution there (Figure 2). Interestingly, the 'comet' by EB proteins reflects the extent of GTP cap of microtubules (Seetapun et al., 2012, Bieling et al., 2007). In addition to the binding of nucleotide-sensitive cap at microtubule ends, EB proteins also contribute to the maturation of microtubules by promoting lateral protofilament interaction and by accelerating reactions of GTP hydrolysis cycle (Maurer et al., 2014).
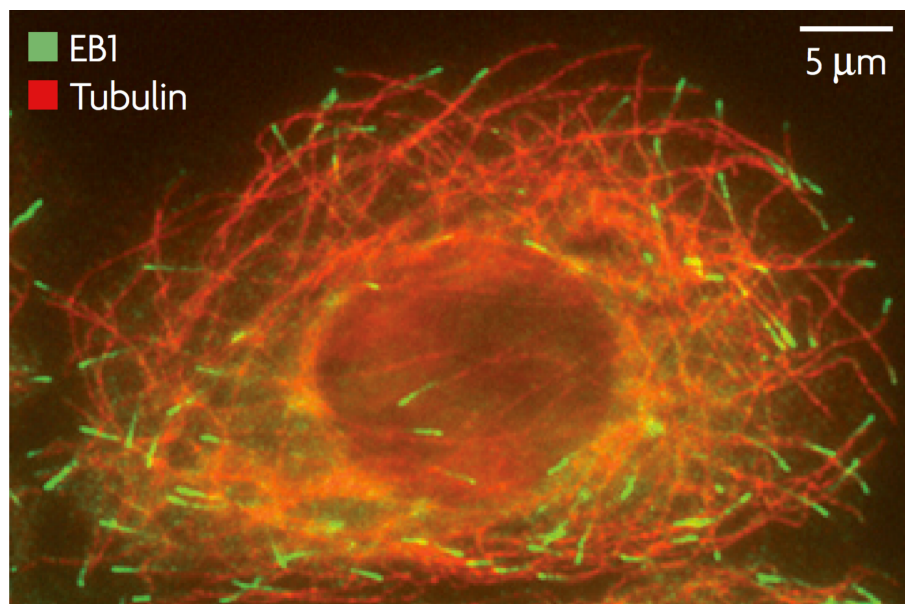
Figure 2. Image of interphase cultured mouse kidney epithelial cells stained for the endogenous EB1 (in green) and β-tubulin (in red). Image is adapted from (Akhmanova and Steinmetz, 2008).

1.1.1.2 Cytoskeleton-associated protein Gly-rich proteins

The cytoskeleton-associated protein Gly-rich (CAP-Gly) domain is a specialized protein module with about 80 a.a., which is highly conserved in all eukaryotes. CAP-Gly domain exists in diverse proteins, such as cytoplasmic linker proteins (CLIPs), the large subunit of the dynactin complex p150^{glued}, tubulin-folding cofactors B and E (TBCB and TBCE)，the centrosome-associated protein 350 (CAP350). Crystal structures of CAP-Gly domain showed a globular-protein fold with a solvent exposed

hydrophobic cavity next to the highly conserved Gly-Lys-Asn-Asp-Gly (GKNDG) motif (Li et al., 2002, Weisbrich et al., 2007). CAP-Gly domains specifically recognize C-terminal EEY/F motifs that are found in EBs, α-tubulin, CLIP170 (Mishima et al., 2007, Honnappa et al., 2006). Here, I concentrate on two proteins from this group: CLIP170 and p150 [glued].

CLIP170 was the first identified +TIP. It consists of two CAP-Gly motifs at its N-terminus responsible for microtubule binding and the C-terminus contain Cys and His residues, which are predicted to form a metal-binding domain. There is a coiled-coil domain between the N-/C-terminus in the center (Figure 3). It has been found that CLIP170 can fold back upon itself, by an intramolecular interaction between the CAP-Gly domains and metal-binding C-terminal domain. The switching between an active extended conformation and an inactive folded conformation is important for inhibiting any unwanted interactions of its N-/C-terminus (Lansbergen et al., 2004). CLIP170 acts as a positive regulator in microtubule growth. For example, studies in Chinese hamster ovary (CHO) cell showed CLIP170 promotes the rescue of microtubule by its N-terminal domain (Komarova et al., 2002). It has been shown that mammalian CLIP170 has a high affinity to tubulin dimer and tracks microtubule plus-ends by a preassociation, copolymerization, and regulated release mechanism (Folker et al., 2005).

p150[glued] is another well-conserved microtubule-interacting protein, which is the largest component of the dynactin complex. The dynactin complex is required for targeting dynein to cargo and for dynein motor processivity (King and Schroer, 2000). p150[glued] contains a microtubule binding CAP-Gly domain and a small serine-rich basic extension at its N-terminus, followed by two predicted coiled-coil regions (Figure 3).

Similar to CLIP170, CAP-Gly domain of p150[glued] is also found at microtubule plus ends and at mitotic kinetochores (Maiato et al., 2004). *In vitro* studies showed that CAP-Gly domain of p150[glued] remains strongly bound to microtubules, acting as a 'parking brake', while the adjacent basic domain not only interacts with microtubule, also 'skating' along microtubules in the absence of molecular motors (Culver-Hanlon et al., 2006). However, the truncation study demonstrated that the entire microtubule-

binding domain of p150^{glued} does not seem to be necessary for normal dynein motility in *Drosophila melanogaster*, nor in yeast (Kim et al., 2007, Kardon et al., 2009). Additionally, p150^{glued} CAP-Gly domain also showed colocalization with other proteins of this class such as CLIP170 and EB1 (Vaughan et al., 1999, Ligon et al., 2003). *In vitro* experiments demonstrated that the p150^{glued} CAP-Gly domain interacts with the C-terminus of EB1 and CLIP170 (Figure 3) (Duellberg et al., 2014). p150^{glued} also localizes at the centrosome where its CAP-Gly domain participates in anchoring microtubule minus ends (Askham and Morrison, 2002, Quintyne et al., 1999).

In addition to the interaction with microtubule independently of cytoplasmic dynein, p150^{glued} also provides a platform for motor binding. For example, solution-binding assays revealed a strong binding between p150^{glued} a. a. 217-548 (coiled-coil 1) and N-terminal fragments of the dynein intermediate chain (Figure 3) (King et al., 2003). Truncation studies of p150^{glued} coiled-coil 1 domain showed that it is required for enhanced motor processivity (Kardon et al., 2009). Additionally, biochemical data demonstrated that p150^{glued} residue 600-811 binds to kinesin II in *Xenopus laevis*, indicating p150^{glued} provides a binding platform for interactions with both dynein and kinesin II (Deacon et al., 2003). The second coiled-coil domain of p150^{glued} interacts with actin-related protein (Arp1), which forms a short actin-like polymer at the base of the dynactin complex (Schroer, 2004). The C-terminus of p150^{glued} acts as a cargo-binding domain, which binds to vesicular adaptors (Fu and Holzbaur, 2014). For example, using the yeast two-hybrid system, the p150^{glued} a. a. 1023-1223 region has been shown to interact with the Huntingtin-associated protein, HAP-1 (Li et al., 1998).
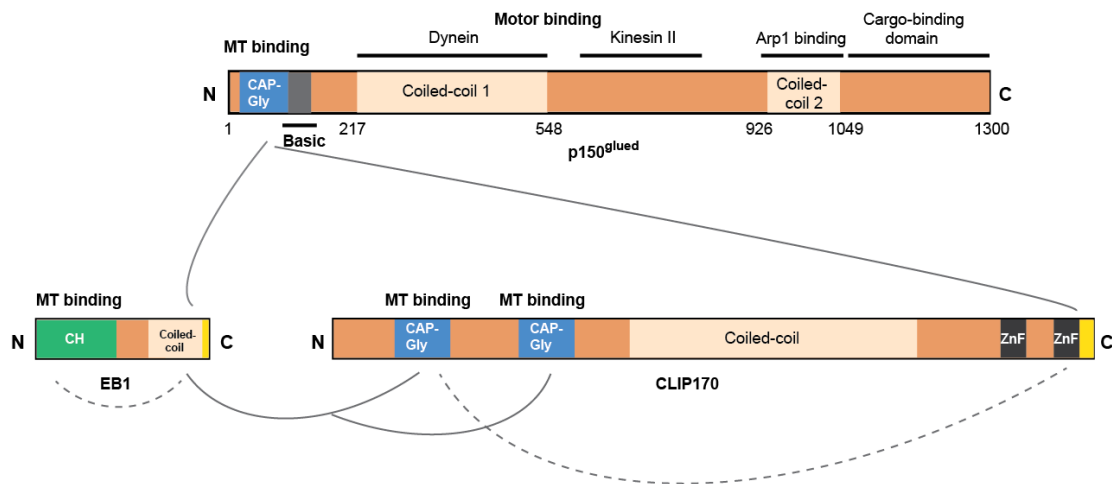
Figure 3. Schematic illustration of the domain organization of p150[glued], EB1, CLIP170 and the protein-protein interaction network between them. CAP-Gly domain of p150[glued] and CLIP170 bind to the C-terminus of EB1. CAP-Gly domain of p150[glued] also interacts with C-terminus of CLIP170. Note that p150[glued], EB1 and CLIP170 form parallel dimers and both EB1 and CLIP170 show autoinhibited by the self-interaction between N- and C-terminus. The solid lines indicate the interactions between two proteins, and dash lines show the self-interaction for autoinhibitory mechanisms.

1.1.1.3 Proteins containing basic and Ser-rich sequences

Another major group of +TIPs are proteins containing low-complexity sequence regions that are rich in basic, serine, and proline residues. They share the small four-residue motif SxIP (where 'x' can be any a.a.), embedded in an intrinsically disordered positively charged sequence region. SxIP motif is specifically recognized by the hydrophobic groove formed by the C-terminal helix bundle of EB proteins. A prominent example of this class of +TIPs is the adenomatous polyposis coli (APC), a well-conserved phosphoprotein with an essential function in cell cycle regulation (Dikovskaya et al., 2001). APC is a well-conserved large multidomain protein and it has been shown that APC binding directly to microtubules throughout its C-terminal basic region (Munemitsu et al., 1994). Apart from the binding with microtubule, C-terminus of APC was found to be a binding partner of EB1 by yeast two-hybrid screen and the conserved APC Ile2805-Pro2806 sequence serves as an anchor for the interaction with hydrophobic cavity of EB1 (Su et al., 1995, Honnappa et al., 2005).

The interaction between APC and EB1 is important for stabilization of microtubule formation and promoting directed cell migration (Wen et al., 2004). Microtubule-actin crosslinking factor (MACF) also contains the SxIP motif enabling the binding to EB1, and they are thus involved in integrating microtubule actin dynamics (Slep et al., 2005, Kodama et al., 2003).

1.1.1.4 Proteins containing TOG or TOG-like domains

Proteins with TOG (tumour overexpressed gene) or TOG-like domains include members of the XMAP215 (*Xenopus* microtubule-associated protein 215) family and CLASP (CLIP170 associated protein). The XMAP215 family contains several tubulin-binding TOG domains and CLASP comprises TOG and TOG-like domains. The higher eukaryotic XMAP215 members are monomeric and have five arrayed TOG domains at their N-terminus, while the yeast homologues suppressor of tubulin 2 (Stu2) has two TOG domains at N-terminus followed by a coiled-coil domain that mediates homodimerization (Slep, 2009). *In vitro* reconstitution studies revealed that XMAP215 binds to tubulin and targets the addition of tubulin dimers to the microtubule growing plus end, while under some conditions XMAP215 can also catalyze microtubule shrinkage (Brouhard et al., 2008). Using high-resolution microscopy techniques, it has been shown the mammalian homologue of XMAP215 (ch-TOG) accumulates at more distal sites along the microtubules than EB1 comets in Hela cells (Figrue 4B) (Nakamura et al., 2012). The selective recognition to the microtubule plus end could be explained based on the fact that TOG:α-/β-tubulin interactions are conformation-selective. Specifically, N-terminal TOG domains preferentially recognize curved unpolymerized α-/β-tubulin and the basic region in the C-terminus provide microtubule lattice affinity, which could only happen at microtubule plus end (Figure 4A) (Ayaz et al., 2012). In CLAPSs, there are also SxIP motifs required for targeting of these proteins to microtubule plus ends (Mimori-Kiyosue et al., 2005).
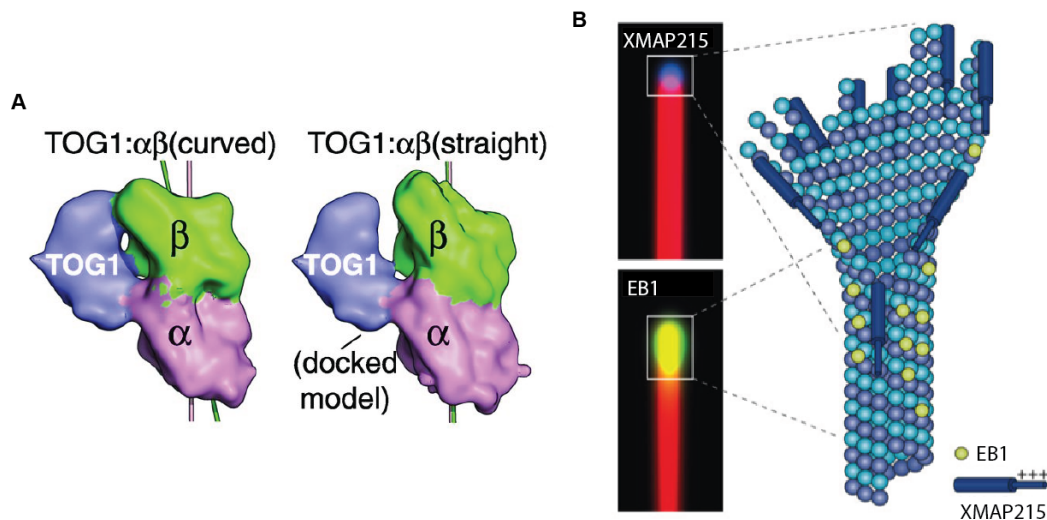
Figure 4. (A) The structure of TOG1:α-/β-tubulin complex (left) and a docked model with straight α-/β-tubulin (right) illustrates how TOG1-contacting epitopes on α- and β-tubulin move relative to each other in the two conformations. (B) Illustration of the distribution of EB1 and XMAP215 at growing microtubule plus ends. The arrangement of TOG domains (blue signal within rectangle) of XMAP215 and the basic region (indicated by +++ in the schematic) drives the specificity of the polymerase for the growing microtubule plus end. Whereas XMAP215 binds to the distal microtubule plus end, EB1 displays the highest accumulation tens of nanometers away from the outermost tip. Model in (A) is adapted from (Ayaz et al., 2012); Schematic in (B) is adapted from (Akhmanova and Steinmetz, 2015).

1.1.1.5 Microtubule motor proteins

Several microtubule plus- and minus-end-directed motor proteins can track growing microtubule ends. Examples are the yeast kinesins Tea2 and Kip2, the microtubule-depolymerizing kinesin 13 MCAK and cytoplasmic dynein (Wu et al., 2006). In the filamentous fungus *Aspergillus nidulans*, cytoplasmic dynein and dynactin accumulate at microtubule plus-end, depending on conventional kinesin (Zhang et al., 2003). Dynein, as a minus-end-directed motor, accumulates at microtubule plus-ends for the following two potential reasons. Firstly, the plus-end dynein may be involved in regulation microtubule-cortex interaction, which is important for spindle positioning. Specifically, studies in budding yeast showed deletion of Bik1 (CILP170 homolog) and Pac1 caused reduction of GFP labeled dynein at microtubule plus end.

The loss of Num1, which is a proposed dynein cortical anchor, resulted in accumulation of dynein on the plus end. On the basis of these observations, the authors presented a model suggesting that dynein is recruited to microtubule plus ends by regulators Bik1 and Pac1. Once microtubule reaches the cortical region, dynein may undergo Num1-dependent activation and get delivered to the region of cortical contact (Sheeman et al., 2003). Secondly, the plus-end dynein cooperates with dynactin and other microtubule plus end proteins to load vesicles and then transport them towards the microtubule minus ends. Dynactin has the ability to accumulate at microtubule plus-end, and it binds vesicular cargo, also recruit dynein for enhancement of its processivity (Schroer, 2004). According to the model proposed by Lansbergen et al., CLIP170 initiates the process by binding to microtubule, then it recruit dynactin, which then recruit cytoplasmic dynein with LIS1. LIS1 might initiate minus-end-directed vesicle movement by releasing dynactin from the complex with CLIP170 (Lansbergen et al., 2004).

1.1.1.6 Plus-end tracking network

Since the discovery of CLIP170 as the first +TIP, more than 20 different +TIP families have been identified (Perez et al., 1999, Akhmanova and Steinmetz, 2010). These proteins form dynamic interaction networks that rely on the protein domains and motifs, like CH, CAP-Gly and SxIP, mostly accumulating at the microtubule plus end. The reason for +TIPs association with microtubule plus ends is the particular structural features of this region comparing to the remainder of the tube, such as the presence of the GTP cap, specific curved tubulin sheets or individual protofilaments, or certain tubulin site (Akhmanova and Steinmetz, 2008).

Among these +TIPs, EBs autonomously bind an extended tubulin-GTP/GDP-Pi structure at microtubule plus end and acts as a key player that recruits a large number of regulatory +TIPs through interactions with CAP-Gly or SxIP motifs. Depending on cooperation or competition between EB1 and other +TIPs, the organization of complex +TIP networks involves both hierarchical and non-hierarchical interactions (Nehlig et al., 2017). *In vitro* experiments with *Drosophila* revealed that both XMAP215 and EB1 with Sentin, one of the EB1 cargos, could promote microtubule

growth. While, in presence of the three components EB1, XMAP215 and Sentin, the microtubule dynamics are cooperatively promoted (Li et al., 2012). In addition, TIP150, another SxIP motifs containing +TIP, promotes the accumulation of MCAK to microtubule plus end. The targeting of both TIP150 and MCAK requires EB1 (Jiang et al., 2009). Another good example to show the cooperation of +TIPs is the study about SLAIN2 in mammalian cells. SLAIN2 is one of the +TIPs that contains multiple SxIP motifs that associates with EBs, CLIPs and ch-TOG. Through the interaction with EBs, SLAIN2 and the ch-TOG complex are enriched at microtubule plus ends and strongly enhance processive microtubule growth (Figure 5A) (van der Vaart et al., 2011). In addition to the cooperation, the dynamic interaction networks through EB1 also depends on a number of potentially competitive and hierarchical interaction modes. For example, *in vitro* reconstitution experiments defined a minimal system for human dynein end tracking, involving in EB1, CLIP170, the dynactin component p150^{glued} and dynein complex. CLIP170 binds relatively efficiently to EB1 and provides new binding sites for p150^{glued}, which in turn recruits the dynein complex to microtubule plus ends. Such an interaction network allows the formation of a platform for recruiting the mammalian dynein motor even in the presence of competitors containing SxIP motif (Figure 5B) (Duellberg et al., 2014).

Since EB dimers can associate with only two CAP-Gly domains or SxIP motifs at the same time, the +TIPs interactions with EBs are quite competitive. Other autonomous enrichment of +TIPs at the microtubule plus ends is required for providing platform for non-autonomous +TIPs (Akhmanova and Steinmetz, 2008). For example, CLASPs interact with the coiled-coil domain of CLIPs independently of EB1 binding (Akhmanova et al., 2001). Another example is the study in budding yeast demonstrating that the Dam1 complex is an autonomous, continuous plus end tracker and recruits Ndc80 to bridge microtubule ends with chromosomes (Lampert et al., 2010). XMAP215 was also shown to track microtubule end autonomously and acts as a microtubule polymerase by binding to microtubule end during multiple rounds of subunits addition (Brouhard et al., 2008). The dynamic crosstalk between +TIPs participates in the regulation of microtubule dynamics, coordinating microtubule attachment to cellular structures, such as mitotic kinetochores or the cell cortex, concentrating signaling molecules.
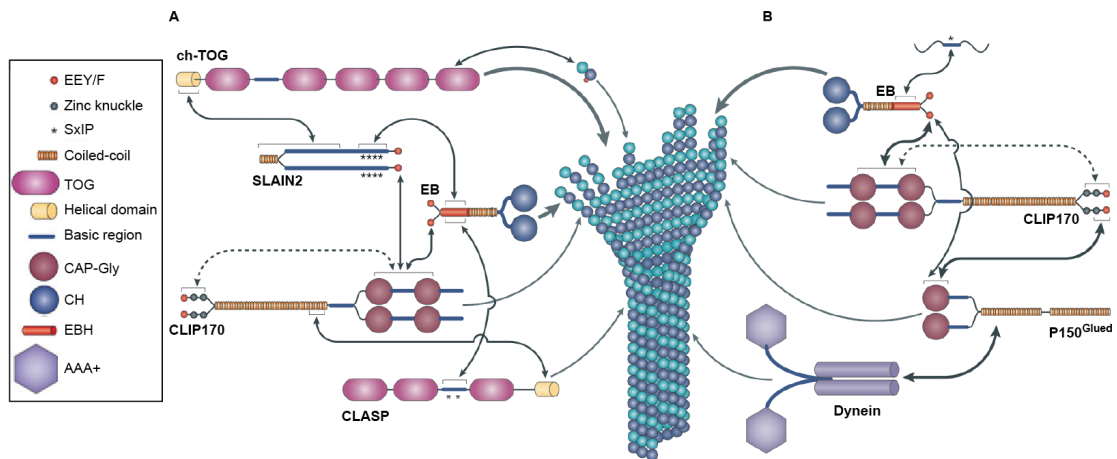
Figure 5. (A), Schematic overview of SLAIN2 interaction site with CLIP170, EB, ch-TOG and microtubule plus end. SLAIN2 enhances ch-TOG accumulation at microtubule plus ends and stimulates processive microtubule polymerization. (B), Scheme of the +TIP network directing the dynein complex to microtubule ends via the p150^{glued}/CLIP170/EB1 interaction module in the presence of SxIP motif containing competitors. Scheme in (A) and (B) are adapted from (Akhmanova and Steinmetz, 2015).

1.1.1.7 Regulation of tubulin

Microtubule dynamic is not only regulated by variable MAPs, but also programmed by the 'tubulin code'- a combination of different tubulin isotypes and the posttranslational modifications (PTMs) on α- and β-tubulin. Tubulins are encoded by multiple genes in most organisms, resulting in highly conserved but still different gene products with variability particularly in the tubulin C-terminal tails. There are nine α-tubulin and nine β-tubulin genes that have been identified in mammals. Tubulin isotypes could influent the structure of tubulin dimers and then affect the properties of the microtubule lattice. It has been shown that the structural elements are differently positioned by comparing the microtubule structures formed with different tubule isotypes. Specific β-tubulin isotypes are enriched in axonemes of cilia and flagellar, and microtubules in neurons. The enrichment of these isotypes may play a role in specific functions of these microtubules (Gadadhar et al., 2017, Janke, 2014).
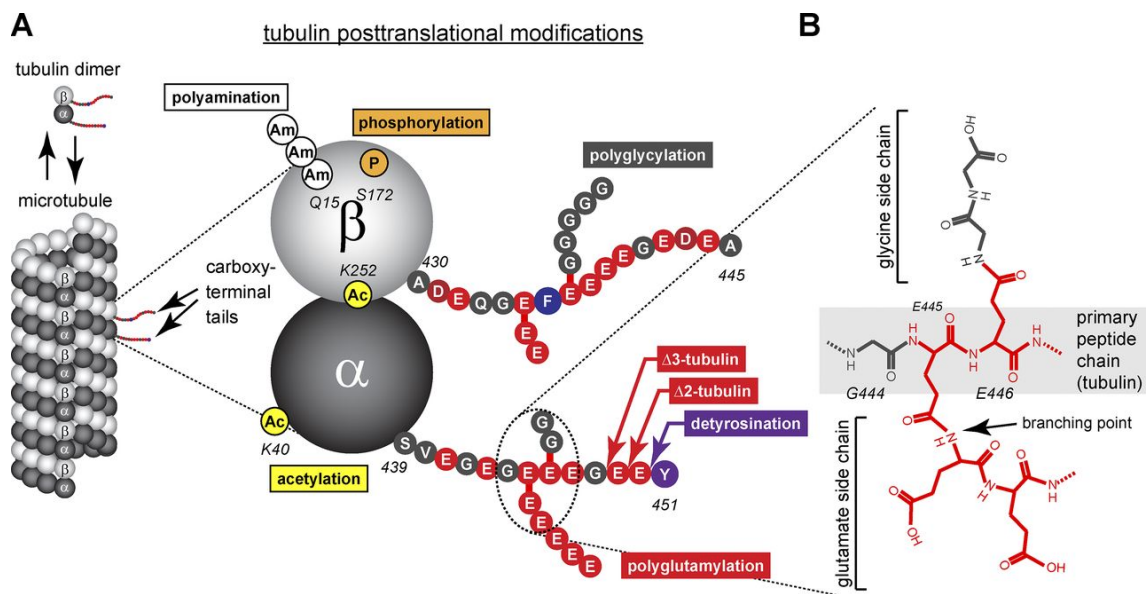
Figure 6. (A), Schematic representation of tubulin posttranslational modifications. Acetylation, phosphorylation and polyamination are identified on the tubulin core. Polyglycylation, detryosination-tryosination and the related Δ2 modification, polyglutamylation are found on the C-terminal tubulin tails. (B), Chemical structure of the branched peptide formed by polyglutamylation and polyglycylation. The scheme is adapted from (Janke, 2014).

Microtubule stability and structure are also regulated by a large range of PTMs, for instance, polyglutamylation, polyglycylation, detryosination-tryosination and the related Δ2 modification are involved in specifically regulation of tubulin and microtubules. Acetylation, methylation and phosphorylation are well-known PTMs that have variety substrates (Figure 6) (Gadadhar et al., 2017, Janke, 2014). In most eukaryotic cells, the C-terminus of α-tubulin is subject to detyrosination, which involves the enzymatically removal of the C-terminal tyrosine of α-tubulin in microtubule. The tyrosine residue can be re-added to the C-terminal glutamate residue of α-tubulin by a reverse tyrosination reaction (Arce et al., 1975). Tyrosination is catalyzed by TTL, while the enzyme catalyzing detyrosination has not been identified (Ersfeld et al., 1993, Gadadhar et al., 2017). One of the important functions of tubulin detryosination-tryosination cycle is to regulate the binding of CAP-Gly containing proteins (Akhmanova and Steinmetz, 2008). For example, in both *Saccharomyces*

cerevisiae and mice fibroblasts, reduction in tyrosinated microtubules disabled interaction of microtubules plus ends CLIP170 and caused defects of mitotic spindles, but not EB1 that lacks a CAP-Gly domain (Badin-Larcon et al., 2004, Peris et al., 2006). Therefore, interactions of tyrosinated α-tubulin and CAP-Gly containing +TIPs may contribute to microtubule-based functions during mitosis and interphase. Furthermore, microtubule-depolymerizing motors are inhibited by the detyrosination of tubulin, resulting in the stabilization of microtubules (Peris et al., 2009). Following detyrosination, remove of the second last amino acid generates Δ2-tubulin. The enzymes involved in this Δ2 modification are members of a family of cytosolic carboxypeptidases (CCPs). It has been shown that the Δ2 modification is an irreversible PTM since Δ2-tubulin cannot undergo retyrosination. Δ2-tubulin is enriched in long-lived microtubules in neurons, axonemes of cilia and flagellar, and also in cellular stabilized microtubules that have been artificially stabilized, like taxol-stabilized microtubule (Paturlelafanechere et al., 1994). Tubulin acetylation happens on residue lysine 40 (K40) of α-tubulin, which is positioned at the luminal face of microtubules (Lhernault and Rosenbaum, 1985, Soppina et al., 2012). Thus, the enzymes required for this process has to access the lumen to generate this modification. The specific function of K40 acetylation remains unclear do far (Howes et al., 2014). Nevertheless, acetylation is used as a marker to judge the stability of microtubules because tubulin acetylation is mainly accumulated on long-lived microtubules (Gadadhar et al., 2017). Besides the acetylation on K40 of α-tubulin, another acetylation has been detected at K252 of β-tubulin (Chu et al., 2011). Taken together, tubulin PTMs are mainly enriched on long-lived stable microtubules in cells and are differently distributed on functional distinct microtubules.

1.2 Cilia and flagella

Cilia and flagella are the Latin words for 'eyelash' and 'whip', and refer to hair-like, microtube-based appendages that extend from cell body. They are present on variable cell types as diverse as single cell protozoa and the retinal pigment epithelial cells of mammals. The shape and morphology of cilia and flagella are variable within different cell types (Figure 7A-D). The length ranges from microns to more than 2 mm in flagella of some insect sperm cells. Cilia play important functions in moving

eggs through oviducts, and clearing mucus out of airways. In addition to the motile functions, cilia serve as sensory organelles to detect extracellular signals, such as growth factors and hormones, odorants and light. Cilia also involved in developmental signaling pathway like hedgehog signaling (Huangfu et al., 2003, Ishikawa and Marshall, 2011, Eggenschwiler and Anderson, 2007).

1.2.1 Ciliary structure and movement

Although cilia and flagella exist in many types of cells and are variable in length and shape, they share a conserved organization, containing a bundle of microtubules, called anxoneme. Based on function and structure, cilia are conventionally categorized into two classes, motile cilia and non-motile cilia, or primary cilia. The '9+2' and '9+0' arrangements of microtubules usually exist in motile and primary cilia, respectively. The minus ends of the ciliary microtubules are anchored in the basal body, which contains nine triplet microtubules. Like centrioles, each of the triplet consists of A, B and C tubules (Figure 7H and I). The A tubule is a complete 13-protofilament microtubule, while B tubule and C tubule are incomplete contain 10 protofilaments (Warner and Satir, 1973, Li et al., 2012). The C tubule terminates at 300-500 nm from the proximal end of the basal body, whereas A tubules and B tubules are attached on the A tubule extends from basal body to form ciliary axoneme (Figure 7F and G). Within cilia, tubulins contributing to long-lived axoneme organization undergo several PTMs (details shown in 1.1.1.7). For example, it was found that acetylation on K40 of α-tubulin marks long-lived microtubules in cilia (Piperno and Fuller, 1985). Localization experiments in *Chlamydomonas* showed that detyrosinated tubulin is enriched on the B tubules of outer doublets, while tyrosinated tubulin can be detected in both A and B tubules and central pairs (Johnson, 1998). In *Tetrahymena*, glutamylated tubulin is present on the outer doublets but not central pairs (Suryavanshi et al., 2010). However, the central pairs of microtubules are glutamylated in sperm of sea urchin *Lytechinus pictus* and *Drosophila melanogaster* (Hoyle et al., 2008). Tubulin glycylation is also present in ciliary axoneme, like *Paramecium* (Redeker et al., 1994). Functional studies revealed that these tubulin PTMs are essential for ciliary movement and proteins transport inside cilia (Wloga et al., 2017).

In motile cilia, the nine outer doublet microtubules and two central singlet are continuous for entire axoneme structure (Ishikawa, 2017). The most proximal region of a cilium is called transition zone, linking the proximal part of the axoneme with ciliary membrane (Figure 7E). Transition fibers show a pin-wheel like structure, emerging from B tubule of the basal body. The tips of transition fibers are thought to anchor microtubules to plasma membrane. Distal to the transition fibers, there are specialized structures that show several parallel strands decorating the ciliary membrane defined as 'ciliary necklace'. These membrane particles were connected to the axoneme by the structure called 'Y-shaped' linkers (Figure 7E) (Gilula and Satir, 1972, Reiter et al., 2012, O'Toole et al., 2007). The transition fibers and transition zone act as a diffusion barrier to prevent the free mixing of membrane proteins between the plasma membrane and the ciliary membrane (Hu and Nelson, 2011). At the base of some motile cilia, there is a membrane domain called 'ciliary pocket', act as a platform for cilia related vesicular trafficking (Figure 7E) (Benmerah, 2013).

Within the axomene of motile cilia, the two central singlet microtubules are connected by periodic bridges and surrounded by fibrous proteins called inner sheath. From the central microtubules, there are radial spokes radiated to the A tubules of outer doublets. The neighboring outer doublet microtubules are interconnected circumferentially by nexin linkers and are attached to the central microtubules through radial spokes (Nicastro et al., 2005). The A and B tubules within one outer doublet is stabilized by tektin filaments, a highly insoluble filaments with physic-chemical properties similar to intermediate filaments (Figure 7F) (Linck et al., 1985). All the interactions between these components play essential roles for maintaining the structural stability of the axoneme. It appears that an axoneme is a highly sophisticated machinery composed of a few hundreds of proteins (Pazour et al., 2005). How dose the various components work together to regulate the ciliary movement? Briefly, ciliary motion is generated by the relative sliding between pairs of doublet microtubules. The sliding of the doublets is powered by ATP and axonemal dyneins, which are classified into outer dynein arms (ODAs) and inner dynein arms (IDAs) (Satir and Christensen, 2008). Both ODAs and IDAs are attached to the A tubule of each doublet microtubule, and these dynein arms reach out to the B tubule of adjacent doublets. By hydrolysis of ATP, dynein arms on the A tubule of one doublet move

towards the end of the neighboring B tubule, producing a local sliding motion between the doublets. Since dynein arms generate unidirectional movement, active sliding in one side of the axoneme produces bending toward one side, whereas dynein arms located on the other side induce bending toward the opposite side. To generate proper ciliary movement bend in both directions, dynein arm activity must be regulated according to timing and location. Previous studies indicated that coordination of dynein activity include radial spokes, central pair microtubules and IDAs and dynein regulatory complex (Heuser et al., 2009, Viswanadha et al., 2017).

The axoneme is surrounded by ciliary membrane. Although the ciliary membrane is an extension from plasma membrane, it has a distinct composition of lipids and proteins. For example, flagellar membranes are enriched in raft-forming phospholipids like phosphatidylethanolamine (PE) and sphingomyelin in *Trypanosama brucei*, compared to membrane of whole cells (Serricchio et al., 2015). Additionally, at the base of cilia – the ciliary pocket region features a highly curved membrane, and the lipid composition is different from the membrane covering the ciliary shaft. It has been suggested that the membrane at base of cilia contains a condensed lipid zone, which acts as a diffusion barrier between plasma membrane and ciliary membrane (Rohatgi and Snell, 2010).
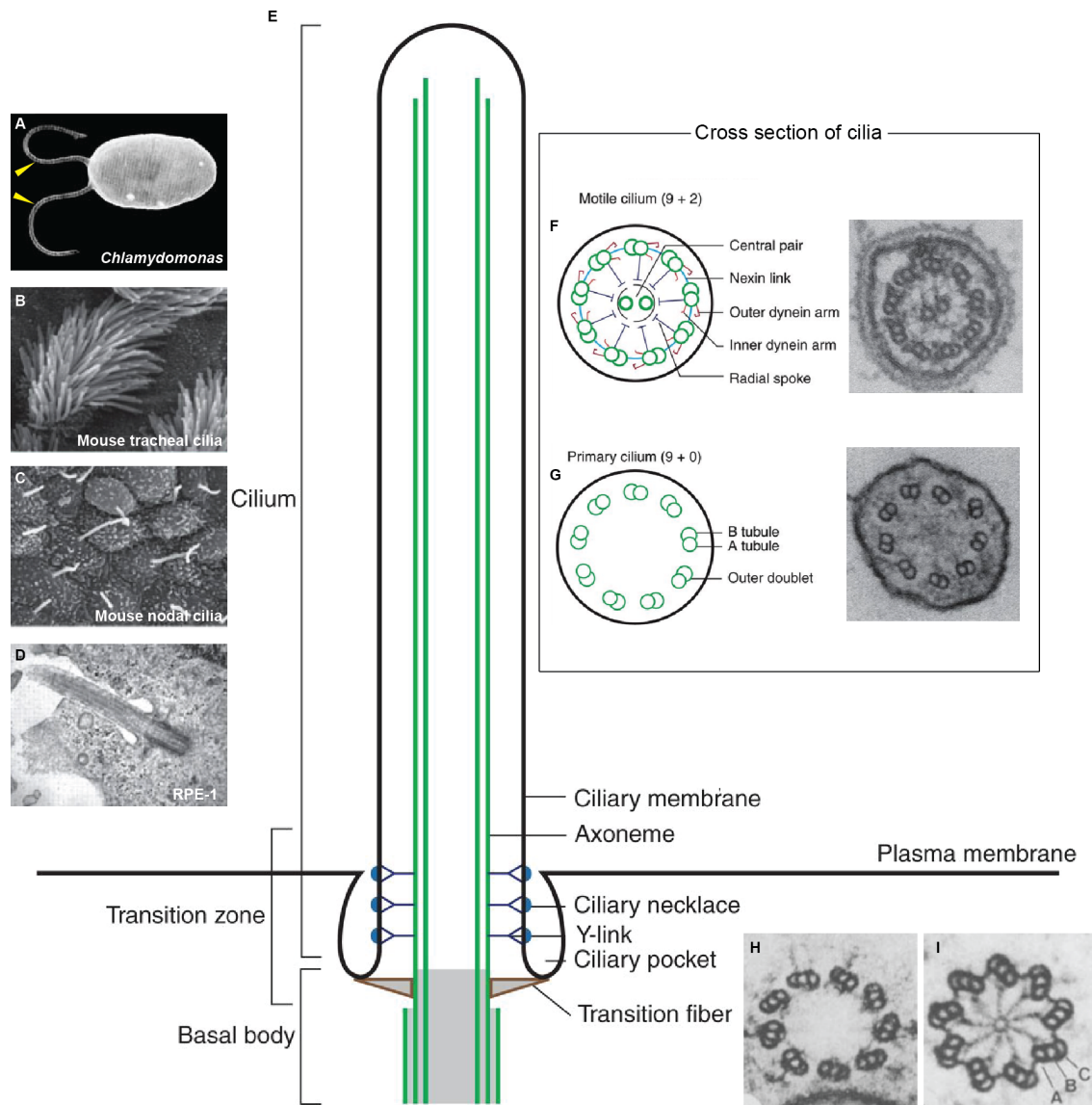
Figure 7. The architecture of cilia. (A), (B), (C), The scanning electron micrograph (Kerssemakers et al.) of flagella extending from a *Chlamydomonas* cell, mouse tracheal motile cilia, mouse nodal cilia. (D), Transmission electron micrograph of the primary cilium of retinal pigment epithelial (RPE-1) cells. (E), Schematic, foreshortened drawing of a longitudinal section of the primary cilium. (F), (G), Schematic and electron micrographs of cross sections of 9+2 structure of the axoneme from *Chlamydomonas*, and 9+0 structure from mouse nodal cilia. (H), (I), Electron micrographs of distal region and proximal region cross sections of flagellar basal bodies in *Trichonympha*. Micrograph in (A) is obtained from (Rosenbaum and Witman, 2002), (B), (C) and (D) are adapted from (Ishikawa and Marshall, 2011). Schematic in (E), (F), and (G) are adapted from (Ishikawa and Marshall, 2017). Micrograph in (F) and (G) are obtained from (Ishikawa, 2017). Micrograph in (H) and (I) are taken from (Gibbons, 1981).

1.2.2 Cilia functions and human diseases

The most striking role of cilia is their contribution in cell motility. In human, ciliary motility is required for sperm cells to propel through the female reproductive system. Vertebrate cilia are important for moving extracellular fluid flow across tissues. For example, cilia are important for protective mucus clearance in the airway; cilia drive polarized fluid flow important for circulation of cerebrospinal fluid in the spinal cord and ventricles of adult brain (Brooks and Wallingford, 2014). Furthermore, in the motile 9+0 cilia of the embryonic node, ciliary motility is required for generating a left-directed flow that is involved in embryonic left-right asymmetry determination (Nonaka et al., 1998b). The primary cilia are generally non-motile since they lack the dynein arms and the central pairs of microtubules, however, they act as 'antenna' to sense the extracellular signals and environments. Primary cilia are also involved in processing various signaling pathways, such as Hedgehog, Notch, Wnt, and growth factor signaling (Drummond, 2012, Goetz and Anderson, 2010).

The primary cilium in mammals was discovered more than 100 years ago, however, the functional importance was largely unknown until the studies linked ciliary dysfunction with polycystic kidney disease (PKD) (Pazour et al., 2000). The polycystic kidney mouse model, the *Tg737*, an insertional mutation that disrupts the gene coding for the protein Polaris, which was found localize below the membrane in the region of the basal bodies and within the cilia (Taulman et al., 2001). Moreover, the orthologs of *Tg737* in *Chlamydomonas* and *C. elegans*, *IFT88* an *osm-55*, respectively, encode proteins functions in ciliogenesis (Haycraft et al., 2001, Pazour et al., 2000). Based on the observation that cilia defects in polycystic kidney mouse model, the conclusion was made that Polaris is required for ciliogenesis. After identification of the PKD as a cilia-related disorder, the function of cilia in human disease has expanded rapidly. Other cilia-related defects were identified such as Bardet-Biedl syndrome (BBS), Nephronophthisis (NPHP), Joubert syndrome (JBTS), and Usher syndrome (Braun and Hildebrandt, 2017, Hildebrandt et al., 2011). These syndromes can be categorized as ciliopathies, a concept that describes a

heterogeneous group of genetic disorders caused by disruption to ciliary structure or its function. Ciliopathies present a complex combination of phenotypes including cystic kidneys, hearing loss, retinal degeneration, and situs inversus. Each disease is the result of mutations in a number of genes, and in general the normal proteins encoded by those genes localize to the primary cilium or basal body (Badano et al., 2006, Fliegauf et al., 2007).

1.2.3 Intraflagllar transport

Assembly of the ciliary axoneme happens exclusively at the distal end of the cilium, and all the materials necessary for cilia assembly are transported from cell body since ribosomes are absent from cilia. The transport of ciliary proteins from cytoplasm to ciliary tip is mediated by a process called intraflagellar tansport (IFT). IFT is a bidirectional protein transport system along axonemal microtubules beneath the ciliary membrane, and it carries ciliary components to ciliary tip and sends the turnover products back to cell body (Figure 8A) (Johnson and Rosenbaum, 1992, Rosenbaum and Witman, 2002). IFT was first observed as the granule-like particles move along the cilia of *Chlamydomonas* by differential interference contrast microscopy, and the anterograde transport is about 2.5 μm/sec, while the retrograde transport rate is ~4 μm/sec (Kozminski et al., 1993). Electron microscopy observation of IFT revealed a varying number of particles assembled into linear arrays (so-called 'IFT-trains') linking outer doublet microtubules to the ciliary membrane (Figure 8B-E) (Rosenbaum and Witman, 2002, Kozminski et al., 1995). The first detailed ultrastructure analysis of IFT trains *in situ* was through electron tomography, two categories of IFT trains were observed. One class of IFT trains is relatively long with about 700 nm and less electron-opaque, with a particle periodicity of ~40 nm. The other class is around 250 nm in length and more compact, with a repeat of ~16 nm. Studies using the retrograde IFT mutant showed the short trains disappeared, therefore, the long and short IFT trains were hypothesized to be involved in anterograde and retrograde transport, respectively (Pigino et al., 2009). However, recently studies revealed that anterograde and retrograde trains are of similar length and show a different periodicity (Stepanek and Pigino, 2016, Vannuccini et al., 2016). Anterograde IFT trains move along B tubules and retrograde trains move along A

tubules. The authors hypothesized that IFT trains moving in opposite directions in different tubules may avoid collisions between them (Stepanek and Pigino, 2016).
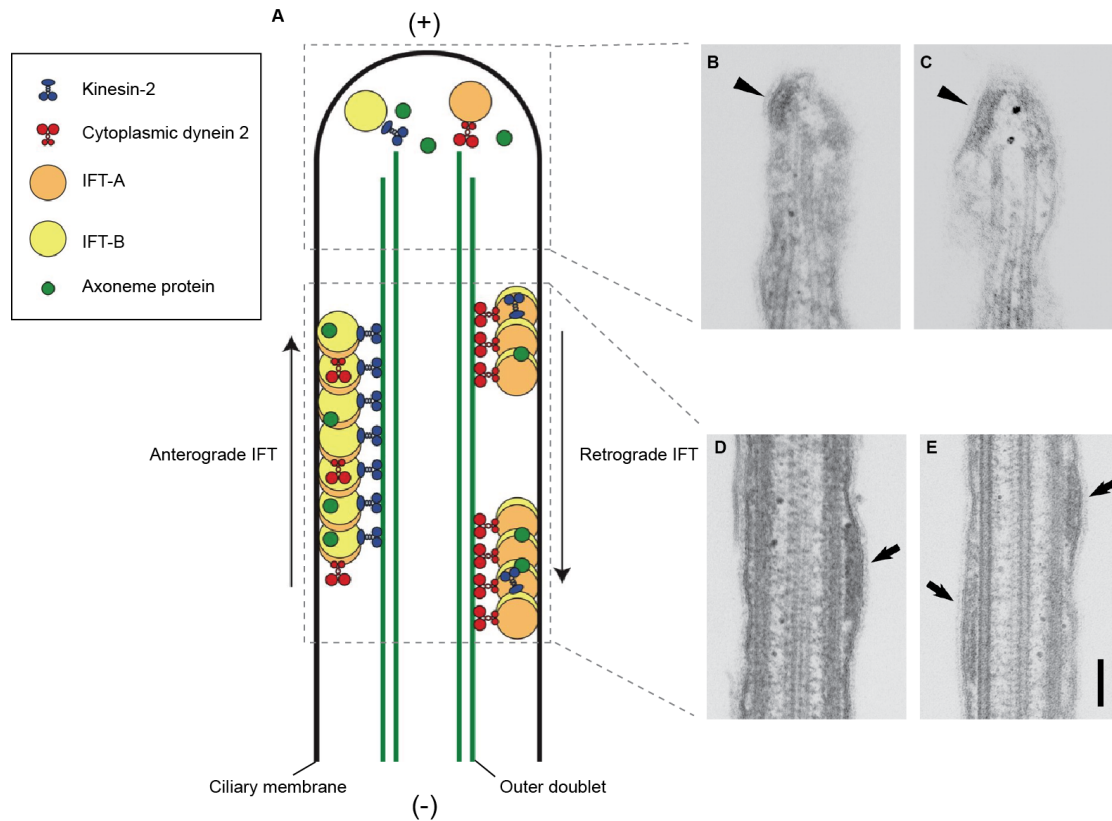
Figure 8. (A), Schematic representation of intraflagellar transport. The antergrade IFT train is powered by kinesin-2 motor to the tip of a cilium. At the cilium tip, anterograde IFT train release cargo and rearrange the conformation for retrograde IFT. Cytoplasmic dynein 2 transports retrograde IFT train to the cell body. (B), (C), EM longitudinal sections of a flagellar tip. Two individual IFT train located in the most distal compartment of the flagellum are visible (arrowhead). (D), (E), IFT trains of different length and density in individual flagella. The scale bar is 100 nm. Schematic in (A) is adapted from (Ishikawa and Marshall, 2017). Micrographs in (B-E) are obtained from (Pedersen et al., 2006).

1.2.4 Building blocks of IFT trains

IFT trains are multimeric protein complexes that consist of IFT motors, IFT particles, cargoes and BBsomes as further described in the following sections.

1.2.4.1 IFT motors

There are two types of microtubule motors that power IFT. Kinesin-2 drives anterograde movement of IFT trains toward ciliary tip, and cytoplasmic dynein 2 moves retrograde IFT trains towards the base of the axoneme. The canonical anterograde IFT motor is heterotrimeric kinesin-2 and is essential for the assembly and maintenance of cilia in most organisms. For example, disruption of KIF3B, one of the kinesin-2 subunits, causes the loss of nodal cilia (Nonaka et al., 1998a). Cytoplasmic dynein 2 is a multiprotein complex identified from sea urchin embryos, and genetic studies indicated the mutations result in the short cilia with accumulation of IFT at the tip (Gibbons et al., 1994, Pazour et al., 1998). Cytoplasmic dynein 2 requires kinesin-2 to reach the ciliary tip, indicating that it travels as an inactive cargo on anterograde IFT trains (Pedersen et al., 2006). Once anterograde IFT trains transport to the ciliary tip, the trains get remodeled and cytoplasmic dynein 2 get activated to power retrograde IFT trains to the cell body (Iomini et al., 2001). In IFT, groups of motor proteins work together to transport a single cargo in a cooperative manner. In *C. elegans* chemosensory cilia, anterograde IFT trains at the ciliary base are mainly driven by kinesin-2 motors, while after a gradual handover of the cargo, OSM-3 replaces kinesin-2 and propels the IFT trains to the ciliary tip (Prevo et al., 2015). IFT is a highly orchestrated event with few aberrant movements, indicating the various motors involved in movement of IFT trains are highly regulated (Prevo et al., 2017).

1.2.4.2 IFT particles

IFT particles serve as adaptors between the cargos and motors during the process of intraflagellar transport. IFT proteins were first purified from cilia of *Chlamydomonas* and identified to consist of two large subcomplexes, IFT-A and IFT-B, by varying the ionic strength during the fractionation. Initial biochemical purification of IFT complex identified IFT144, 140, 139, 122 for IFT-A and IFT172, 88, 81, 80, 74/72, 57/55, 52, 46, 27, 20 for IFT-B (Piperno and Mead, 1997, Cole et al., 1998).

Subsequent studies have added IFT121 and IFT43 to IFT-A, and IFT70, IFT25, IFT54, IFT56, IFT38 and IFT22 to IFT-B (Ishikawa et al., 2014, Subota et al., 2014, Blacque et al., 2006, Fan et al., 2010, Follit et al., 2009). The IFT-B complex is further divided into IFT-B1 (known as IFT-B core containing IFT88, 81, 74, 70, 56, 52, 46, 27, 25, 22) and IFT-B2 (known as IFT-B peripheral subunits comprising six subunits, IFT172, 80, 57, 54, 38, and 20), both of them are capable of assembling into stable complexes (Taschner et al., 2016, Taschner et al., 2014, Lucker et al., 2005). Bioinformatics analysis of IFT proteins showed protein-protein interaction motifs such as WD-40 repeats, coiled-coil heptad repeats and tetratricopeptide (TPR) are widespread displaying in IFT proteins, most of which are required for interaction among IFT proteins, as well as the interactions with ciliary cargos and motors (Taschner and Lorentzen, 2016). Mutations affecting IFT proteins cause defects of ciliary structure and function. In most cases, loss of subunits in IFT-B results in short or absent cilia (Haycraft et al., 2003, Pazour et al., 2000, Fujiwara et al., 1999). On the contrary, mutations in IFT-A subunits are often compatible with a partial or a complete assembly of cilia, but with accumulation of IFT proteins (Efimenko et al., 2006, Tsao and Gorovsky, 2008). Thus, IFT-A and IFT-B play complementary but distinct parts in the transport of ciliary proteins. In most cases, IFT-B is required for anterograde transport and is essential for assembly and maintenance of cilia, while IFT-A contributes to retrograde transport that returns proteins to the cell body.

1.2.4.3 IFT cargo

The IFT complex is proposed to bind a variety of cargo proteins, such as ciliary tubulins, and dynein arms and IFT motors (Prevo et al., 2017). Tubulin is the major structural protein of the axoneme. Tubulin subunits get transported to ciliary tip by IFT in low amounts when the assembling cilia reach its steady-state length. On the contrary, the amount of tubulin is upregulated during the elongation phase of ciliogenesis (Hao et al., 2011, Craft et al., 2015). Structural studies showed N-terminal domains of IFT81 and IFT74 in IFT-B1 form a heterodimer that bind tubulin *in vitro*. Specifically, the calponin homology (CH) domain of IFT81 binds to tubulin dimer and the binding affinity is enhanced by the positively charged N-terminus of IFT74, which interacts electrostatically to the acidic C-terminal tails of tubulin

(Bhogaraju et al., 2013). Consistent with the structure model, disruption of either the CH-domain of IFT81 or IFT74 N-terminal domain resulted in a reduced rate of flagellar regeneration. The mutations of both domains caused the assembly of short flagellar (Kubo et al., 2016). Besides the CH domain of IFT81, there are several other IFT-B proteins (IFT57, IFT54 and IFT38) that contain CH domains. It has been demonstrated that IFT54 also binds to tubulin and polymerized microtubules (Taschner et al., 2016). Moreover, it has been found that IFT46 has specific roles in transporting outer dynein arms through the interaction with the cargo adaptor ODA16 (Ahmed and Mitchell, 2005, Hou et al., 2007, Taschner et al., 2017). The inner dynein arms, have been shown by genetic studies in zebrafish embryos and *Chlamydomonas*, get delivered into cilia by IFT56 (Ishikawa et al., 2014).

1.2.4.4 BBSome

The BBSome is a complex comprising eight Bardet-Biedl syndrome (BBS) protein subunits (BBS-1, 2, 3, 4, 5, 8, 9, BBIP10) (Loktev et al., 2008). In *C. elegans*, dysfunction of BBSomes caused instability and incorrect assembly of the IFT complex, resulting in dissociation of IFT-A and IFT-B complexes. It suggests that there is a functional interaction between the BBSome and IFT-A and IFT-B in *C. elegans* (Blacque et al., 2004, Wei et al., 2012). However, the BBSome appears to be highly substoichiometric to IFT-A and IFT-B in *Chlamydomonas*. It has been suggested that the BBSome serve as an adaptor required for exporting signaling proteins from cilia, rather than as an integral component of IFT particles (Lechtreck et al., 2009). Mouse *IFT27* mutants showed the accumulation of BBSomes in their cilia, indicating that IFT27, together with IFT25, might form a docking site for BBSome export from cilia (Eguether et al., 2014, Liew et al., 2014). In addition, the BBSome is also required for cilium membrane biogenesis and is linked to the membrane of the cilium through the small GTPase ARL6/BBS3 (Nachury et al., 2007). Interestingly, the BBSome is not conserved in all eukaryotic species. For example, *Batrachochytrium dendrobatidis* and *Toxoplasma gonidii* have functional cilia with the loss of BBSome, indicating the function of it is nonessential in some species (van Dam et al., 2013).

1.2.5 Functions of IFT proteins: beyond the ciliogenesis

As discussed in the previous chapter, IFT plays critical roles in the building and maintenance of cilia. Apart from the functions in ciliogenesis, IFT proteins are also found in different membrane system in cells and are involved in various functions. Here I will discuss the structural basis of IFT protein for membrane trafficking and then several examples will be shown.

The IFT system is universally and ancestrally associated with cilia and IFT subunits are also remarkably conserved at the sequence level across eukaryotes. Interestingly, a comparative analysis of IFT proteins revealed that several IFT subunits (IFT144, IFT140, IFT122 and IFT121 in IFT-A; IFT172 and IFT80 in IFT-B) are clearly members of the protocoatomer family, sharing secondary structure folds and elements with vesicle coat complex involved in membrane trafficking (COPI, COPII and clathrin/adaptin complex) (van Dam et al., 2013, Jekely and Arendt, 2006). COPI and clathrin/adaptin complex consist of one or two β-propellers, an α-solenoid-like domain, exclusively in the order of β-α (Devos et al., 2004). The same domain architecture was recognized in subunits of the COPII, nuclear pore complex (NPC), as well as IFT complex. Based on these observations, it has been proposed that clathrin, COPI, COPII, NPC and IFT complex share a common origin in an ancestral protocoatomer (Rout and Field, 2017). More specifically, phylogenetic reconstruction and structural analysis demonstrated that IFT proteins are closely related to the COPI complex. IFT-A, IFT-B and BBSome subunits were classified into four groups based on the homology relationships to COPI complex (Figure 9). IFT144, IFT140, IFT122, IFT121, IFT172 and IFT80 in the first group share domain structure with COP-α and -β' subunits. The second group has domain structure similar as COP-ε, consisting IFT139, IFT88, IFT70, IFT56, BBS4 and BBS8. The third group comprises the small GTPases, including IFT22, IFT27 and BBS3. The last group contains BBS1, BBS2, BBS7 and BBS9, representing four homologous subunits in the BBSome (van Dam et al., 2013). The similarity between IFT proteins and BBSome subunits with vesicle trafficking proteins implies these proteins may share similar evolutionary roots and perform similar functions.
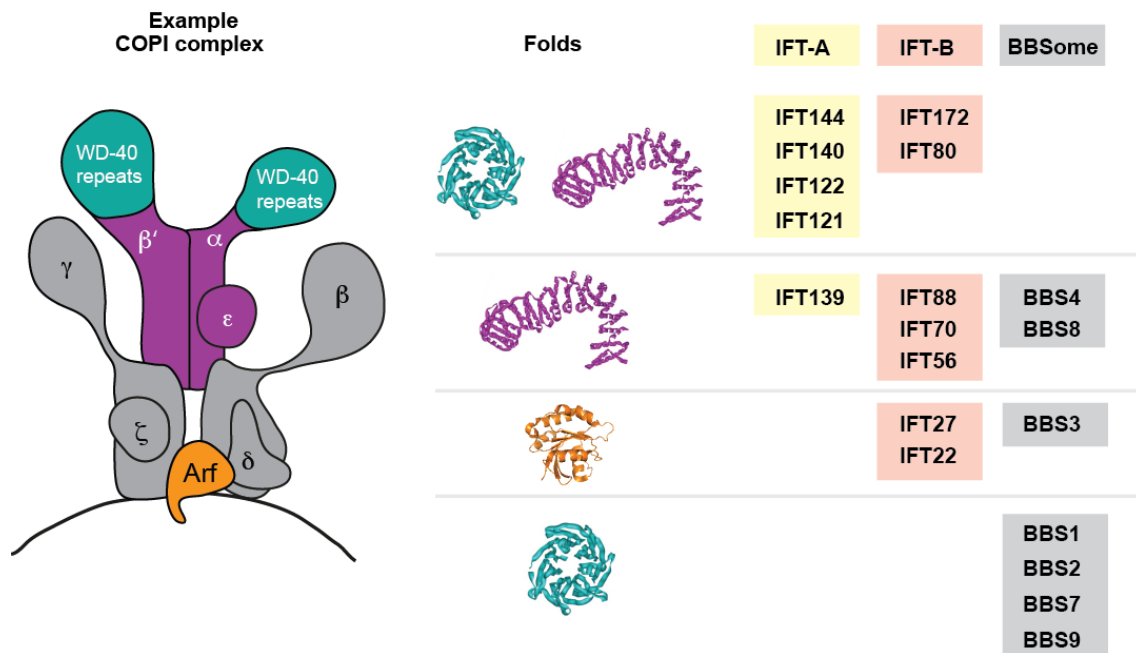
Figure 9. IFT complex and COPI share a common domain architecture. A diagram of the organization of the COPI coated vesicle complex is shown on the left. β-propeller regions, α-solenoid regions and the small GTPases Arf are colored in cyan, purple and green, respectively. The sample models for each fold are shown in the center. The classification of the IFT and BBSome proteins are based on secondary structure prediction from (Taschner et al., 2012) and phylogenetic analysis from (van Dam et al., 2013).

Based on the proposal above, multiple studies have provided evidence for IFT proteins function in vesicle trafficking. The first detailed report showing that IFT proteins might be involved in membrane trafficking other than ciliogenesis is that IFT20 is localized at the Golgi complex, by anchoring to the Golgi polypeptide, GMAP210. The knock down of IFT20 affects the amount of ploycystin-2 localized to the cilia, indicating that IFT20 is involved in delivering ciliary membrane proteins from Golgi complex to cilia (Follit et al., 2006, Follit et al., 2008). Additionally, recent evidence showed that IFT88 associates with vesicles from endoplasmic reticulum (ER) exit site to primary cilium. Diacylglycerol kinase δ (DGKδ), a residential lipid kinase in the ER, binds to IFT88 and triggers the release of IFT88-containing vesicles (Ding et al., 2017). By extracting cytoplasmic vesicles from *Chlamydomonas* and doing immunogold labeling, it has been found IFT46, radial

spoke proteins (RSPs), α-tubulin associated with the outside surface of cytoplasmic vesicles (Wood and Rosenbaum, 2014). Additionally, in *Chlamydomonas*, IFT27, IFT46, IFT72 and IFT139 were found re-localized from flagella and basal body to the cleavage furrow during cell division, and the location of IFT27 was pinpointed to surface of membrane vesicles (Wood et al., 2012). Moreover, it has been observed that vesicles pinch off from the tip of cilia and get released into the extracellular environment, which is called ciliary ectosomes. A recent study showed that growth induction triggers vesiculation of the cilia tips and IFT-B proteins were detected in these ciliary vesicles (Phua et al., 2017, Wood and Rosenbaum, 2015). The BBSome complex, also sharing common structure elements with vesicle coat protein, has been proposed to be involved in sorting membrane proteins to primary cilia. *In vitro* reconstitution showed BBSome proteins coat on the lipid surface and the coating is initiated by a small GTPase BBS3 (Jin et al., 2010).

Furthermore, the IFT system has been found in non-ciliated cells, associated with membrane. For example, IFT20 was found co-localize with Golgi and post Golgi membrane compartments in T-lymphocytes, similar to the localization of IFT20 in ciliated cilia (Follit et al., 2006, Finetti et al., 2009). When T-cells interact with antigen presenting cells, the proteins and lipids on the contact area rapidly redistribution and form an interface known as immune synapse (Cemerski and Shaw, 2006). During this process, it was found IFT20 is recruited together with other IFT proteins (IFT57, IFT88) to the immune synapse. Knockdown of IFT20 was found interfere with the formation of immune synapse. It is the first evidence that IFT is involved in membrane trafficking in non-ciliated cells (Finetti et al., 2009). In non-ciliated retina neurons, subsets of IFT proteins like IFT20, IFT52, and IFT57, are found associated with cytoplasmic membrane vesicles at the postsynaptic terminal region (Sedmak and Wolfrum, 2010). In summary, IFT system is not only required for building and maintenance of cilia in ciliated cells, it also functions in multiple cell biological processes like membrane trafficking, cellular secretory in both ciliated and non-ciliated cells.

2. Results

2.1 Chapter I

2.1.1 Structural basis for the extended CAP-Gly domains of p150^{glued} binding to microtubules and the implication for tubulin dynamics

Structural basis for the extended CAP-Gly domains of p150^glued binding to microtubules and the implication for tubulin dynamics

Qianmin Wang[a], Alvaro H. Crevenna[b], Ines Kunze[a], and Naoko Mizuno[a,1]

[a]Cellular and Membrane Trafficking, Max Planck Institute of Biochemistry, D-82152 Martinsried, Germany; and [b]Physical Chemistry, Department for Chemistry and Biochemistry and Center for NanoScience, Ludwig-Maximilians-Universität München, D-81377 Munich, Germany

p150^glued belongs to a group of proteins accumulating at microtubule plus ends (+TIPs). It plays a key role in initiating retrograde transport by recruiting and tethering endosomes and dynein to microtubules. p150^glued contains an N-terminal microtubule-binding cytoskeleton-associated protein glycine-rich (CAP-Gly) domain that accelerates tubulin polymerization. Although this copolymerization is well-studied using light microscopic techniques, structural consequences of this interaction are elusive. Here, using electron-microscopic and spectroscopic approaches, we provide a detailed structural view of p150^glued CAP-Gly binding to microtubules and tubulin. Cryo-EM 3D reconstructions of p150^glued-CAP-Gly complexed with microtubules revealed the recognition of the microtubule surface, including tubulin C-terminal tails by CAP-Gly. These binding surfaces differ from other retrograde initiation proteins like EB1 or dynein, which could facilitate the simultaneous attachment of all accessory components. Furthermore, the CAP-Gly domain, with its basic extensions, facilitates lateral and longitudinal interactions of tubulin molecules by covering the tubulin acidic tails. This shielding effect of CAP-Gly and its basic extensions may provide a molecular basis of the roles of p150^glued in microtubule dynamics.

dynamic instability | dynactin | cytoskeleton | electron microscopy

The great variety of microtubule-associated proteins and the complexity of their interactions (1) are beginning to rival that of the actin-associated proteins. This complexity reflects the many different roles that actin and microtubules play in cellular cytoskeletal organization and activity. Our study focuses on the structural interactions of tubulin/microtubules with protein fragments corresponding to N-terminal portions of the p150^glued subunit of the megadalton dynactin complex. Of particular interest is the 80-amino acid cytoskeleton-associated protein glycine-rich (CAP-Gly) domain (p150^glued residues 25–105), which, when harboring critical mutations in neuronal dynactin, leads to devastating neurological disorders (2).

Several studies have characterized the interactions of p150^glued with various +end-binding proteins (+TIPs), including end-binding protein 1 (EB1) and CLIP-170 (3–5), and the role of the negatively charged, C-terminal tubulin tails in binding positively charged domains of these proteins to the tubulin surface (6–9). Biophysical observations showed the ability of the +TIPs to promote microtubule polymerization (5, 6, 10). Recently, Lazarus et al. (11) have demonstrated that the N-terminal dimeric portion of p150^glued is a neuron-specific anticatastrophe factor acting at the microtubule +end; a mutation in the CAP-Gly domain, which causes the lethal Perry syndrome, when introduced in their recombinant dimeric construct, abolishes the protective anticatastrophic depolymerization activity.

Here, by focusing on a single CAP-Gly domain of p150^glued, intrinsic interactions with tubulin and microtubules were identified. The basic p150 fragments cause the lateral association of microtubules by neutralizing their repulsive negative surface charge. By limiting the extent of bundling, cryo-electron microscopic (cryo-EM) 3D reconstructions were obtained for CAP-Gly plus basic extensions connected to the negatively charged, flexible tails of tubulin. These reconstructions indicated a flexible

connection of the CAP-Gly domain. Furthermore, this domain facilitated the assembly of tubulins into longitudinally connected oligomers at low temperatures and initiation of polymerization, likely through activating lateral associations of tubulin. The lateral interaction is likely due to the masking of the acidic charge of the tubulin surface. These two observed interactions provide a basis for the microtubule recovery following catastrophes. The properties of the +TIPs are much more than the sum of their parts. However, the identification of intrinsic properties of the components builds a foundation for exploring their cooperative interactions.

Results

EM Observation Shows That the Microtubule Lateral Association Is Induced by p150^glued. To understand the interaction between p150^glued and microtubules in a structural context, we observed the p150^glued–microtubule complex using cryo-EM. We generated several p150^glued fragments containing the microtubule-binding CAP-Gly domain: namely, the CAP-Gly core [p150(25–105)]; 25 additional N-terminal residues [p150(1–105)]; 40 additional, unstructured C-terminal residues [p150(25–144)]; and both N- and C-terminal extensions [p150(1–144)] (Fig. S1) (12, 13). Both extensions contain several basic residues with predicted pI values of 12.0 and 12.6, respectively, as opposed to rather mild basic pI of 8.9 for CAP-Gly. A microtubule-pelleting assay showed that the binding of CAP-Gly alone to microtubules appears to be fairly weak (Fig. S1B, marked with an *), but addition of the upstream/downstream basic patches increased the binding affinity. Quantitative pelleting assays showed that CAP-Gly can recognize both alpha and beta tubulin at saturating levels (Fig. S2A). In the presence of 2 μM microtubules with 20 μM p150^glued

Significance

This study presents a direct visualization of the microtubule-p150glued(CAP-Gly) complex by cryo-EM and seeks to describe the molecular mechanism of the control of tubulin dynamics by p150 CAP-Gly. It highlights the neutralization of the acidic tubulin surface by the basic extensions of CAP-Gly, resulting in the activation of tubulin polymerization. In the condition where the lateral association is impeded (i.e., at low temperature), the extended CAP-Gly domain induces tubulin dimers to connect longitudinally. The two directional modes of self-association of tubulin suggest a foundation for its dynamic behavior at the tip of microtubules and its regulation.

BIOCHEMISTRY

Fig. 1. (*A*) Shown are 3D reconstructions of microtubules with p150(1–105) (*Left*), p150(25–144) (*Center*), and p150(25–105) (*Right*). The sample was prepared by mixing 20-µM protein fragments with 2-µM microtubules in 80 mM Pipes-Na (pH 6.8), 1 mM MgCl₂, and 1 mM EGTA. Chicken-wire densities show the reconstructions without amplifying the high-resolution density whereas the amplitude-corrected reconstruction is presented as a solid density, resulting in weakening the density of the decoration. A fitted tubulin atomic model is shown in green (PDB ID code 1TUB). Tubulin E-hooks are missing from the atomic model. The last visible residue from the atomic model is labeled "C." Tu, tubulin protofilament. (*B*) Schematics of the interaction between E-hook and p150^glued CAP-Gly. The N- and C-terminal parts of the atomic model of CAP-Gly (PDB ID code 1TXQ) are marked in yellow (N25) and pink (C97), respectively. The N- and C-terminal extensions of the CAP-Gly core are depicted as yellow and pink lines, respectively. These extensions are predicted to be disordered, but the experiments confirm the interactions with tubulin E-hooks (green line). The GKNDG motif interacting with tyrosine at the C terminus of the alpha tubulin E-hook is colored in blue. The mean orientations of the flexibly connected p150(1–105) (*Left*) and p150(25–144) in the reconstructions in *A* are suggested. (*C*) Lateral projection of one protofilament decorated with p150(1–105) (*Left*) and p150(25–144) (*Right*). Circles, CAP-Gly core; arrowheads, the highest density (CAP-Gly core). The dashed line indicates the position of the neck.

fragments, saturation of the proteins on microtubules was achieved, except for p150(25–105) (*SI Discussion* and Figs. S1*B* and S2).

The corresponding complexes observed under cryo-EM showed that microtubules associate with each other to form a lateral assembly (Fig. S1*C*). This assembly was not observed for p150(25–105). These microtubules sometimes opened up showing a sheet-like structure. We selected p150(25–105), p150(1–105), and p150(25–144) for further analysis because they yielded complexes in which microtubules were separated enough for image processing. In contrast, p150(1–144) caused strong microtubule bundling, which hampered structure analysis.

Cryo-EM Reconstruction Shows a Neck Formation of Tubulin E-Hooks and the CAP-Gly Basic Patch. The reconstruction of microtubules bound to the CAP-Gly core p150(25–105) showed nondetectable

protein decoration (Fig. 1*A*, *Right*) reflecting the weak interaction. p150(1–105) and p150(25–144) gave enough density to visualize the spatial relation of the CAP-Gly domains bound to the microtubules (Fig. 1*A*, *Left* and *Center*). The CAP-Gly density is located ∼2 nm away from the microtubule surface, connected through a neck protruding out from the microtubule surface. The reconstruction of p150(1–105) (chicken wire displayed density) gave an interpretable density corresponding to the CAP-Gly core, which has comparable size to the crystal structure of the CAP-Gly (PDB ID code 1TXQ) (Fig. 1*B*). We chose not to fit the crystal structure to the reconstruction due to the flexibility of the CAP-Gly binding.

There is no apparent interaction between the core of the microtubules and the CAP-Gly. By adjusting the amplitude of relatively high frequency signals (*SI Materials and Methods*), the microtubule density started revealing secondary structure elements (Fig. 1*A*, gray solid density), which made it feasible to fit the atomic structure of a tubulin dimer. The molecular fitting showed that the C terminus of tubulin is connected to the neck (Fig. 1*A*, labeled with "C"). The ∼15 aa, negatively charged C-terminal tubulin tail (termed the E-hook) was not resolved in the atomic model (PDB ID code 1TUB) because of its flexible nature (14). Judging from the connection of the E-hook containing neck and the tubulin monomer, E-hook is leaning toward the minus end of the microtubule in the p150(1–105)-microtubule reconstruction. As the CAP-Gly core itself attaches to the neck, the neck density should also consist of the mass of the CAP-Gly basic extensions. Proteolytic treatment of the tubulin E-hooks by subtilisin abolished the binding of the CAP-Gly fragments (Fig. S2), also confirming the exclusive binding of the CAP-Gly fragments to E-hooks. On the other hand, the reconstruction of p150(25–144)-microtubule showed a decoration connected along the microtubule axis although the general flat bean-like shapes of CAP-Gly were recognizable by changing the density threshold (Fig. 1*A*, *Center* and 1*C*, *Right*). This density is connected through the neck, indicating that the essential interaction happens through the E-hook.

Based on the pelleting assay (Fig. S1*B*), the binding of the p150 fragments to the microtubules was greatly increased upon the addition of the basic patches (amino acids 1–25 and 106–144). Therefore, the densities connecting CAP-Gly and tubulin core (Fig. 1*A*, neck) likely correspond to E-hooks and the 1–25 basic patch for p150(1–105), and E-hooks and the 106–144 basic patch for p150(25–144) (Table 1). This observation indicates that the binding of CAP-Gly–containing fragments depends on oppositely charged surface interactions rather than a set of specific/conserved interactions. Moreover, the binding affinity of the CAP-Gly core to the tyrosinated E-hook was 11 µM whereas virtually no detectable binding was observed for the detyrosinated E-hook (>130 µM) (Table 1). This increase of the affinity agrees with previous reports (7) showing the recognition of the CAP-Gly core GKNDG motif by tyrosine at the end of the alpha E-hook. It suggests that the GKNDG motif is interacting with the C terminus of tubulin whereas the basic patches 1–25 and 106–144 wrap around the rest of the E-hook to secure the binding (Fig. 1*B*).

Table 1. Dissociation constants (*K*ₐ, µM) of p150^glued fragments to E-hook peptides using fluorescence correlation spectroscopy

p150 fragments	αY	αE	βC
1–210 dimer	0.8 ± 0.3	3 ± 1	0.8 ± 0.3
1–105	6 ± 3	35 ± 20	9 ± 5
25–105	11 ± 5	> 130	46 ± 20
25–144	5.4 ± 1.5	28 ± 30	10 ± 4
1–144	7 ± 3	13 ± 4	7 ± 2

αY, tyrosinated alpha tubulin E-hook; αE, detyrosinated alpha tubulin E-hook, βC; beta tubulin E-hook.

p150[glued] CAP-Gly Fragments Flexibly Recognize the Microtubule Surface. The computational amplitude adjustment of the reconstruction weakened the density of the CAP-Gly to a close-to-noise level. This faint density suggests either that the occupancy of the protein fragments is low or that their attachment to the microtubule surface is very flexible. However, the pelleting assay in the corresponding conditions showed the saturation of p150 fragments on the microtubules, supporting a possibility that the blurred density is due to the flexible binding of the p150 fragments.

To explore this aspect in detail, density contours of the reconstructions were calculated. The lateral projections of the reconstructions from radius ~130–180 Å (Fig. 1C) showed the strongest density of the p150(1–105) decoration to be 4 Å lower than the neck position (Fig. 1C, Left, red arrowhead), shifted toward the minus end, but 8 Å for p150(25–144) (Fig. 1C, Right, red arrowhead). This position corresponds to the core of CAP-Gly, and it suggests a flexible binding mode for the interaction of CAP-Gly fragments with E-hooks. Comparing the overall shapes of the CAP-Gly core densities raises the possibility that the orientation of the CAP-Gly may be flipped between p150(1–105) and p150(25–144) reconstructions (direction shown in Fig. 1B).

Further, the recognition site of CAP-Gly was mapped onto microtubules (Fig. 2, blue) and compared with the ones of dynein (Fig. 2A, yellow) (15) as well as the yeast EB protein Mal3 (Fig. 2A, pink) (16), a binding partner of p150[glued] during endosomal recruitment. Interestingly, all binding surfaces differ from each other, and there is enough space for all proteins to bind simultaneously to the same microtubule unit. p150[glued] binds to tubulin where the C-terminal E-hook is located (Fig. 2A, marked "C" in red) at the "neck" of the reconstruction. This position is well-separated from the binding sites for dynein/kinesin or EBs. The pelleting assay of the p150(1–144), EB1 CH domain and kinesin head to the microtubule also showed that they all bind to the microtubule surface (Fig. 2B, rightmost lane).

Microtubule Lateral Association Is Caused by Shielding of E-Hooks. The saturated decoration of p150[glued] fragments on the microtubule surface caused microtubules to laterally associate with each other, which made the structural analysis particularly challenging. However, this observation drew our interest and led us to investigate the cause of the bundling triggered by CAP-Gly fragments.

We hypothesized that the lateral association of the microtubules may occur by the fact that CAP-Gly fragments cover the E-hooks. The negatively charged, flexible E-hooks could serve as an electrostatic shield that repels a close approach of neighboring microtubules. Binding of the positively charged p150[glued] segments to the negatively charged tubulin E-hooks may collapse

the mobile barrier that keeps the microtubules apart. To test this hypothesis, we measured the change of turbidity at 400 nm by adding several p150[glued] fragments to taxol-stabilized microtubules (Fig. S3). The scattering increased as highly positively charged protein fragments were added, from 0.29 for microtubules alone up to 1.7 for p150(1–144) (net charge, +12.7). The degree of the increase in scattering correlates with the lateral association of microtubules observed in the corresponding electron micrographs (Fig. S1C). The turbidity was not increased for p150(25–105) (net charge, +1.6), which does not contain any basic patches. Interestingly, the addition of the construct p150 (106–144), which has a net charge of +7 but does not contain CAP-Gly, also caused an increase of turbidity to 0.76 and the bundling of the microtubules. Consistent with this finding, we also observed the increase of turbidity and the lateral association of microtubules when tubulin E-hooks were removed by subtilisin (Fig. S3B). Further, we tested the change of turbidity with a control protein that has a high basic charge but is not derived from p150[glued]. For this purpose, we used histone H2A (15 kDa, net charge, +12.6) as a test case and measured the turbidity changing to 0.81, an increase similar to p150(106–144).

These results altogether suggest that the E-hooks of tubulin form a negative shield on the microtubule surface. The neutralization of the charge by basic proteins repels the shielding and leads to the lateral association of microtubules. The degree of the turbidity increase generally correlates well with the net charge of added protein fragments. This phenomenon does not require any specific protein interaction with microtubules as shown for the case of histone H2A or p150(106–144).

Longitudinal Tubulin Oligomerization Is Induced by CAP-Gly Plus Basic Patch at Low Temperatures. The masking of the acidic tails of tubulin by CAP-Gly plus basic patches causes the lateral association of tubulin. Moreover, previous reports established the ability of p150 fragments to promote the polymerization of microtubules (5, 11). Therefore, we sought to correlate polymerization activity with the charge effects of various CAP-Gly fragments. First, the light scattering of tubulin below the critical concentration for spontaneous polymerization (2 μM) was monitored during a temperature shift from 4 °C to 37 °C (Fig. S4A, Tu). Consistent with previous reports, light scattering was elevated: i.e., tubulin polymerization, in the presence of the dimerized CAP-Gly, with its basic extensions [p150(1–210) dimer] (Fig. S4A) (11). We also observed assisted tubulin polymerization with p150(1–144) fragments (Fig. S4B) although the effect was much less, compared with the dimerized CAP-Gly. The stepwise change of ionic strength in the assay buffer confirmed the sensitivity of the process to the salt concentration,
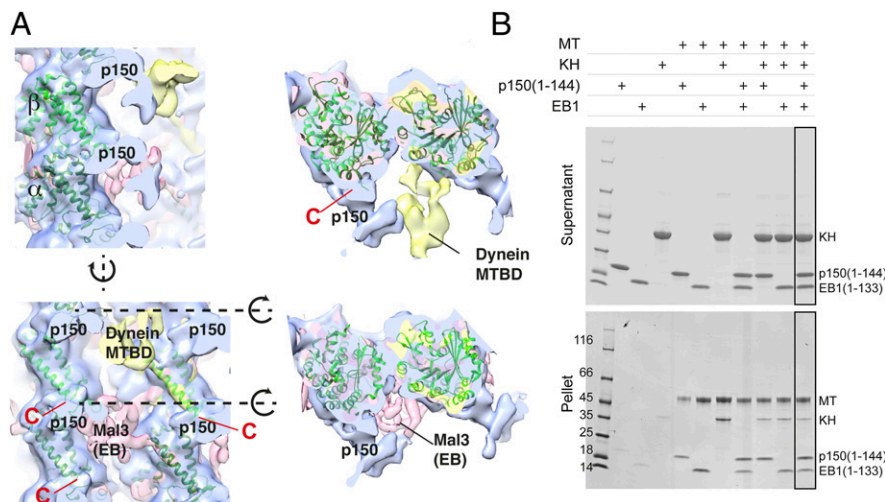

Fig. 2. (A) Comparison of the binding surfaces on tubulins for p150[glued] neck, dynein (MTBD), and Mal3 (EB). The recognition sites of these proteins differ from each other. Red C, the C-terminal end of the tubulin atomic model, which precedes the flexible 15–16 residue E-hooks. Cross-sections of the surface of the side view (dotted line) are shown Right. (B) Pelleting assay of p150(1–144), kinesin head (KH), EB1 CH domain, and GTPgammaS-stabilized microtubules. The 2-μM microtubules and 20-μM proteins were mixed. Added proteins are indicated as "+." The three proteins bind to microtubules simultaneously.

BIOCHEMISTRY

as expected from the electrostatic binding properties of the proteins. The pronounced tubulin copolymerization with p150 (1–144) was observed when the tubulin concentration was high enough to self-promote polymerization (10 μM) (Fig. S4C, red lines).

To connect the tested protein fragments in the context of tubulin polymerization, we used the latter experimental condition to further examine the behavior of tubulins. The light-scattering profiles revealed an elevation of scattering with CAP-Gly, which included the C terminus basic extensions [p150(1–144), p150(25–144)] (Fig. S4C, red and purple) whereas the fragments without the extension [p150(1–105), p150(25–105)] did not have a significant influence. Interestingly, the profiles also showed that the presence of the C-terminal extension alone (residues 106–144) increased the final saturation level, agreeing with the increase of the turbidity seen with already polymerized, taxol-stabilized microtubules (Fig. S4C, pink). We further detected a striking increase in scattering for tubulin-CAP-Gly mixtures at the stage before the initiation of polymerization at 4 °C (Fig. S5A).

To visualize this rise, we analyzed the reaction mixtures using electron microscopy. The protein fragments were confirmed to bind to unpolymerized tubulins (Fig. S5B) and the CAP-Gly fragments containing the basic patches 1–25 or 106–144 induced tubulins (Fig. 3) with a radius of curvature of ~17 nm. These oligomers have the same morphology as the separated, curled protofilaments observed in vitro (17).

This similarity indicates that the interaction of the CAP-Gly fragments to tubulin dimers at 4 °C increases tubulin's longitudinal self-affinity.

The degree of oligomerization increased when more positively charged residues were present (Fig. 3 and Fig. S5C). When tubulin oligomer formation was induced by the p150(1–210) dimer, which has the most prominent effect on tubulin polymerization (Fig. S4A) (11), large agglomerates of tubulin oligomers were visible in EM (Fig. 3). Therefore, it is not feasible to quantify the degree of oligomerization using EM, even though light-scattering experiments showed comparable values with p150(1–144)-induced oligomers (Fig. S5A). In contrast, the longitudinal tubulin association did not occur in the presence of only CAP-Gly core, p150(25–105), or the basic patch without CAP-Gly, p150(106–144). These observations suggest that the activation of the longitudinal assembly of tubulin is facilitated by the bridging of both CAP-Gly and the basic extension, possibly like the way shown in the reconstruction of p150(25–144) (Fig. 1A, Center).

In comparison, CLIP-170 is a member of +TIPs that contains tandem-connected CAP-Gly domains. It has been reported that a CLIP-170 fragment containing only one CAP-Gly (CLIP-170S) does not enhance the polymerization of tubulin whereas a variant containing both CAP-Gly domains (CLIP-170L) increases the polymerization rate (18, 19). We extended this analysis to test whether oligomerization would occur with a CLIP-170-tubulin mixture using EM (Fig. 3). We detected that CLIP-170L induces tubulin oligomerization strongly whereas there was only sporadic oligomer formation with CLIP-170S. These results are consistent with the indication that the observed oligomers have a direct effect on microtubule polymerization.

Tubulin Oligomers Function as Intermediates During Polymerization.
To understand the copolymerization of longitudinally connected tubulin oligomers induced by CAP-Gly fragments, we followed the process by dynamic light scattering (DLS). Although tubulin control showed a population of <10 nm (Fig. 4A, Top, red), the mixture of tubulin with p150(1–144) exhibited the population only at a size distribution of ~100–1,000 nm (Fig. 4A, Top, green) at 4 °C. When tubulin polymerization was initiated by a temperature shift to 37 °C, a growing population of an ~1,000–10,000 nm species was observed after 60–90 s (Fig. 4A, 90 s, blue arrow). At the same time, the population of the 100–1,000 nm decreased. After 150 s, the size distribution became comparable with microtubules alone (Fig. 4A, Top, blue). During this polymerization, the signal of tubulin dimers (1–10 nm) was not detected,
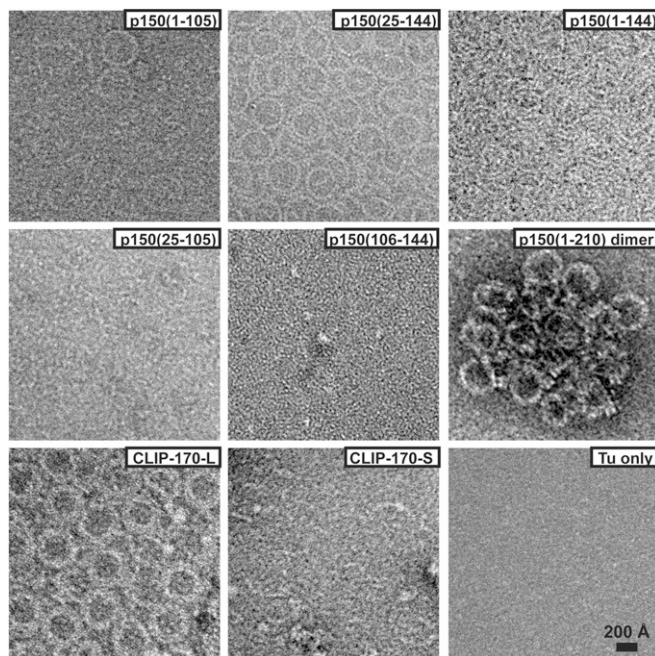

Fig. 3. Negative stain EM observation of tubulin oligomers (10 μM) induced by p150[glued] fragments (10 μM) at 4 °C. Oligomer formation happens with p150(1–144) and p150(25–144), but there is very little or no oligomerization for p150(1–105), p150(25–105), and p150(106–144). p150(1–210) dimer causes tubulin oligomers and further clustering of the oligomers. CLIP-170L with two tandem CAP-Gly shows similar oligomer formation whereas CLIP-170S with one CAP-Gly shows no oligomeric formation.

strongly indicating that the oligomeric formation of tubulin and p150(1–144) directly transitions to tubulin polymers without disassembling into dimer units.

Further, snapshots of the copolymerization at 300 s were taken by cryo-EM and epifluorescence light microscopy. Consistent with the observations by dynamic light scattering, we could readily detect formations of microtubules. The striking population of laterally connected, sheet-like tubulin polymers was observed as well (Fig. 4C, marked as "S" and Fig. S6). The lateral interaction is promoted upon the temperature change to 37 °C. The ends of the closed microtubules often showed a flared morphology, sometimes with fragments of straightened oligomers attached to each other (Fig. S6, guided in magenta). The corresponding experiment using light microscopy revealed a strong colocalization of p150(1–144) at the end of microtubules as well as a weak colocalization on the surface of growing microtubules (Fig. 4B, arrows).

Taken together, the preformed, longitudinally connected tubulin oligomers (before tubulin polymerization) activate their lateral interactions upon temperature change, resulting in sheet-like formations. The oligomers tend to cluster at the end of the closed growing microtubule, likely incorporating into the microtubule structure.

GTP Hydrolysis Is Not Required for Tubulin Oligomer Formation. The tubulin oligomers that are induced by p150[glued] have a linear, curved formation that could act as a building block for tubulin polymerization. Similar observations have been made for CLIP-170 (19). This curved morphology of tubulin oligomers can also be observed in GDP-tubulin rings (20), which is actually the preferred nucleotide state for depolymerized tubulin (21). Furthermore, curved protofilaments are observed at the depolymerizing ends of microtubules (17, 22, 23). Therefore, we asked whether the hydrolysis of GTP occurs coincidently with tubulin oligomerization. For this purpose, we measured the concentration of inorganic phosphate (P_i) released in the presence
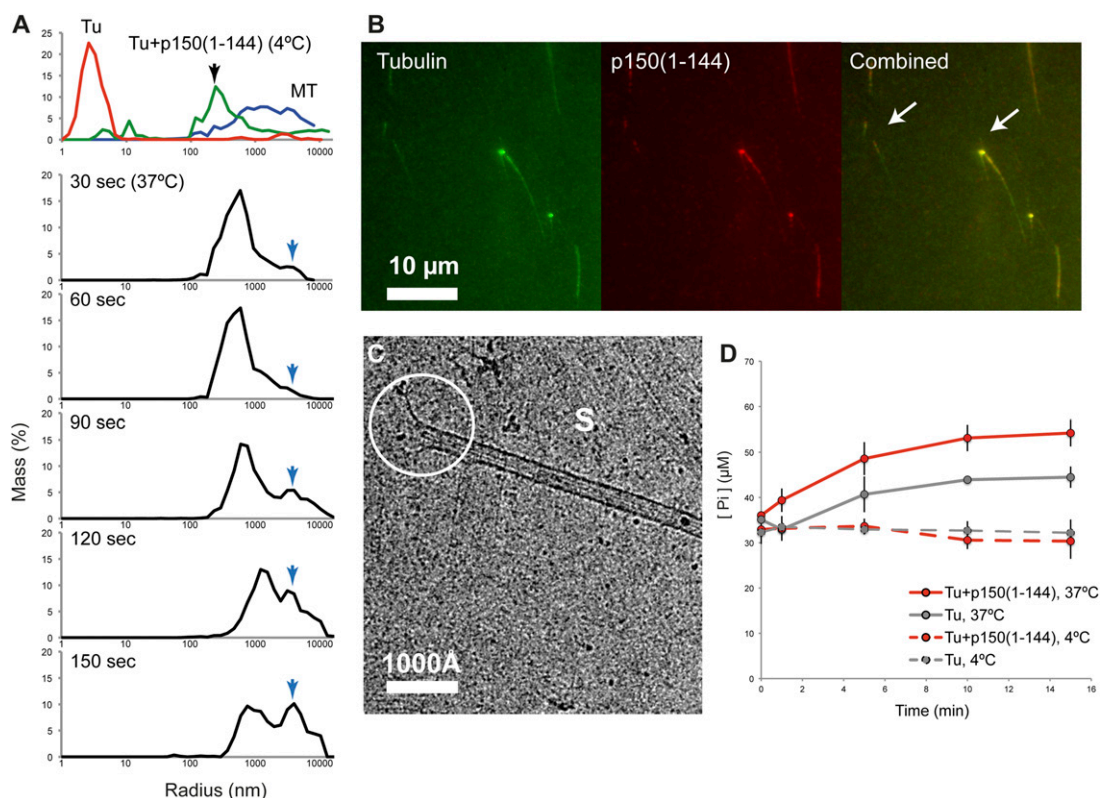
Fig. 4. Intermediates of tubulin polymerization induced by p150(1–144). (*A*) DLS measurements of the mixture of tubulin and p150(1–144). (First row) The control scattering profile of tubulin at 4 °C (red), tubulin with p150(1–144) (green), and microtubule at 37 °C (blue). (second to sixth row) Scattering profiles of the mixture of tubulin-p150(1–144) after incubation at the indicated time points at 37 °C. The blue arrow traces the growth of the microtubules and sheets. (*B*) Copolymerization of p150(1–144) and tubulin into microtubules at 5 min observed by fluorescence microscopy. Two examples of the colocalization of CAP-Gly and tubulin are indicated by arrows. (*C*) Cryo-EM observation of tubulin and p150(1–144) copolymerization 5 min after mixing. S, sheet together with thin fibrils, which are precursors of protofilaments. The active end of a microtubule is indicated with a white circle. (*D*) GTPase activity measurements of tubulin alone (gray, dotted line), tubulin with p150(1–144) (red, dotted line) at 4 °C, and the corresponding curves at 37 °C (solid lines, respectively). Error bars (SD) are calculated from three independent measurements.

of tubulin and p150(1–144) during the formation of curved oligomers. Surprisingly, we did not observe any significant differences in [P$_i$] at any time of incubation (Fig. 4*D*, dotted lines): 32.7 μM (SD 2.4) (Tu only) vs. 32.1 μM (SD 2.0) [Tu plus p150(1–144)]. It indicates that GTP hydrolysis is not coupled to tubulin oligomerization. We also observed that tubulin-p150(1–144) oligomerizes in the presence of GMPCPP (a nonhydrolyzable analog of GTP) and that the oligomers retained their curved shape (Fig. S7). Thus, the observed curved tubulin oligomers are not due to GTP hydrolysis. On the contrary, the GTPase activity of tubulin was activated in the presence of p150(1–144) more than the tubulin control (Fig. 4*D*, red solid line) after the initiation of tubulin polymerization, suggesting that GTP hydrolysis is required only when the incorporation of the tubulin oligomers into the microtubule lattice occurs.

Deletion of Tubulin E-Hook Activates Tubulin Polymerization. Our assays showed that the binding to CAP-Gly is mediated by tubulin E-hooks, in agreement with previous biochemical reports (6–9, 13, 24), and that the coverage of E-hooks by the basic extension activates tubulin polymerization. A similar activation of tubulin polymerization was observed by subtilisin-treated tubulin alone (Fig. S8) (25, 26). The resulting polymerized products showed bundling of the microtubules or open and connected sheets under EM (Fig. S8*B*), supporting the notion that the E-hooks shield tubulins from the lateral connection. Altogether, these findings suggest the importance of E-hooks to control tubulin polymerization kinetics using a negatively charged patch as a shield. The positively charged CAP-Gly fragments may

modulate the tubulin polymerization by neutralizing the electrostatic shield of the E-hooks.

Discussion

Our study describes the interaction of tubulin E-hooks with p150[glued] from a structural point of view and seeks to describe the relationship of the molecular interaction with tubulin polymerization activity. p150[glued] CAP-Gly plus its adjacent basic patches recognizes the negative electrostatic surface of the tubulin acidic E-hooks. Its binding surface differs from other microtubule-binding proteins in the endosomal recruitment pathway. The basic patches affect tubulin self-assembly through interactions with tubulin's E-hooks. From our observations, we surmise a possible role of tubulin E-hooks in the context of CAP-Gly interaction. Namely, CAP-Gly and its basic patches may work as a cross-linker of tubulins. This crosslinking effect could be seen as oligomeric association when tubulin is not spontaneously associable (4 °C). Upon the change of the temperature to 37 °C, lateral association of protofilaments may be immediately activated. These two directional associations may lead to the acceleration of the polymerization. The effect is likely more efficient when CAP-Gly forms dimers (11), presumably due to the increase of the local concentration. We in fact observed a stronger local clustering of tubulin oligomers in the presence of the dimeric protein (Fig. 3). This bridging could serve as a stabilizer for tubulin to adopt a polymerizable conformation. In a cellular environment, this nucleation mechanism of p150[glued] may be facilitated when microtubules undergo the phase change from rapid shrinkage to growth. Efficient growth of the microtubules at the plus ends can be achieved if

Wang et al.   PNAS | **August 5, 2014** | vol. 111 | no. 31 | **11351**

38

tubulin oligomers are used as the basic building block. Similar models were suggested for other +TIP proteins (18), and a comprehensive analysis combining these components is necessary.

Implications of the Nonoverlapping Recognition of p150^{glued}, EB, and Dynein and of the Surfing Activity of p150^{glued}. Our structural analysis directly identified the interaction interface between p150^{glued} CAP-Gly and tubulin E-hooks. Interestingly, this binding surface on tubulin is distinct from those of EBs and dynein (Fig. 2). CAP-Gly recognizes tubulin E-hooks protruding from the outer surface of the microtubule whereas EBs recognize the nucleotide-binding pocket at the groove between the microtubule protofilaments. Dynein binds to an area closer to helices H11/H12 of tubulin, which is also the binding site for the other major microtubule-motor protein kinesin (27) (Fig. 2). Moreover, p150^{glued} has been reported to form a complex with EB1 and CLIP-170, and this +TIPs complex would track the plus ends of microtubules (1). Our finding that the binding sites of these three microtubule-associated proteins do not sterically hinder each other may facilitate a smooth bridging of the plus-end tracking and subsequent vesicle tethering to the dynein motor.

p150^{glued} has been reported to diffuse one-dimensionally along the microtubule surface, termed surfing/skating (12, 28). Considering the main function of p150^{glued} as an anchor for vesicles at the plus end of microtubules (29–32), it is conceivable that the surfing activity is a way of maximizing the chance of encountering EB proteins that directly recognize GTP-tubulin at the end of microtubules. Our study provides a molecular basis for this surfing mechanism. E-hooks, which are incorporated into the microtubule surface, provide a periodic array of negative electrostatic charges. CAP-Gly, with its basic patches, recognizes this surface. CAP-Gly also has a specific interaction with E-hooks, which can ensure efficient binding to microtubules. E-hooks give an opportunity for CAP-Gly to diffuse laterally to the next binding site by providing the continuous charged surface.

The Role of Tyrosinated Tubulin for p150^{glued}. It has been reported that p150^{glued} CAP-Gly domains bind preferably to alpha tubulin that is tyrosinated at the C-terminal E-hook (7). Tubulin tyrosination occurs in its depolymerized form (33) and so freshly incorporated alpha tubulin harbors the modification at microtubule plus ends. This biased distribution of tyrosinated tubulin is likely the key for the microtubule plus-end recognition by CAP-Gly (7, 34). In our assays, p150^{glued} CAP-Gly core has a higher affinity to the tyrosinated alpha E-hook compared with the detyrosinated E-hook and beta E-hook (Table 1), but the basic extensions increase the binding affinity of CAP-Gly fragments to other E-hooks. CAP-Gly prefers tyrosinated tubulin to bias itself toward the plus ends of microtubules. The situation in a cell, however, might be more complex. E-hooks are variable in isoforms in addition to the diverse decoration by posttranslational modifications. The weak interaction through basic extensions might play a role for reinforcing the affinity of p150^{glued} to microtubules. Further studies are needed to understand the functions of different tubulin isoforms in the context of posttranslational modifications.

Materials and Methods

Recombinant proteins of p150^{glued} fragments, CLIP-170, EB1, and KH are expressed in *E. coli*. Protein purifications and subsequent biochemical analyses were carried out as described in *SI Material and Methods*. Details of electron microscopic analyses are also found in *SI Material and Methods*, as well as in Fig. S9.

1. Akhmanova A, Steinmetz MO (2008) Tracking the ends: A dynamic protein network controls the fate of microtubule tips. *Nat Rev Mol Cell Biol* 9(4):309–322.
2. Cronin MA, Schwarz TL (2012) The CAP-Gly of p150: One domain, two diseases, and a function at the end. *Neuron* 74(2):211–213.
3. Watson P, Stephens DJ (2006) Microtubule plus-end loading of p150(Glued) is mediated by EB1 and CLIP-170 but is not required for intracellular membrane traffic in mammalian cells. *J Cell Sci* 119(Pt 13):2758–2767.
4. Lansbergen G, et al. (2004) Conformational changes in CLIP-170 regulate its binding to microtubules and dynactin localization. *J Cell Biol* 166(7):1003–1014.
5. Ligon LA, Shelly SS, Tokito M, Holzbaur ELF (2003) The microtubule plus-end proteins EB1 and dynactin have differential effects on microtubule polymerization. *Mol Biol Cell* 14(4):1405–1417.
6. Hayashi I, Wilde A, Mal TK, Ikura M (2005) Structural basis for the activation of microtubule assembly by the EB1 and p150Glued complex. *Mol Cell* 19(4):449–460.
7. Peris L, et al. (2006) Tubulin tyrosination is a major factor affecting the recruitment of CAP-Gly proteins at microtubule plus ends. *J Cell Biol* 174(6):839–849.
8. Honnappa S, et al. (2006) Key interaction modes of dynamic +TIP networks. *Mol Cell* 23(5):663–671.
9. Weisbrich A, et al. (2007) Structure-function relationship of CAP-Gly domains. *Nat Struct Mol Biol* 14(10):959–967.
10. Bieling P, et al. (2008) CLIP-170 tracks growing microtubule ends by dynamically recognizing composite EB1/tubulin-binding sites. *J Cell Biol* 183(7):1223–1233.
11. Lazarus JE, Moughamian AJ, Tokito MK, Holzbaur ELF (2013) Dynactin subunit p150 (Glued) is a neuron-specific anti-catastrophe factor. *PLoS Biol* 11(7):e1001611.
12. Culver-Hanlon TL, Lex SA, Stephens AD, Quintyne NJ, King SJ (2006) A microtubule-binding domain in dynactin increases dynein processivity by skating along microtubules. *Nat Cell Biol* 8(3):264–270.
13. Kobayashi T, Shiroguchi K, Edamatsu M, Toyoshima YY (2006) Microtubule-binding properties of dynactin p150 expedient for dynein motility. *Biochem Biophys Res Commun* 340(1):23–28.
14. Sui H, Downing KH (2010) Structural basis of interprotofilament interaction and lateral deformation of microtubules. *Structure* 18:1022–1031.
15. Redwine WB, et al. (2012) Structural basis for microtubule binding and release by dynein. *Science* 337(6101):1532–1536.
16. Maurer SP, Fourniol FJ, Bohner G, Moores CA, Surrey T (2012) EBs recognize a nucleotide-dependent structural cap at growing microtubule ends. *Cell* 149(2):371–382.
17. Mandelkow EM, Mandelkow E, Milligan RA (1991) Microtubule dynamics and microtubule caps: A time-resolved cryo-electron microscopy study. *J Cell Biol* 114(5):977–991.
18. Slep KC, Vale RD (2007) Structural basis of microtubule plus end tracking by XMAP215, CLIP-170, and EB1. *Mol Cell* 27(6):976–991.
19. Arnal I, Heichette C, Diamantopoulos GS, Chrétien D (2004) CLIP-170/tubulin-curved oligomers coassemble at microtubule ends and promote rescues. *Curr Biol* 14(23):2086–2095.
20. Nicholson WV, Lee M, Downing KH, Nogales E (1999) Cryo-electron microscopy of GDP-tubulin rings. *Cell Biochem Biophys* 31(2):175–183.
21. Tran PT, Joshi P, Salmon ED (1997) How tubulin subunits are lost from the shortening ends of microtubules. *J Struct Biol* 118(2):107–118.
22. Moores CA, et al. (2002) A mechanism for microtubule depolymerization by KinI kinesins. *Mol Cell* 9(4):903–909.
23. Asenjo AB, et al. (2013) Structural model for tubulin recognition and deformation by kinesin-13 microtubule depolymerases. *Cell Reports* 3(3):759–768.
24. Bu W, Su L-K (2003) Characterization of functional domains of human EB1 family proteins. *J Biol Chem* 278(50):49721–49731.
25. Sackett DL, Bhattacharyya B, Wolff J (1985) Tubulin subunit carboxyl termini determine polymerization efficiency. *J Biol Chem* 260(1):43–45.
26. Peyrot V, Briand C, Andreu JM (1990) C-terminal cleavage of tubulin by subtilisin enhances ring formation. *Arch Biochem Biophys* 279(2):328–337.
27. Mizuno N, et al. (2004) Dynein and kinesin share an overlapping microtubule-binding site. *EMBO J* 23(13):2459–2467.
28. King SJ, Schroer TA (2000) Dynactin increases the processivity of the cytoplasmic dynein motor. *Nat Cell Biol* 2(1):20–24.
29. Kim H, et al. (2007) Microtubule binding by dynactin is required for microtubule organization but not cargo transport. *J Cell Biol* 176(5):641–651.
30. Chevalier-Larsen ES, Wallace KE, Pennise CR, Holzbaur ELF (2008) Lysosomal proliferation and distal degeneration in motor neurons expressing the G59S mutation in the p150Glued subunit of dynactin. *Hum Mol Genet* 17(13):1946–1955.
31. Moughamian AJ, Holzbaur ELF (2012) Dynactin is required for transport initiation from the distal axon. *Neuron* 74(2):331–343.
32. Kardon JR, Reck-Peterson SL, Vale RD (2009) Regulation of the processivity and intracellular localization of Saccharomyces cerevisiae dynein by dynactin. *Proc Natl Acad Sci USA* 106(14):5669–5674.
33. Janke C, Bulinski JC (2011) Post-translational regulation of the microtubule cytoskeleton: Mechanisms and functions. *Nat Rev Mol Cell Biol* 12(12):773–786.
34. Mishima M, et al. (2007) Structural basis for tubulin recognition by cytoplasmic linker protein 170 and its autoinhibition. *Proc Natl Acad Sci USA* 104(25):10346–10351.

39

Supporting Information

Wang et al. 10.1073/pnas.1403135111

SI Discussion

To understand the binding of cytoskeleton-associated protein glycine-rich (CAP-Gly) and tubulins in our experimental system, we chemically cross-linked p150^{glued} CAP-Gly fragments to microtubules that were treated with subtilisin. Subtilisin digests the E-hooks of beta and alpha tubulin in a time-dependent manner (Fig. S2A). After 30 min of digestion, in which subtilisin removes only the E-hook of beta tubulin, we observed a decrease of cross-linked products. After 4–6 h of incubation, when also alpha tubulin E-hooks are digested, the cross-linking of CAP-Gly to tubulin is no longer detectable, indicating that the p150^{glued} CAP-Gly-microtubule interaction was maintained by tubulin E-hooks. The binding affinities of the peptides (alpha, tyrosinated, and detyrosinated tubulin E-hooks and beta tubulin E-hooks) and p150^{glued} fragments were further determined by a binding assay using fluorescence correlation spectroscopy (Table 1). This binding was also confirmed by cross-linking CAP-Gly to chemically synthesized E-hook peptides (Fig. S2D). Next, we determined the stoichiometry of CAP-Gly-tubulin complexes using a microtubule-pelleting assay with p150^{glued} CAP-Gly and polymerized, taxol-stabilized microtubules. The binding of CAP-Gly itself to microtubules appears to be fairly weak (Fig. S1A, marked with an *), but CAP-Gly containing the upstream/downstream basic patches increased the binding affinity. The quantitative pelleting assay of p150(1–144) and microtubules shows a K_d of 2.2 μM, with a stoichiometry of two proteins per tubulin dimer (Fig. S2A). Altogether, our experiments indicate that p150^{glued} CAP-Gly recognizes both alpha and beta tubulins at saturation levels. The stoichiometry of 2 was also used to define the asymmetric unit for the 3D reconstruction.

SI Materials and Methods

Protein Preparation and Purification. For all cloned constructs, DNA was obtained from the Mammalian Gene Collection (MGC, Source BioScience LifeSciences) or the Berkeley Drosophila Genome Project (BDGP) Gold cDNA Collection (*Drosophila* Genomic Resource Center) and further modified by PCR. Human p150^{glued} (25–105, 1–105, 25–144, 1–144), CLIP-170 (CLIP-170L, 1–350; CLIP-170S, 57–210), and end-binding protein 1 (EB1) (1-133) were expressed as His-tagged recombinant proteins using the *Escherichia coli* BL21 (DE3) Gold strain. For p150(106–144) and *Drosophila* kinesin head (KH, 1–342), the fragment was expressed as a SUMO fusion protein, and SUMO tag was cleaved using Senp2 protease. Proteins were purified using Ni^{2+}-affinity chromatography (HisTrap; GE Healthcare) followed by MonoS ionic exchange chromatography (GE Healthcare) and gel-filtration chromatography (Superdex 75; GE Healthcare).

Tubulin was purified from porcine brains or purchased from Cytoskeleton, Inc. Histone H2A is a generous gift from Jürg Müller (Max Planck Institute of Biochemistry, Martinsried, Germany). Proteins were stored in 20 mM Pipes-NaOH (pH 6.8), 1 mM MgCl$_2$, 1 mM EGTA, 100 mM NaCl, and 1 mM DTT or BRB80 [80 mM Pipes-Na (pH 6.8), 1 mM MgCl$_2$, 1 mM EGTA] supplemented with 1 mM DTT. All experiments were performed in BRB80 buffer or with BRB80 supplemented with an additional 35 mM or 70 mM KCl. Ionic strengths of the buffers were measured using the conductivity detector of an Aekta Purifier system (GE Healthcare) calibrated with NaCl solutions of known concentrations. BRB80 was corresponded to ~80 mM, BRB80 plus 35 mM KCl to 115 mM, and BRB80 plus 70 mM KCl to 150 mM.

Kinetics Measurement of Tubulin Polymerization. For measurement of microtubule polymerization, a Bio Photometer plus (Eppendorf) spectrophotometer was used. The copolymerization assays below the critical concentration of tubulin were performed with 2 μM tubulin with 1 μM of the protein fragments, 1 mM GTP, and 8% (vol/vol) DMSO in BRB80, with ionic strengths corresponding to 80/115/150 mM. The assays were performed in a room with controlled temperature at 37 °C. There was a systematic error of the perturbation of scattering for the first 3 min, presumably because of the experimental setup; therefore, the initial time was not considered for the measurement. The measurement was performed up to 30 min and repeated three times. For the measurement of the tubulin polymerization above the critical concentration, 10 μM tubulin, 5 μM protein fragments, 1 mM GTP, and 8% DMSO were mixed in BRB80, and the measurements were carried out as described above.

Dynamic Light Scattering. The measurement was performed using a Wyatt NanoStar (Wyatt Technology). For each measurement, a 10-μl sample was prepared containing 1 mM GTP and 10 μM tubulin as a control, and 5 μM p150(1–144) was added for the test experiments. The measurements were repeated every 3 s, and the results were averaged over 10 measurements. To follow the transition of different species during tubulin polymerization, data corresponding to a time of 30 s were averaged. The temperature was set to either 4 °C or 37 °C as indicated. Concentrations of samples were adjusted to avoid detector saturation.

Fluorescence Microscopy. For labeling, p150^{glued} CAP-Gly was modified (C81S), and an additional cysteine was inserted at residue 105 because labeling of the wild-type constructs caused a loss of the tubulin nucleator activity: i.e., no oligomeric formation was observed. Modified protein was purified as described above. Labeling was performed using atto565-maleimide, and the activity of the labeled protein was confirmed by kinetics experiments as well as the observation of the curved tubulin oligomers. Labeled tubulin was purchased from Cytoskeleton, Inc. An upright epifluorescence microscope (Zeiss) was used for image acquisition equipped with a filter set (FITC and TRITC) and an EM CCD camera (X-ion Andor). MetaMorph was used for microscope control and image acquisition.

Phosphate Release Detection. The release of phosphate was measured by using PhosFree Phosphate Assay BIOCHEM kit (BK050) from Cytoskeleton Inc. Then, 20 μM tubulin was mixed with 20 μM p150(1–144) in a total volume of 50 μl. The reaction was quenched at 0 min, 1 min, 5 min, 10 min, and 15 min after the samples were mixed at 4 °C and 37 °C. The quenched mixture was centrifuged at 20,000 × g, and the supernatant was used for detection of phosphate using malachite green staining and absorbance measurements at λ = 650 nm according to the manufacturer's manual. To minimize errors, we used the same batches of GTP and tubulin for all measurements. The measurements were repeated three times.

Microtubule-Binding Assay. Polymerized and taxol-stabilized microtubules (2 μM) were mixed with various concentrations of p150^{glued} proteins. After incubating for 20 min at room temperature, the 40-μL mixture was ultracentrifuged for 20 min at 280,000 × g at 25 °C. The supernatant was recovered, and the pellet was carefully washed with BRB80 once. p150^{glued}-CAP-Gly bound to microtubules was quantified using SDS/PAGE and ImageJ. For assessment of the simultaneous microtubule

bindings of p150(1–144), EB1, and KH, microtubules were polymerized using GTPgammaS instead of GTP for ensuring EB1 binding. Then, microtubules (2 μM) were mixed with the proteins (20 μM), and the pelleting assay was performed as described above.

EDC Cross-Linking. For the cross-linking assay, 5 μM polymerized/unpolymerized tubulins were mixed with proteins, and 1-Ethyl-3-[3-dimethylaminopropyl]carbodiimide hydrochloride (EDC) (Fisher) was added to a final concentration of 5 mM. Samples were incubated either on ice or at room temperature for 1 h. The EDC reaction was stopped by adding SDS sample buffer.

Subtilisin Treatment on Microtubule and Tubulin. For the treatment of microtubules, 15 μM taxol-stabilized microtubules were mixed with 5.6 μM subtilisin (Sigma Aldrich) and incubated for 1 min, 10 min, 30 min, 60 min, 120 min, 240 min, 360 min, or 480 min at room temperature or 10 min, 30 min, 60 min, or 90 min at 37 °C. It is known that the beta E-hooks are cleaved first, followed by the alpha E-hooks (1). The cleavage of E-hooks was confirmed by band shifts in SDS/PAGE (4–20% gradient) and Western blotting against anti-alpha tubulin, clone YL1/2 (Merck Millipore) that recognizes alpha tubulin E-hooks (Fig. S2C). The enzymatic reaction was stopped by adding 2.5 mM PMSF. Subtilisin-treated microtubules were further purified by ultracentrifugation, and the pellet was resuspended gently to achieve the desired concentration for further experiments. For the treatment of tubulins, 20 μM tubulin was mixed with 7.4 μM subtilisin, and the mixture was incubated for 30 min in 30 °C followed by an addition of 2.5 mM PMSF.

Peptide Binding Assay. Peptides were synthesized by the Max Planck Institute of Biochemistry Core Facility. We prepared peptides corresponding to the tyrosinated E-hook of alpha tubulin (alpha CY, biotin-GSSVEGEGEEEGEEY), the detyrosinated (glutamated) tail of alpha tubulin (alpha CE, biotin-GSSVEGEGEEEGEE), and the E-hook of beta tubulin (beta C, biotin-GSGEFEEEGEEDEA). Then, peptides (25 μM) and p150[glued] proteins (100 μM) were mixed, and chemical cross-linking assays were performed using EDC. The results were evaluated on SDS/PAGE.

Fluorescence Correlation Spectroscopy. Fluorescence correlation spectroscopy was carried out using a system previously described (2). Peptides labeled with atto488 at the N termini were synthesized by the Max Planck Institute of Biochemistry Core Facility. Peptides (1 nM) and p150[glued] fragments (0.01–100 μM) were mixed in BRB80 and allowed to reach steady-state binding for 20 min before the measurement. Data were acquired for 10 min using a laser power of 15 μW. All analysis was carried out using custom-written programs in MATLAB. To calculate diffusion coefficients of the protein–peptide complexes, the focus size was fixed using a 400 μm^2/s diffusion coefficient of atto488 free carboxylic acid (taken from http://www.picoquant.com/appnotes.htm).

Sample Preparations for Electron Microscopy. For the observation of tubulin oligomerization, tubulin (10 μM) was mixed with proteins (10 μM) and incubated for 5 min on ice. The sample was applied to the grid without dilution because dilution causes the dissociation of oligomers. For the observation of polymerization intermediates, tubulin (10 μM) and proteins (10 μM) were mixed and incubated at 37 °C for 5 min. The samples were immediately vitrified using a Vitrobot (FEI). For the observation of the microtubule–protein mixture, taxol-stabilized microtubule (2 μM) was mixed with proteins (20 μM), and the sample was vitrified immediately.

Electron Microscopy Operation. For negative-stain EM, carbon-coated and freshly glow-discharged grids were prepared. Then,

5 μL of sample were applied to the grids. Excess solution was removed by filter paper followed by rinsing with H_2O, and staining with two drops of 1% uranyl acetate. Samples were observed with a CM200-FEG (FEI) operating at 160 kV with the nominal magnification of 38,000×, corresponding to 2.78 Å per pixel.

For cryo-EM, holey carbon grids purchased from Quantifoil were used. After glow discharge, the samples were applied to the grids, and vitrification was immediately carried out using a vitrobot (FEI). For observation, a Tecnai F20 (FEI) was used with an acceleration voltage of 200 kV and with a nominal magnification of 50,000× corresponding to a pixel size of 2.21 Å per pixel. The images were taken with a CCD camera (FEI, Eagle) with a defocus range of 1–3 μm.

Image Processing. Image processing was carried out using BSOFT (3), SPIDER (4), and IHRSR (5) for single-particle microtubule reconstruction.

For cryo-EM image processing, defocus values of the collected images were measured using ctffind3 (6), and the contrast transfer function (CTF) was corrected by phase-flipping. Microtubules were computationally boxed out to squares with a size of 200 × 200 pixels (corresponding to 442 × 442 Å) by tracing the central axis of the tubes. Opened or bundled microtubules were not selected. The selected microtubules were tested by applying multireference alignment using the reprojections of available microtubule maps (EMDB ID: emd_5193/5194/5195/5196) with various protofilament numbers, namely microtubules with 13 protofilaments, 14 protofilaments, 15 protofilaments, and 16 protofilaments as references, and the numbers of the protofilaments of individual boxes were determined using the highest cross-correlation value of the alignments. The consistency of the protofilament number within a filament and the characteristic Moiré patterns based on the protofilament numbers were taken into consideration as well.

p150[glued] binds to every tubulin monomer, confirmed by chemical cross-linking and pelleting assays as well. This observation facilitated the use of the most commonly found 14-protofilament microtubules as test samples, and further reconstructions were performed using 14-protofilament microtubules.

Reconstructions were done using the iterative helical real space reconstruction (IHRSR) approach by applying the helical parameters of microtubules. The helical parameters were defined to be 231° azimuthal rotation and 2.98 Å rise per asymmetric unit as a tubulin monomer. We used 56,000 asymmetric particles, for the final reconstruction of p150(1–105), 52,700 asymmetric particles for p150(25–144), and 12,000 asymmetric particles for p150(25–105) reconstructions. A cylindrical density of the same size as the 14-protofilament microtubule was created as an initial volume, and the iterative reconstruction was performed 50 times. During each iteration, a reference was created by calculating reprojections of the reconstruction from the previous cycle by rotating every 4° toward the azimuthal direction, which produced 90 reference images. The new reconstruction was created by back projection, and then the helical parameters were imposed. As a refinement, the number of the reference images was increased to 3,690 images including out-of-plane tilt alignment, and the refinement process was iterated for a further 20 times. The amplitudes of high frequency components in the CAP-Gly1-105-microtubule reconstruction were adjusted by fitting helically symmetrized atomic models of tubulin (PDB ID code 1TUB) into the EM envelope as reference. By adjusting the amplitudes, the density of the CAP-Gly1-105 weakened; therefore, the maps used for the detection of the protein decoration were not amplitude-corrected. The resolution of the map was measured by calculating the Fourier shell correlation (FSC) of two reconstructions that were individually calculated from the initial cylindrical volumes. Before the FSC calculations, a mask was

created by using the volumes of the reconstructions, generously including surrounding noise densities, followed by five times of a dilation and smoothing procedure provided by bsoft, and the mask was applied to the reconstruction to be compared. The resolution was estimated to be 9.7 Å according to FSC (0.5) criteria (Fig. S9*B*) for the p150(1–105)–microtubule complex and 10.2 Å for the p150(25–144)–microtubule complex.

Atomic models of tubulin (PDB ID code 1TUB) were used for molecular fitting into the microtubule-CAP-Gly1-105 reconstruction. For the mapping of the dynein and Mal3 (EB1) binding regions on the microtubule, the EM maps of dynein-microtubule (EMDB ID 5439) and Mal3-microtubule (EMDB ID 2005) were used. In both cases, we manually fit the maps using UCSF Chimera (University of California, San Francisco).

1. Redeker V, Melki R, Promé D, Le Caer JP, Rossier J (1992) Structure of tubulin C-terminal domain obtained by subtilisin treatment: The major alpha and beta tubulin isotypes from pig brain are glutamylated. *FEBS Lett* 313(2):185–192.
2. Müller BK, Zaychikov E, Bräuchle C, Lamb DC (2005) Pulsed interleaved excitation. *Biophys J* 89(5):3508–3522.
3. Heymann JB, Belnap DM (2007) Bsoft: image processing and molecular modeling for electron microscopy. *J Struct Biol* 157(1):3–18.
4. Frank J, et al. (1996) SPIDER and WEB: Processing and visualization of images in 3D electron microscopy and related fields. *J Struct Biol* 116(1):190–199.
5. Egelman EH (2007) The iterative helical real space reconstruction method: Surmounting the problems posed by real polymers. *J Struct Biol* 157(1):83–94.
6. Mindell JA, Grigorieff N (2003) Accurate determination of local defocus and specimen tilt in electron microscopy. *J Struct Biol* 142(3):334–347.

Fig. S1. (*A*) Scheme of the protein fragments used for this study. (*B*) Microtubule pelleting assay showing the affinity of CAP-Gly fragments to microtubules: p150(1–144) > p150(25–144) > p150(1–105) > p150(25–105). Microtubules (2 μM) and individual proteins (2 μM or 20 μM) were used. In the presence of 20-μM protein fragments, the bound proteins to 2 μM microtubules (dimer as a unit) are calculated to be 2.7 μM [p150(25–105), 5.2 μM (p150(1–105), 5.3 μM (p150(25–144)] and 5.2 μM [p150(1–144)]. (*C*) Cryo-EM observations of taxol-stabilized microtubules mixed with p150^{glued}-CAP-Gly fragments. CAP-Gly with additional basic patches cause lateral association of microtubules.

Fig. S2. (*A*, *Left*) An example of the quantitative copelleting assay of microtubules (2 μM) and various concentrations of p150(1–144) (from left: 1 μM, 5 μM, 10 μM, 15 μM). (*Right*) Quantification of the copelleting assay showing the saturation of bound protein at 2.5 mol/tubulin dimer, indicating that p150(1–144) recognizes both alpha and beta tubulin. $K_d = 2.23$ μM. Note that this K_d is a combination of the CAP-Gly binding to alpha and beta tubulin E-hooks. (*B*) EDC cross-linking of subtilisin-treated microtubules and p150glued-CAP-Gly. Cross-linked products are marked with arrowheads. E-hook of beta tubulin is removed in ~30 min, and the alpha tubulin E-hook is truncated at ~4–6 h. Concomitantly, the binding of tubulin to p150[glued]-CAP-Gly is lost. (*C*) Western blotting of subtilisin-treated microtubules in 25 °C (*Left*) and 37 °C (*Right*), showing the completion of the cleavage of E-hooks at 6 h (25 °C) and 1 h (37 °C), respectively. For staining, anti-alpha tyrosinated tubulin was used, which detects tyrosine at the end of alpha tubulin E-hooks. (*D*) p150[glued]-CAP-Gly is cross-linked with peptides of alpha [both tyrosinated (marked as αY) and detyrosinated (αE)] and beta E-hooks (βC).

Fig. S3. (*A*) Turbidity change of 10-μM taxol-stabilized microtubules was measured upon additions of the 10-μM protein fragments. The ionic strength of reacting buffer was 80 mM (black bar), 115 mM (dark gray bar), and 150 mM (light gray bar). (*B*) Negative stain EM observations of subtilisin-treated microtubules (2.5 h in 37 °C) showing lateral associations. Examples of bundles and single microtubules are labeled by B and S, respectively.

Fig. S4. Turbidity change as a function of time. The turbidity caused by the polymerization of microtubules was measured at an absorbance at 400 nm. The experiments were repeated more than three times for each condition. Only the upper half of error bars are shown for representation purposes. (*A* and *B*) The 2-μM tubulin does not polymerize on its own (gray lines), but, in the presence of 1 μM p150(1–210) dimer, polymerization is promoted as well as in the presence of p150(1–144) to a lesser extent. These phenomena are ionic strength- dependent, which is indicated in the graph legend. (*C*) Tubulin polymerization profiles of 10-μM tubulin and 5-μM p150 fragments. The effect is greater with higher concentrations. Addition of p150(1–105) or p150(25–105) does not increase the turbidity of the microtubule growth, but, with the C-terminal appended basic patches, an increase of the signal occurs.

Fig. S5. (*A*) Turbidity change when 10-μM tubulin and 10-μM protein fragments were mixed together. Black bar, 80-mM ionic strength; gray bar, 115-mM ionic strength. The turbidity change also shows ionic strength dependency, consistent with copolymerization. (*B*) EDC chemical cross-link shows the CAP-Gly fragments cross-linked to unpolymerized tubulin (arrow) at 4 °C. The cross-link reactions happen for both unpolymerized tubulins and polymerized micro-tubules. (*C*) Density of tubulin oligomers shown in Fig. 3. More than 10 images (1.1 × 1.1 μm^2) of the tubulin oligomers induced by the proteins were collected and counted per 100 × 100 nm^2.

Fig. S6. Cryo-EM observation of CAP-Gly1–144 and tubulin copolymerization at t = 300 s. Compared with the normal tubulin polymerization (*Upper Right*), formation of significantly more sheets and curved oligomers is visible in the background. (*Lower*) Zoomed-in views of the sheet-like structures. Pink dotted lines in the upper row are guidelines for the observed densities as shown unperturbed in the lower row. The arrangements of the curved oligomers to sheet-like polymers are shown in the presence of CAP-Gly1–144 (*Left*) in comparison with tubulin alone (*Right*).
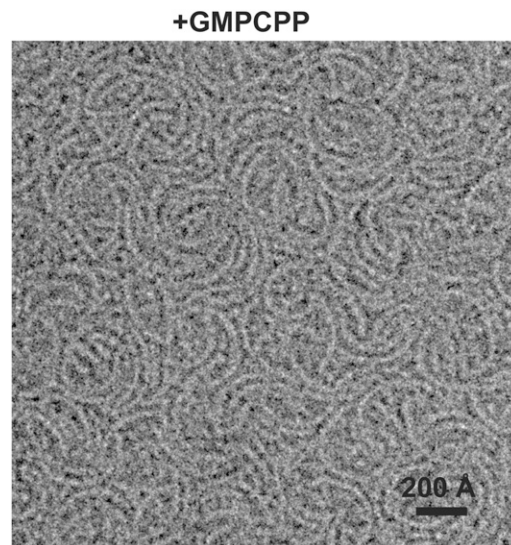
+GMPCPP

Fig. S7. Tubulin oligomers in the presence of p150(1–144) and GMPCPP, showing curved tubulin oligomers as well.

Fig. S8. Polymerization profile of subtilisin-treated tubulins (sTu). (*A*) sTu polymerization profile. Increase of the scattering is observed. (*B*) The polymerized products show mostly bundles or open sheets laterally associated with each other.
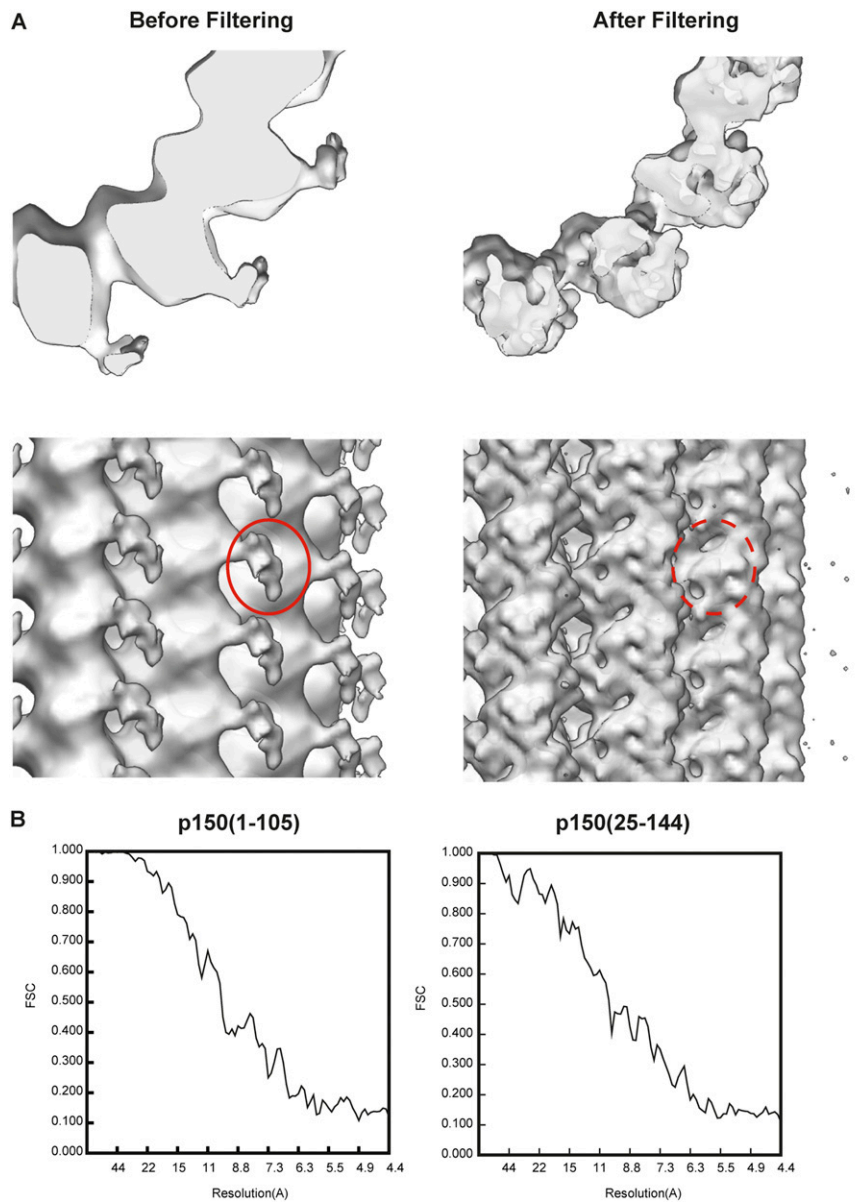
Fig. S9. (*A*) A 3D reconstructions of the microtubule-p150(1–105) complex. Due to the flexible binding of p150(1–105) to the microtubule, amplitude-corrected reconstructions (After Filtering) no longer show the densities corresponding to the CAP-Gly (red dotted circle on the side view) whereas the amplitude-uncorrected reconstructions clearly show the CAP-Gly decorations (red solid circle). (*B*) Fourier shell correlations (FSCs) of the reconstructions of p150(1–105)-microtubules (*Left*) and p150(25–144)-microtubules (*Right*).

2.1.2 Extended discussion

2.1.2.1 The preference of p150^{glued} CAP-Gly domain on tyrosinated α-tubulin

As mentioned in the introduction, microtubule plays a large variety cellular roles mediated by different microtubule-associated proteins (MAPs) and posttranslational modifications (PTMs) on α- and β-tubulin. In most eukaryotic cells, the C-terminus of α-tubulin is subject to the tyrosination-detyrosination cycle. It has been shown that CAP-Gly domains of CLIP170 and p150^{glued} bind more efficiently to tyrosinated microtubules than to detyrosination polymers (Bieling et al., 2008, Peris et al., 2006). In our study, using fluorescence correlation spectroscopy, we also observed that CAP-Gly domain of p150^{glued} shows higher affinity to tyrosinated α-tubulin and the two basic extensions of CAP-Gly domain enhance the binding. However, the cellular function of the binding preference of p150^{glued} to tyrosinated tubulin was elusive by then. A recent work *in vitro* showed the motility of mammalian dynactin-dynein complex was about four times higher on tyrosinated microtubules than on detyrosinated microtubules. The reason for this is likely that CAP-Gly domain of p150^{glued} interacts preferably with tyrosinated α-tubulin for initiation of processive motility. However, this interaction is not required for the subsequent continuation of processive motility (McKenney et al., 2016). Another study in *C. elegans* suggested that transport initiation function of p150^{glued} CAP-Gly domain on tyrosinated microtubule is required for generating cytoplasmic pulling forces for centrosome centration (Barbosa et al., 2017). In the future, it will be interesting to explore the function link between p150^{glued} on tyrosinated microtubule and other cellular activities.

2.1.2.2 Positively charged residues in p150^{glued} are essential for microtubule stabilization

Microtubule polymerization is initiated by self-assemble of tubulin dimer into linear protofilaments. Tubulins of adjacent protofilaments are laterally linked through

homologous monomer contacts α-α, β-β to form sheet of protofilments, which closes into a tube as microtubule. Our studies about p150[glued] provided evidences to suggest that p150[glued] promotes the process of microtubule polymerization, consistent with previous studies showing p150[glued] increases microtubule polymerization rates and inhibits catastrophe (Lazarus et al., 2013). p150[glued] induces the formation of the curved tubulin oligomer below the critical concentration for spontaneous polymerization, and tubulin oligomer can be used as direct building bock for efficient microtubule polymerization. Actually, these tubulin protofilament rings have been observed for both microtubule-stabilizing and -destabilizing factors. Kinesin-13 proteins are homodimeric catastrophe factors are thought to function by bending individual protofilaments around the motor to generate protofiliament rings (Moores and Milligan, 2006). CLIP170 promotes microtubule rescue and the N-terminal CAP-Gly domains induce the formation of tubule rings, similar as CAP-Gly domain of p150[glued] in our study. Indeed, it was found microtubules could increase their overall length by addition of tubule oligomers (Kerssemakers et al., 2006). Moreover, p150[glued] promotes laterally association of protofilaments by covering the acid tails of the tubulin, since the acid tails of tubulin act as shields to avoid the laterally interaction. Interestingly, the laterally tubulin interaction does not need any specific protein associate with microtubule, while the charge of the protein is the key factor. Altogether, p150[glued] is one of the microtubule-stabilizing factors by promoting the tubulin association two dimensionally.

Besides p150[glued], there are some other factors that stabilize microtubules via different mechanisms. For instance, APC decorates the plus ends of microtubules to prevent the catastrophe happen (Kita et al., 2006). CLASPs have been shown to be required for the stability of microtubules by promoting the pause state based on the observation that microtubules showed constantly growing or shrinking in the CLASPs depleted cells (Sousa et al., 2007). As mentioned in the introduction, XMAP215 enhances microtubule growth by catalyzing addition of multiple individual tubulin subunits to the growing microtubule ends (Brouhard et al., 2008)

2.2 Chapter II

2.2.1 Membrane Association and Remodeling by Intraflagellar Transport Protein IFT172

Membrane Association and Remodeling by Intraflagellar Transport Protein IFT172

Qianmin Wang[1], Michael Taschner[1*], Kristina Ganzinger[2], Petra Schwille[2], Esben Lorentzen[1], Naoko Mizuno[1]**

Affiliations:

[1] Max Planck Institute of Biochemistry, Department of Structural Cell Biology, Am Klopferspitz 18, D-82152 Martinsried, Germany

[2] Max Planck Institute of Biochemistry, Department of Cellular and molecular biophysics, Am Klopferspitz 18, D-82152 Martinsried, Germany

*Current address: University of Lausanne, Department of Fundamental Microbiology, Switzerland

**Current address: Department of Molecular Biology and Genetics, Aarhus University, Gustav Wieds Vej 10c, DK-8000 Aarhus C, Denmark

ABSTRACT

The cilium is an important organelle for motility and cellular signaling and is found on most mammalian cells and on some unicellular eukaryotes. Cilia formation requires the process of Intraflagellar Transport (IFT) to move ciliary building blocks and signaling components into the cilium. How ciliary components move from their sites of synthesis in the cell body to the base of the cilium is currently poorly understood. IFT172 is a 200 kDa protein, the largest subunit of the IFT complex and is essential for ciliogenesis in a wide range of organisms, but has due to its large size it has been challenging to study structurally. Here, we report the biochemically characterization of recombinantly purified IFT172, and show that IFT172 is a membrane interacting protein with an ability to remodel large membrane surfaces into small vesicles. We show by electron microscopy that purified IFT172 has an architecture of two globular domains with a long rod-like protrusion, resembling to the domain organization of coatomer proteins such as COPI-II or clathrin. IFT172 adopts two different conformations that can be manipulated by lipids or detergents: 1) an extended elongated conformation and 2) a globular closed architecture. Furthermore, we demonstrate that the association of IFT172 with membranes is mutually exclusive with IFT57, implicating module-like role of IFT172 within the IFT system.

INTRODUCTION

Eukaryotic cells are organized into different compartments and organelles. One such organelle is the cilium or flagellum (interchangeable terms) that protrudes from the surface of most eukaryotic cells and serves important functions in motility, sensory reception and signaling (Ishikawa & Marshall, 2011). Motile cilia are usually present in several copies on the surface of cells and beat in coordinated waves to create movement. Less well known is the fact that most animal cells contain a primary cilium (in general non-motile) that is normally present in one copy per cell (Ishikawa & Marshall, 2011). Although primary cilia on mammalian cells were discovered at the end of the nineteenth century (Wheatley, 2005), research in this area was largely neglected for a century because of the view that eukaryotic primary cilia might only be vestigial and relatively unimportant organelles. This view has radically changed by evidence that primary cilia function in sensory perception, important both during development and in normal physiology (Wheatley, 2005). Furthermore, cilia are important to a number of signaling pathways such as platelet-derived growth factor receptor α (PDGFRα), Sonic hedgehog (Shh), Epidermal Growth Factor (EGF), WNT and 5HT$_6$ serotonin signaling (Veland *et al*, 2009). Both sensory reception and signaling in the cilium is a result of increased clustering of receptors in the ciliary membrane. Besides the loss of sight and smell, defects in cilia can lead to many other human genetic diseases collectively termed ciliopathies (Braun & Hildebrandt, 2017). These include polycystic kidney disease, cognitive impairment, limb deformities, obesity, *situs inversus* (visceral organs have their position inverted), respiratory distress, ectopic pregnancy and sterility (Braun & Hildebrandt, 2017). Understanding the molecular basis for the structure and function of cilia is thus crucial.

At the molecular level, all cilia have a common architecture consisting of a microtubular axoneme surrounded by a membrane that is continuous with the cellular plasma membrane (Ishikawa & Marshall, 2011). A barrel-shaped basal body, originating from a centriole, anchors the axoneme in the cell (Nigg & Raff, 2009). The cilium consists of more than 600 different proteins including structural axonemal proteins such as tubulin subunits, dynein motors, but also small GTPases, receptors and ion channels, glycolytic enzymes and proteins directly involved in transport

processes (Pazour *et al*, 2005). Moreover, flagellum elongation takes place by addition of new subunits at the distal end (Rosenbaum *et al*, 1969; Marshall & Rosenbaum, 2001; Johnson & Rosenbaum, 1992). Consequently, proteins destined for the cilium are actively transported along the outer microtubules of the axoneme, a process termed intraflagellar transport (IFT) (Rosenbaum & Witman, 2002). IFT is necessary for the assembly of cilia or flagella in almost all species studied so far, from protists to mammals. The process of IFT is mediated by a large ~22-subunit protein complex termed the IFT particle. Ciliary cargoe is transported on large trains of IFT particles to the tip of the flagellum (anterograde transport) in a kinesin-II motor-dependent manner (Kozminski *et al*, 1993; 1995) although the molecular basis for train formation is currently unknown. The IFT trains are sandwiched between the ciliary membrane and the axoneme suggesting that IFT proteins may have some affinity for membranes although no membrane interacting domains are predicted in any IFT subunit (Taschner *et al*, 2012). IFT complexes are also shown to associate with various membrane systems of diverse functions. These include the well-studied association of IFT20 with the Golgi and with vesicles being transported from the Golgi to the cilium in mammalian cells (Follit *et al*, 2006). Other studies demonstrated that IFT proteins associate with vesicles in ciliated and non-ciliated neurons (Sedmak & Wolfrum, 2010) as well as on vesicles at the cleavage furrow of dividing *Chlamydomonas* cells (Wood *et al*, 2012). Additionally, IFT proteins were observed on vesicles destined for the cilium in *Chlamydomonas* (Proteins of the ciliary axoneme are found on cytoplasmic membrane vesicles during growth of cilia., 2014) and membrane shedding from cilia was observed for a number of organisms and cell types including *Chlamydomonas* and *C.elegans* (Wang *et al*, 2014; Nager *et al*, 2017; Wood & Rosenbaum, 2015). These observations suggest that subunits of the IFT complex subunits may have affinity for membranes although the molecular mechanisms of such IFT-membrane interactions remain elusive.

The IFT particle can be fractionated into two complexes termed IFT-A (made of 6 proteins, required for retrograde transport) and IFT-B (made of at least 16 proteins, essential for anterograde transport) (Cole *et al*, 1998). The IFT-B complex can be further sub-divided into a 10 subunit IFT-B1 and a 6 subunit (IFT172, IFT80, IFT57, IFT54, IFT38 and IFT20) IFT-B2 complex (Taschner *et al*, 2016). IFT172 is the largest of the IFT proteins with a molecular weight of 200kDa and belongs to the IFT-

B2 complex (Taschner *et al*, 2016; Cole *et al*, 1998; Piperno & Mead, 1997). Genetic studies showed that IFT172 is required for ciliogenesis in *Chlamydonomas* (Cole, 2003), *Trypanosoma brucei* (Absalon *et al*, 2008), *Tetrahymena* (Avidor-Reiss *et al*, 2004; Tsao & Gorovsky, 2008), *D.melanogaster* neurons (Avidor-Reiss *et al*, 2004) and for cilium mediated hedgehog signaling in mouse embryos (Huangfu *et al*, 2003), and null alleles of *IFT172* in mice are embryonic lethal. Mutations in the human IFT172 gene result in skeletal ciliopathies (Halbritter *et al*, 2013). Endogenous IFT172 is found to localize to punctate foci clustering at the base of the cilium (Halbritter *et al*, 2013) as well as at the tip of the cilium, where it may be involved in IFT-train tip-turnaround via an unknown mechanism (Pedersen & Rosenbaum, 2008). IFT172 is incorporated into the IFT complex through a salt-labile interaction with the calponin homology (CH) domain of IFT57 (Taschner *et al*, 2016). However, the molecular organization of IFT172 is not well understood.

In this report, we characterized the molecular properties of purified *Chlamydomonas* IFT172 and found that IFT172 interacts with membranes. Recombinantly prepared IFT172 showed an architecture of two ~10 nm-sized globular domains followed by a rod-like extension, which is consistent with the bioinformatics prediction of two beta-propeller domains appended by a long stretch of alpha-solenoids. Interestingly, IFT172 can also employ the second distinct conformation, with a square shaped organization (closed conformation). Furthermore, using GUVs and cryo-EM, we found that IFT172 interacts with membrane surfaces and surprisingly to remodel membranes into small vesicles of ~20 nm in size. The pinching of the vesicle surface happens with as little as 50 nM of IFT172 by clustering onto a certain surface of a membrane.

RESULTS

IFT172 readily associates with lipids

IFT172 is a ~200 kDa, the largest component of the IFT-B (Cole *et al*, 1998; Piperno & Mead, 1997). Bioinformatics analyses using HHpred/Phyre2 (Kelley *et al*, 2015; Söding *et al*, 2005) revealed that IFT172 has two N-terminal β-propellers (~65 kDa) followed by a ~1100 residues α-solenoid (~100 kDa), with significant sequence similarity to known vesicle coatomer proteins such as COPI-II and clathrin subunits (Fig. 1A). To characterize the behavior of IFT172 *in vitro*, we recombinantly prepared *Chlamydomonas* IFT172 using an eukaryotic insect cell expression system. IFT172 expressed with a C-terminal His-tag appeared in the soluble fraction after centrifugation of the cell lysate but the elusion from Ni-NTA beads resulted in a turbid white solution indicative of a high lipid content (supplementary Table). While previously we have used purified IFT172 (Taschner *at al*, 2016) eluted at the molecular weight of around400 kDa in size exclusion chromatography (SEC), significant fraction of IFT172 eluted in the void volume suggesting a molecular weight of more than 670 kDa (Fig. 1B). Although elution of the void volume is normally a sign of protein aggregation, dynamic light scattering (DLS) analysis showed a uniform particle size distribution of IFT172 with an average diameter of ~120 nm suggesting an oligomeric assembly of the proteins (Fig. 1C). To further characterize the SEC-purified IFT172 lipid-associated mixture, negative-stain electron microscopy (EM) was performed, revealing rather-uniform, large, globular objects with a size of ~75 nm (Fig. 1D). These were composed of IFT172 and various small components with molecular weights in the range of lipids according to the mass spectrometric analysis (Supplementary Table). Based on this, we hypothesized that these oligomers may compose of a vesicle-core covered with IFT172. To test this hypothesis, the IFT172-oligomers were treated with the protease trypsin and SEC was carried out to separate proteolyzed products (Fig. 1E). SEC showed new appearances of proteolyzed protein signals (Fig. 1E, left, labelled 1-3) in addition to the original void signal, which no longer had prominent IFT172 signals (Fig. 1E, right). The EM observation of the void product showed smooth, round particles (Fig. 1F), typical of liposome (Fig. 1G).

IFT172 adopts closed and open conformations

To isolate monomeric IFT172 from the IFT172 oligomers, the detergent n-dodecyl β-D-maltoside (DDM) was added to solubilize IFT172. Upon the addition of DDM, the fraction of the large IFT172- oligomers was lowered, and instead, an increase of the IFT172 peak to ~450 kDa occurred by SEC (Fig. 2A). This corresponding fraction showed the size of ~11 nm by DLS (Fig. 2B). To visualize the domain architecture of IFT172, negative-stain EM of this detergent purified IFT172 was carried out (Fig. 2C). The purified IFT172 showed two different morphologies, 1) a 30-nm long rod-like architecture (rod), with a ~10 nm globular attachment (head) (Fig. 2C, square, and Fig. 2D), and 2) a globular architecture (Fig. 2C, circle, and Fig. 2E). The rod-like architecture is largely consistent with the predicted domain organization of the IFT172 (Fig. 1A). 2D averages focusing on the head domain (Fig. 2F-H) yielded more defined features of IFT172 architecture, revealing two individual ~5 nm, globular densities, likely corresponding to the two beta-propeller domains. Surprisingly, the density of the rod domain was subdivided into four small globular domains with a size of 4 nm each (Fig. 2H). The rod domain is comprised of alpha-solenoidal TPR alpha solenoidal motifs predicted from the sequencing analysis (Fig. 1A) but the sub-domain organization have been unknown. On the other hand, 2D averages of the compact IFT172 revealed a size of ~12 nm globular structure with 4 subdomains inside (Fig. 2G). Presumably, the two of these subdomains correspond to the WD40 beta-propeller domains, and the rod domain might be closed up by connecting to the head domains (Fig. 2I).

To avoid the influence of the residual detergent during the detergent-dependent IFT172 purification, we revised the purification by employing Q sepharose anion ion-exchange chromatography without using detergent. Interestingly, the purified IFT172 without detergent only contained a closed conformation (supplementary Fig. 1A), indicating that the DDM facilitates the opening of IFT172. We then added DDM to the purified, globular IFT172, confirming that IFT172 converts into the open conformation, showing that IFT172 can employ both closed and open conformations (supplementary Fig. 1A-C).

IFT172 interacts directly with and vesiculates membranes

Based on the observation that IFT172 co-purifies with lipids, we hypothesized that IFT172 may interact directly with membranes. To test this hypothesis, detergent-free

monomeric IFT172 was mixed with liposomes (Folch fraction I) and protein-liposome co-sedimentation assays were performed. While IFT172 alone did not sediment, a substantial amount of IFT172 (up to 40%) was co-sedimented in the presence of 0.5 mM liposome (Fig. 3A). IFT172 did not show any apparent preference to different sizes of vesicles (Fig. 3B and 3C), indicating that membrane curvature is not a critical factor for the binding of IFT172 to membrane surface. We rather observed a preference for negatively charged lipids (Fig. 3D and 3E). Further, using analytical DLS, the interaction of IFT172 with membrane was tested. Immediately after adding 500 nM IFT172, we observed that the average size of liposomes of 200 nm in diameter increased by 33 % presumably due to the binding of the protein on the surface of vesicles (Fig. 4A). Then gradually, the peak position of vesicles shifted to smaller sizes, while the size distribution became broader. This change of the vesicle size suggests remodeling of liposomes in the presence of IFT172. Using GUVs (giant unilamellar vesicles) and fluorescently labeled lipids, the interaction of venus-tagged IFT172 with membranes was directly observed (Fig. 4B). Supporting the DLS observation, an association of the IFT172-Venus with GUVs was observed (Fig. 4B and 4C). To follow the dynamics of the interaction, real-time recordings for GUVs were performed (Fig. 4B). IFT172-Venus started to cover the surface of a GUV immediately after addition and the intensity of decorated IFT172 maximized within ~2-4 min. When the IFT172 concentration was at its detection limit (50 nM), IFT172 displayed an uneven coverage of GUVs (Fig. 4B, arrowheads), indicating a clustering of the protein on the membrane surface. Interestingly, we observed ~60% GUVs collapsed within 10 min after loading IFT172 (Fig. 4D and 4E left). Some of the GUVs that remodeled into smaller entities were trapped on the supporting chip (Fig. 4D, "4 min"). The frequency of collapsing of GUVs depended on the concentration of added IFT172, as the frequency is increased by 10 times upon addition of 250 nM IFT172 (Fig. 4E right). The critical concentration for remodeling membrane appears to be ~10 nM in the given experimental condition as the effect of collapsing vesicles was not visible anymore below this concentration. These results show that IFT172 interacts with membranes, clusters on the membrane surface, and remodel the membrane surface.

To more closely examine the remodeling events of vesicles by IFT172, the mixture of IFT172 with liposomes was observed by negative-stain EM. Compared to intact liposomes (Fig. 5A), the addition of 1 μM IFT172 to 200 μM, 200-nm liposome

resulted in broken pieces of liposomes in the background (Fig. 5B). Lowering the protein concentration to 250 nM facilitated a better visualization of the process, showing the striking association of IFT172 and the forming of relatively uniform, ~18 nm ring-like structures 'budding out' from liposomes (Fig. 5C and 5D, arrowheads). Next, the IFT172-liposome mixture was fractionated by SEC (Supplementary Fig. 2A). The fraction of ring-like structures (Supplementary Fig. 2B) shifted to longer elution times and mass spectrometry confirmed that it contained both lipids and IFT172. (Supplementary Fig. 2C and D)

IFT172 membrane affinity maps to the N-terminal beta-propeller region

To assess which domain of IFT172 is involved in membrane binding, two fragments lacking either the N-terminal globular domain (residues 590-1755, IFT172ΔN), or lacking the C-terminal rod domain (residues 1-968, IFT172ΔC) (Fig. 6) were prepared and tested for liposome interaction. A co-sedimentation assay of IFT172ΔN with liposomes showed that the protein does not bind to membranes (Fig. 6A), and no apparent remodeling of membrane surface was observed by negative stain EM (Fig. 6B). On the other hand, IFT172ΔC showed interactions with liposomes in a co-sedimentation assay (Fig. 6C). The breakage of GUVs was also observed after loading IFT172ΔC, similar to IFT172FL in GUV assay (Fig. 6E). The mixture of IFT172ΔC with liposomes was observed by negative-stain EM, and the deformation of the liposomes was observed (Fig. 6D). These results together indicate that the association of IFT172 with membranes is mediated by the N-terminal beta-propeller.

IFT57 competes with lipids for the binding to IFT172

IFT57 is reported to be a direct interaction partner of IFT172 within the IFT-B2 complex and a previous interaction analysis showed that the interaction is mediated by the IFT172ΔC and the IFT57 Calponin Homology (CH) domain (Taschner *et al*, 2016). We therefore tested the binding of IFT57 to IFT172 in the presence of membranes. The liposome co-sedimentation assay showed that IFT57 has no interaction with membranes (Fig. 7A). As more IFT57 is added to IFT172-liposome mixture, the amount of pelleted IFT172 decreased, showing that less IFT172 interacts with membrane surfaces in the presence of IFT57 (Fig. 7B). Notably, IFT57 does not co-sediment in any of these conditions, indicating that the IFT57-IFT172 complex does not interact liposomes.

IFT172 co-localizes to the axoneme in cells and forms foci in the cytoplasm

IFT172 is implicated in ciliogenesis and endogenous IFT172 localizes to punctate foci clustering at the base of the cilium (Halbritter *et al*, 2013). In addition, IFT proteins from both IFT-A and IFT-B complexes are found to associate with vesicles in various cell types (Ding *et al*, 2017; Wood *et al*, 2012; Sedmak & Wolfrum, 2010; Wood & Rosenbaum, 2014). To test the subcellular location of IFT172, we performed immunofluorescence microscopy using RPE-1 cells (human retinal pigment epithelium cells) (Supplementary Fig. 3A) as well as HeLa (Henrietta Lacks cervical cancer cell line) cells (Supplementary Fig. 3B). Upon starvation for 24h, which facilitates ciliogenesis in these cells, IFT172 showed co-localization with a well-known cilia marker Arl13b (ADP-ribosylation factor-like 13b) at the axoneme inside cells (Fig. 3C). This is in agreement with a previous report (Kowal & Falk, 2015), also validating the specificity of the antibody. In addition to the localization in the primary cilia, IFT172 formed foci in the cytoplasm (Supplementary Fig. 3A-C) both in ciliated or the control cells without starving. These foci did not colocalizes with IFT20, Rab5 and lysozyme C (Fig. 3D-F), which are known to be in Golgi, early endosome, and secreting vesicles from Golgi respectively. Furthermore, RPE-1 cell lysate without starvation was further fractionated using a centrifugation-based fractionation procedure (Itzhak *et al*, 2016). IFT172 was found in the membrane rich fraction, which supports the notion that IFT172 co-localizes with membranes (Supplementary Fig. 3G).

DISCUSSION

Mechanism of IFT172 membrane recognition

We have observed that IFT172 clusters on membrane surfaces with as little as a concentration of 50 nM, showing a strong membrane affinity. Furthermore, we mapped membrane interaction to the N-terminal domain of IFT172. Interestingly, the beta-propeller domains of IFT172 has a basic surface at the inner lumen of the blade1, according to homology modeling, similar to the charge distribution on the surface of beta COPI (Dodonova *et al*, 2015). The COPI complex contains a direct membrane binding subunit (Arf1) (Beck *et al*, 2008), however, the charged surface of beta COPI is also located proximal to membrane surface. This may implicate that IFT172 recognizes membrane surfaces through its blade surface. Other than that, IFT172 does

not have an obvious membrane binding or curving domain. Interestingly, it was recently reported that membrane curvature formation resulting in a fission event could occur due to the crowding of proteins (Snead *et al*, 2017). It is possible that membrane remodeling by IFT172 is induced by the local crowding, which might be facilitated by self-association of IFT172 on a certain surface of the membrane. Negatively charged lipids might be a key candidate facilitating the clustering of IFT172, as we observed preferential binding of IFT172 to this class of lipids (Fig. 3D and 3E).

Role of ITF172 in IFT turnaround at ciliary tip

What are the mechanisms for switching between anterograde and retrograde IFT at the ciliary tip allowing for a full transport cycle? When kinesin II-driven anterograde IFT trains reach the distal end of the axoneme, they are rapidly converted into dynein 2-driven retrograde IFT trains through poorly understood mechanisms. Photobleaching experiments revealed that this process takes less than 3 seconds in trypanosomes(Morga & Bastin, 2013). IFT172 was shown to be required for tip-turnaround in *Chlamydomonas,* as a temperature sensitive C-terminal point-mutant of IFT172 accumulates IFT proteins at the ciliary tip (Pedersen *et al*, 2005). Consistently, it is known that IFT172 truncations lacking parts of the alpha-solenoid at the C-terminus are sufficient to support anterograde IFT in *Tetrahymena*, but accumulate at the ciliary tip together with other IFT proteins indicative of a tip-turnaround defect (Tsao & Gorovsky, 2008). It thus appears that the N-terminal β-propeller domain of IFT172 is involved in IFT train formation and anterograde transport while the C-terminal domains are required at the ciliary tip to switch to retrograde transport. Our *in vitro* observation showed that the N-terminal beta propeller has a mutually exclusive interaction with IFT57 and membrane. This may mean that the membrane binding module of IFT172 is inhibited when it is incooporated in the IFT complex to form a train. During the IFT turnaround, disassembly and reconfiguration of IFT trains, IFT172 may park at the membrane surface by associating with the membrane at the tip of cilia On the other hand, the alpha-solenoid rod domain may play an additional role in re-association of IFT172 to the rest of IFT complex therefore the dissociation of IFT172 to the membrane occurs during the switching of the direction of the IFT trains (Tsao & Gorovsky, 2008).

Missing components for the coatomer formation

Archetypical vesicle coat proteins such as clathrin or COPI/II proteins (Lee & Goldberg, 2010; McMahon & Mills, 2004; Faini *et al*, 2013; Rout & Field, 2017) form well-ordered coatomers with internal symmetry (Rout & Field, 2017). Previous studies suggested the similarities between IFT172 and proteins that are involved in coatomer formation (Jékely & Arendt, 2006). Our homology detection using HHpred (Söding *et al*, 2005) also indicated that clathrin has significant similarity (E-value of 10^{-29}) to IFT172. Our purified IFT172 showed a striking interaction with vesicles leading to an immediate interaction and remodeling membrane surface enough to pinch off small vesicle-like structure. Furthermore we showed that the interaction of the IFT172 with membranes are held through the beta-propeller domain, resembling the proximal location of the COPI beta-propeller domain to the membrane surface of COPI-vesicles (Dodonova *et al*, 2015). Taken altogether, we speculate that IFT172 interacts with liposomes, possibly to pinch off a small lipid fracture or to result in well-ordered coat formation given the complete interaction partners.

In the course of the search for the binding partners that possibly facilitate an organized coat-like formation, our primary choice was the known IFT172 binding partner IFT57 that together forms a IFT periphery complex. Interestingly, we observed a competitive effect of IFT57 towards IFT172's membrane bindings. It is interesting to note that IFT172 may indeed be a loose module in the IFT peripheral complex as seen by (Cole *et al*, 1998) and that it may modulate between the IFT-B2 and membrane and/or other peripheral membrane proteins. In this sense, IFT172 might be a modulated "cargo adapter" that is carried by IFT, or the glue that is first anchored to the membrane surface at the base of cilia, and then, recruits other IFT components to assemble together.

IFT172 as a multi-functional module for train formation

Possible biological functions of IFT172 have been suggested to be Golgi to cilium transport of vesicles (Wang & Deretic, 2014), endo/exo-cytosis at the ciliary pocket (Benmerah, 2013), involvement in train formation (Pigino *et al*, 2009), participation in cell division at the cleavage furrow (Wood *et al*, 2012) and the IFT train turnaround at the ciliary tip (Pedersen *et al*, 2005). Many of these suggested functions of IFT172 require an interaction of the protein with the membrane surface. From

these points of view, it is sensible to observe that IFT172 has an association to membranes. In spite of the reported interaction of IFT components to membrane or vesicular environment, so far, we did not find any other recombinantly produced *Chlamydomonas* IFT-B proteins to associate to lipids or membranes. In addition, we found clustering of IFT172 protein to a membrane surface. This strong association with membrane may be the driving force for the IFT complex to be proximal to membrane surface.

Together with studies in in *Trypanosoma* and *Chlamydomonas* and from mutations in human patients, our results suggest that IFT172 could be an important actor in several key steps of IFT: (1) the way by which IFT proteins/complexes reach the flagellum base and the possible role of post-Golgi vesicles in this process; (2) the mechanisms leading to the formation of trains from IFT complexes and (3) the procedure to convert anterograde trains to retrograde trains.

Although the functions of IFT172 appear fairly discrete, our attempt of visualizing IFT172 and test colocalization with known vesicle markers in cells was unsuccessful. However the implication was rather that IFT172 may be making a microstructure in the cytosol, independent of large organelles. It is possible that IFT172 has more detectable, distinct functions during ciliogenesis or cilia-maintenance phase. For that sense, further studies are necessary on IFT172 to connect the protein biochemistry and the cellular functions.

ACKNOWLEDGEMENTS

METHODS

Protein expression and purification

The coding sequence of IFT172, IFT172ΔN (residues 590-1755) and IFT172ΔC (residues 1-968) from *Chlamydomonas* were gene synthesized, or sub-cloned into multiple cloning site 2 (MCS2) of pFL vector, and a His-tag (6×HIS) was added to the C-terminus of IFT172 by PCR. Then DH10 BAC cells were transformed with the plasmid for making recombinant production of baculoviral DNA. Sf9/21 insect cells were transfected with recombinant viral DNA for making recombinant baculoviruses. HighFive cells (Invitrogen) (200 ml, 1×10^6 cells/ml) were infected with IFT172-His tag virus and incubated at 26°C for 3 days. The cells were harvested by centrifugation (1,000 g, 15min), and resuspended in 5 times lysis buffer (20 mM Hepes pH 7.4, 10 mM KCl, 1.5 mM $MgCl_2$, 250 mM sucrose) with freshly a protease inhibitor tablet (complete tablet, EDTA-free; Roche) and 5 mM β-mercaptoethanol. Cells were transferred to a Dounce homogenizer and homogenized around 20 strokes, and it was left on ice for 20 min for completely break up. The crude cell lysate was centrifuged at 750 g for 10 min to pellet the nuclei. Additional NaCl was added to the supernatant to a final concentration of 200 mM, followed by further centrifugation (10,000 g, 30 min, 10°C). His60 Ni Resin (Clontech) was used for affinity binding, and the Ni Resin was washed with 20 mM Hepes pH 7.4, 150 mM NaCl, 1 mM DTT. The protein was eluted with 20 mM Hepes pH 7.4, 150 mM NaCl, 300 mM imidazole and 1 mM DTT. The eluted IFT172 was concentrated and loaded onto a Superose 6 10/300 (GE Healthcare) size-exclusion chromatography column equilibrated with 20 mM Hepes pH 7.4, 150 mM NaCl, and 1 mM DTT. To further investigate the IFT172 association with lipids, vesicle fractions were purified by ultracentrifugation starting from insect cell material over-expressing IFT172. The results of this procedure showed that IFT172 co-purified in the lipid-fraction after the last centrifugation step at 100.000g, 30 min.

To purify the IFT172 monomer, the same purification procedure was used except that 0.1% DDM was added to all the buffers. To purify the detergent-free IFT172 monomer and IFT172-venus for membrane binding assays, the elution from His60 Ni Resin was then loaded onto anion-exchange column (5 ml HiTrapQ-Sepharose, GE Healthcare) before size-exclusion chromatography and DDM was omitted in the purification last steps.

Purification of IFT57 was carried out as described in (Taschner *et al*, 2016) except that we employed a bacteria expression system. Briefly, full length *Chlamydomonas* IFT57 was cloned into pEC vector with N-terminal cleavable His tag and expressed in E. coil BL21 (DE3). The bacterial culture was grown in TB medium at 37 ^{o}C until O.D. (600 nm) around 2, then the temperature was reduced to 18 ^{o}C and 0.5 mM IPTG was added for over-expression overnight. Cells were harvested and lysed in 50 mM Tris-HCl pH 7.5, 150 mM NaCl, 10% glycerol, 5 mM β-mercaptoethanol, 1 mM PMSF, 25 μg/ml DNase I. The soluble fraction was loaded on a Ni^{2+}-NTA column (5 ml, Roche). The column was washed with lysis buffer with additional 1 M NaCl and the protein was eluted with lysis buffer contains 500 mM imidazole. The eluted fraction was dialyzed against 20 mM Tris-HCl pH 7.5, 50 mM NaCl, 10% glycerol, 5 mM β-mercaptoethanol with TEV protease to remove the His tag. The dialysis product was further purified by an ion-exchange column (anion exchanger, 5 ml HiTrapQ-Sepharose, GE Healthcare) to remove contamination and cleavage tags. Size exclusion chromatography (SEC) was finally applied with 10 mM Hepes pH 7.5, 150 mM NaCl, 1 mM DTT.

Limited proteolysis

Limited proteolysis of IFT172-lipid oligomers was performed in 20 mM Hepes pH 7.4, 150 mM NaCl, and 1 mM DTT. 0.05 mg/ml final concentration of Trypsin was incubated with IFT172-lipid oligomer at room temperature for 2 hours. Samples were analysed by SDS-PAGE and size-exclusion chromatography on Superose 6 10/300 (GE Healthcare) column.

Liposomes preparation

Liposomes were prepared from a bovine brain extract, Folch Fraction I (Sigma Aldrich) by evaporating the chloroform of the lipid under a nitrogen-stream and further incubation under vacuum. Multi-lamellar vesicles (MLVs) were generated by hydrating the dried lipid with 20 mM Hepes, 150 mM NaCl, pH 7.5 to a concentration of 2 mg/ml. Large unilamellar vesicles were generated by extruding the MLV-suspension through filter (Avanti) with pore sizes of 200 nm, 100 nm, and 50 nm.

GUVs were generated using the gentle hydration method(Akashi *et al*, 1996). Briefly, 100 ul of 10 mg/ml Folch Fraction I with 0.1% ATTO 655 labeled DOPE (ATTO-

TEC) dissolved in 20:9:1 chloroform: methanol: H_2O was dried on glass test tube under a nitrogen-stream and subsequent incubation under vacuum, then 1 ml of 10 mM Hepes, 240 mM sucrose, pH 7.5 was added gently to the glass tube without disturb the lipid layers. The tube was incubated at 75°C water bath overnight. The bulky cloud floating in the middle of the solution, which contains GUVs was transferred to 10 mM Hepes, 150 mM NaCl, pH 7.5 for fluorescence imaging.

Liposomes sedimentation assay

IFT172 or IFT172/57 in 20 mM Hepes, 150 mM NaCl, pH 7.5 was incubated with MLVs or large unilamellar vesicles for 15 min on ice. Soluble proteins were separated from liposome-bound proteins by ultracentrifugation for 20 min at 50,000 rpm using a TLA100.3 rotor in a TL-100 tabletop ultracentrifuge (Beckman). Both supernatant and pellet fractions were collected and analyzed using SDS-PAGE.

Negative stain EM

To observe IFT172 in lipid binding form and monomer form from SEC, samples (0.05 μM) were applied to homemade carbon grids. For liposomes conformation changing observation by IFT172, IFT172ΔC and IFT172ΔN, 0.25 uM proteins were mixed with 0.2 mM MLV or 200 nm LUV, grids were made without dilution. The grids were staining with 1% (w/v) uranyl-acetate staining and images were recorded on a CM200 (FEI, 160 kV) under low-dose mode with magnification of 50,000 corresponding to 2.16 Å/pixel. We use e2boxer.py from EMAN2 package for semi-automatically particle picking. Two-dimensional (2D) reference-free classification was performed with RELION 1.4. For IFT172 monomer architecture analysis, micrographs were recorded with magnification of 38,000x corresponding to 2.78 Å/pixel. e2boxer.py from EMAN2 package (Tang *et al*, 2007)for semi-automatically particle picking and two-dimensional (2D) reference-free classification was performed using the RELION software package (Scheres, 2012). To obtain the domain architecture of open conformation of IFT172, about 6000 particles were picked and applied for domain masking and an assembly strategy. Soft masks for each domain were generated by Fiji. After drawing the domain shapes by the 'wand tool' in Fiji (Schindelin *et al*, 2012), the masks were soft-edged by enlarging ~9 pixels and filtering with Guassian blur in Fiji. Masks for N-terminal beta propeller globular domain of IFT172 and the C-terminal alpha-solenoid rod were applied to individual,

aligned single particles images using 'bmask' from BSOFT software package (Heymann & Belnap, 2007), and the resulting images for each domain were further aligned and average using Relion, and the 2D averages were combined with 'badd' from BSOFT.

Cryo-EM

For the observation of IFT172 interaction with membrane under cyro-EM, IFT172 (0.5 μM) and LUVs in 200 nm (0.4 mM) were mixed and vitrified immediately. 4 μl sample without dilution was placed onto a glow-discharged Quantifoil grids (Cu, R2/2) and then blotted for 6 s with blot force 6 to remove the excess solution with Vitrobot Mark IV (FEI). The Vitrobot chamber was operated at 4^oC with 100% humidity. The grids were observed on a Tecnai F20 (FEI) with an acceleration voltage of 200 kV with a nominal magnification of 29,000x corresponding to a pixel size 3.72 Å/pixel. The micrographs were taken with a CCD camera (FEI, Eagle) with a defocus range of -2 to -4 μm.

Microfluidic chip fabrication and preparation

PDMS microfluidic chips with vesicle traps were fabricated using soft lithography. The vesicle trap geometry was adapted from (Robinson *et al*, 2013). We firstly increased the trap density to facilitate time-lapse imaging of multiple vesicles in a single field of view. We secondly used a layered arrangement of progressively narrower trap posts. The first quadrants had 8 μm spacing between trap posts, with subsequent quadrants narrowing to nominally 6, 4.5, and 3 μm gaps between both trap posts. In this arrangement, smaller vesicles that could not be capture in the wide traps were trapped in the narrower traps downstream. SU8 master moulds of 10 and 20 μm were produced on a 4 inch silicon wafer (University Wafer) using SU-8 2010 or 2015 (Microchem corp.), according to the manufacturers data sheet and developed using PGMEA. To facilitate intact release of the small PDMS features of traps, the developed SU8 master was surface-treated with a fluorophilic coating by spin coating about 200 μl of 1:20 Cytop CTL-809M in CTsolv.100E (both from Asahi Glass Co. Ltd., Japan) onto the master. For this the Cytop dilution was directly pipetted onto the SU8 features and then spin-coated at 3000 rpm for 1 min, using a 500 rpm/s ramp. The wafer was then hard-baked for 30 min at 453 K on a hot plate to simultaneously drive SU8 polymerization to completion whilst also covalently anchoring the coating.

The master was then allowed to slowly cool down to room temperature by turning off the hot plate.

PDMS base and curing agent (Sylgart 184, Dow Corning) were mixed at a ratio of 10:1, and poured to about 4 mm thickness onto the master in a petri-dish. After degassing for about 15 min, PDMS prepolymer was cured on the silicone master at 80 ºC for at least one hour. The PDMS was then peeled off the silicon wafer, cut to size and fluid ports were punched with a 4 mm and 0.5 mm diameter biopsy puncher (World-Precision-Instuments) for the reservoir and outlet, respectively. The PDMS microchannels were then sealed by plasma bonding them onto glass cover slips (24x50 mm, VWR) using oxygen plasma (15 s at 0.3mbar, 30% power, Diener, ZEPTO) and bonded for 15-30 min at 80 ºC. Before introduction of GUVs, the bottom layer channels were filled, via centrifugation (900g, 10 min), with 1% (w/v) pluronic F-127 (Sigma) solution in PBS to coat the channels. This prevents vesicle rupture upon contact with the walls. After coating, a syringe-pump (neMESYS, cetoni, Germany) was used to draw the GUV solution and reagents through the fluid channels during the experiments using a flow rate of 4 µl/h.

Confocal microscopy

Imaging was performed with an LSM 780/CC3 confocal microscope (Carl Zeiss, Germany) equipped with a C-Apochromat, 40x/1.2W objective. We used PMT detectors (integration mode) to detect fluorescence emission (excitation at 488 nm for YFP and 640 nm for DOPE-ATTO 655) and record confocal images, typically focusing on the equatorial plane of the GUVs. After some of the GUVs got trapped on the chip for imaging, the buffer was pumped to the chip for about 10 min to remove the small membrane pieces in the background. Afterwards, individual GUVs were picked and focused. For the control experiments to quantify the stability of the GUVs, freshly sample buffer was loaded for 10 min and images of individual GUVs was taken every minute. For IFT172-Veuns membrane binding test, diluted IFT172 to 250 nM and 50 nM was loaded after buffer wash and images of individual GUVs was taken every minute. The osmolality of all the buffers and diluted protein solutions were match (name of the equipment). All images were analyzed using ImageJ.

Antibodies and cell culture

The following antibodies were used in this study: Anti-IFT172 (mouse monoclone, sc-398393; Santa Cruz), Anti-Arl13b (1711-1-A; Proteintech)The secondary antibodies Alexa Fluor 488 mouse (A21202) and Alexa Fluor 568 rabbit (A10042) were purchased from Thermo Fisher Scientific. HeLa cells were grown in DMEM medium containing 10% FCS at 37°C with 5% CO_2. RPE-1 cells were grown in DMEM/F12 medium containing 10% FCS at 37°C with 5% CO_2.

Cell fractionation assay

To identify IFT172 in subcellular compartments of RPE-1 cell, RPE-1 cells were fractionated according to the previously described protocol (Itzhak *et al*, 2016). Briefly, cells from two 10 cm cell culture plates were collected in 4 ml lysis buffer (25 mM Tris-HCl, pH 7.5, 50 mM sucrose, 0.5 mM $MgCl_2$, 0.2 mM EGTA), followed by homogenization with a Dounce homogenizer. The sucrose concentration was restored to 250 mM afterwards. Nuclear materials were removed by centrifugation at 1000 g for 10 min (Multifuge 1L, Heraeus). The supernatant was collected and further centrifuged at 38,000 rpm for 30 min (Optima MAX Ultracentrifuge, Beckman Coulter) to separate cytosolic (supernatant) and organellar (pellet) fractions. The pellet was resuspended in SDS buffer (2.5% SDS, 50 mM Tris pH 8.1) for western blotting. Total cell lysate, cytosolic fraction and organellar fraction were separated by SDS-PAGE and analyzed with western blotting. Anti-IFT172 antibody used with 1:100 dilution and goat anti-mouse IgG (62-6520, Thermo Fisher) was used as secondary antibody with 1:5000 dilution.

Immunofluorescence microscopy

RPE-1 and HeLa cultured on glass cover slips were used for immunostaining. Cells were fixed with 4% formaldehyde (Thermo Fisher Scientific) for 10 min, washed with PBS for 3 times, followed by the permeabilization in 0.01% Triton X-100 for 15 min. After rinsing with PBS, the cover slips were blocked with 4% BSA for 30 min, rinsed again with PBS, and then incubate with primary antibodies diluted in PBS containing 4% BSA for overnight at 4°C. The samples were rinsed three times with PBS containing 4% BSA and then incubated with secondary antibodies diluted in PBS containing 4% BSA for 1h at room temperature. Slides were then washed and mounted with Prolong gold antifade reagent (Thermo Fisher Scientific) and checked

at room temperature on CF2 Leica TCS SP8 microscope equipped with a 63×1.40 OIL lens. The images were merged and processed using Fiji (Schindelin *et al*, 2012).

To overexpress Rab5-GFP or lysozyme C-mCherry in Hela cell for co-staining with IFT172, the plasmids encoding Rab5-GFP or lysozyme C-mCherry (plasmids obtained as gifts by Dr. Julia von Blume) was transfected into Hela cells followed with 24 h incubation at 37 °C.

Dynamic light scattering

For measuring the size of the purified IFT172, dynamic light scattering was carried out on a DynaPro NanoStar Instrument (Wyatt) using 50-μl cuvettes and IFT172 volume of 20 μl at 4°C. Raw data were analyzed by the DYNAMICS software package. The dispersity of the solution was assessed, and the average hydrodynamic radius (RH) was calculated.

For measuring the size of the liposomes, a Malvern Zetasizer Nano ZSP system (Malvern, UK) was used using disposable micro cuvettes (ZEN0040; Malvern, Malvern, UK) with the backscatter (173°). For each experiment, 3 scans (6-10 runs each) were measured at 25 °C with an initial equilibration time of 3 min. Dispersant viscosity and refractive index (r.i.) were set to 0.8882 cP and 1.330, respectively, and the pre-defined settings for liposomes were used for the scattering material (abs 0.001, r.i. 1.330). The liposome concentration was 0.1mg/ml in all experiments to allow measurements with an attenuator of 7 or 8 (mean adjusted count rate of ~20,000). For all measurements, the fits of the raw correlation data met the manufacturer's quality criterion. The values plotted for each experimental condition are the mean size distributions for 3 runs as obtained from the instrument software (based on the measured intensities and the general purpose model (normal resolution)). The count rate for control measurements with IFT172 alone was ~10-fold lower than for experiments with liposomes, and the mean of the size distribution was at 64±13 nm. Therefore, we assess that the shift in the size distribution observed after protein addition is due to the absorption of the protein to the liposomes.
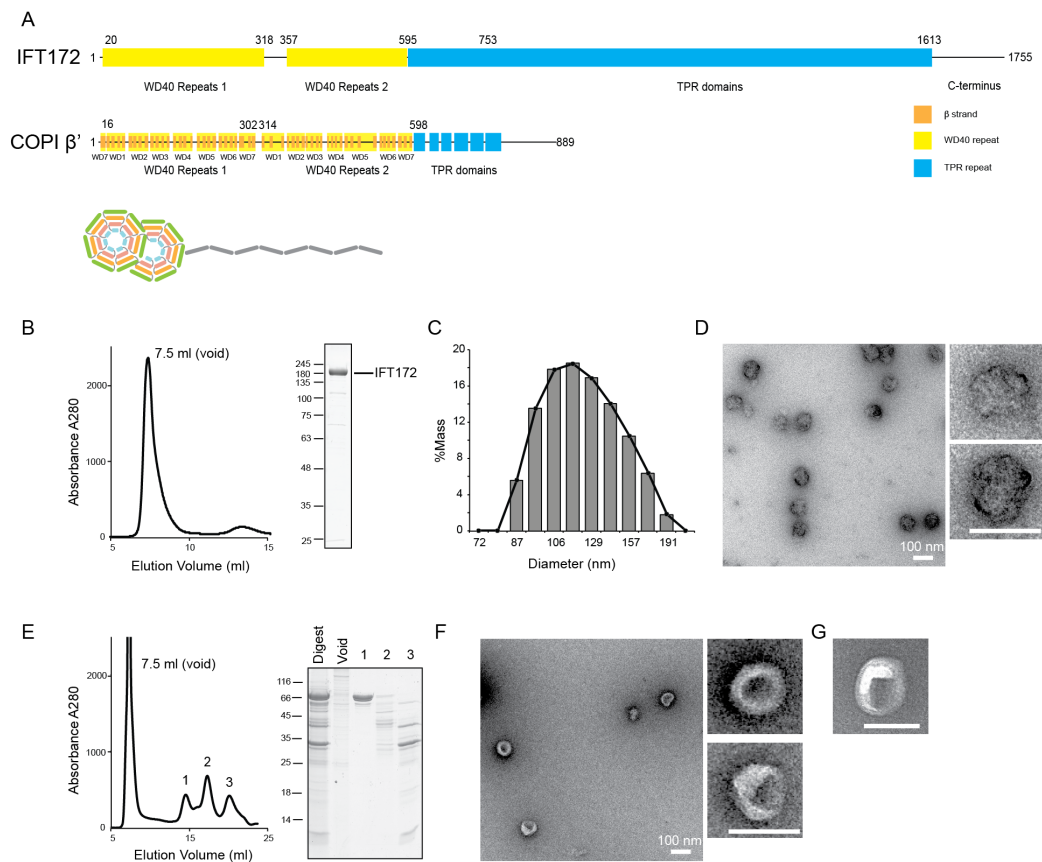
FIGURES

Figure 1 - Purification of recombinant IFT172 from *Chlamydomonas.*

A. Predicted domain architecture of IFT172 from *Chlamydomonas.* The predicted WD40 repeats (in yellow) and TPR (tetratricopeptide repeat) domain (in blue) were defined by HHpred. IFT172 shows a similar domain organization to COPI-II and clathrin. COPI β' from *Saccharomyces cerevisiae* is shown for comparison. **B.** Size-exclusion chromatogram (SEC) of recombinant full-length IFT172 and Coomassie-stained SDS-PAGE analysis of recombinant IFT172 after size-exclusion chromatography. **C.** Dynamic light scattering (DLS) measurement of IFT172 shows a uniform particle size distribution of IFT172 with an average diameter of ~120 nm with 100% mass. **D.** Negative stain EM micrograph of the IFT172 showing globular oligomer formation. **E.** SEC profile of IFT172 proteolyzed products after limited-proteolysis (left) and SDS-PAGE of the peak fractions from SEC is shown (right). **F.** Negative stain EM micrograph of the fraction from void peak in (E) shows round

particles with smooth surface. **G.** Negative stain EM micrograph of the liposome from Folch fraction I as a control.
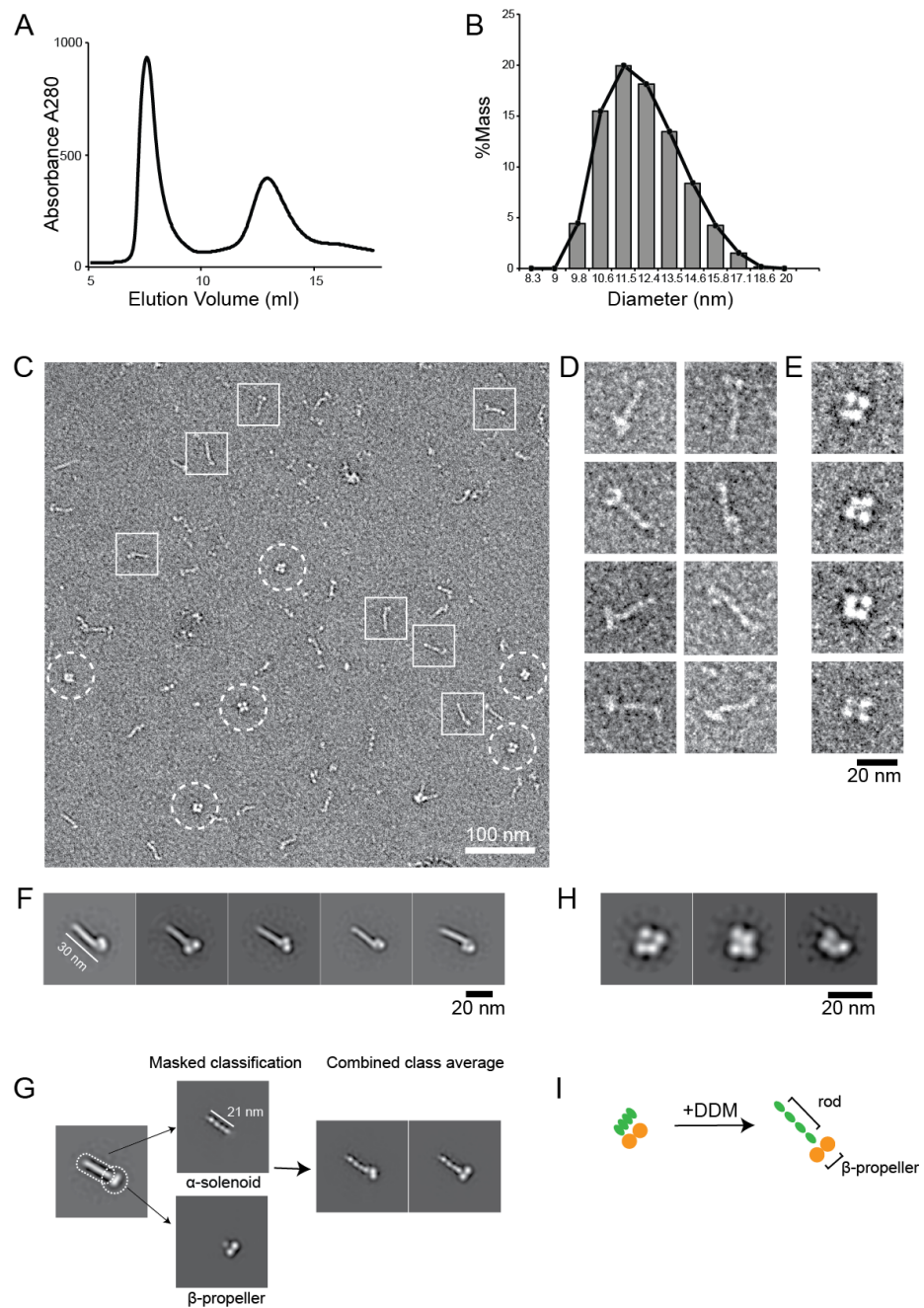
Figure 2 - Monomer architecture of recombinant IFT172 from *Chlamydomonas.*
A. SEC profile of recombinant full-length IFT172 with 0.1% DDM shows an
increased amount of the monomer peak. **B.** DLS measurement of IFT172 monomer
shows the size of the particle is around 11 nm. **C.** Negative stain EM micrograph of

monomer IFT172 with 0.1% DDM, showing an open (square) and a closed (circle) conformation. **D, E.** Representative IFT172 monomers in an open (D) conformation and closed (E) conformation , respectively. **F, G.** Reference-free 2D class averages of IFT172 in an open conformation (F) and a closed conformation (G), respectively. The open conformation shows a rod-like structure with 30 nm in length, while the closed IFT172 contains 4 sub-domains. **H.** Detailed 2D averages of IFT172 by domain masking and assembly strategy. The original average views are shown on the left side. To obtain detailed features for each domain, soft masks (dotted lines) were applied to facilitate an individual alignment of the head domain and tail domain. Two complete IFT172 molecular are generated by aligning the two components. The N-terminal head region shows two globular density with a size of ~5 nm each. The rod part shows 4 globular domains with 4 nm each, which could be the features by TPR alpha solenoid motifs. **I.** Schematic representation of the conformation changing of monomer IFT172 by DDM.
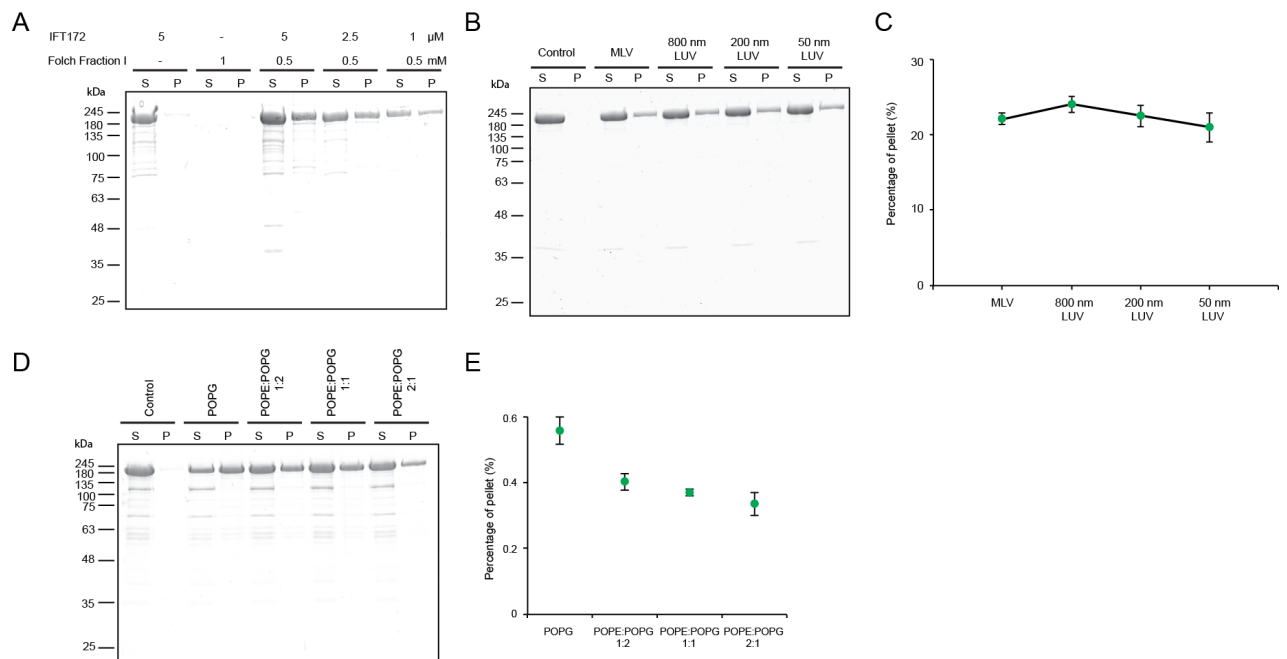
Figure 3 - Liposome sedimentation assays of IFT172 from *Chlamydomonas.*

A. Co-sedimentation assay of IFT172 with Folch fraction I multilamellar vesicles (MLV). Showing the direct binding of IFT172 to membrane. **B, C.** Co-sedimentation assay of IFT172 with Folch fraction I MLV and large unilamellar vesicles (LUVs) of different sizes (B) and their quantification (C). IFT172 has no preference to different curvatures of the membrane. **D, E.** Co-sedimentation assay of IFT172 with different ratio of POPE, POPG mixture (D) and their quantifications (E). IFT172 has a preference to negatively charge lipid. Error bars depict standard deviations from three separate experiments.
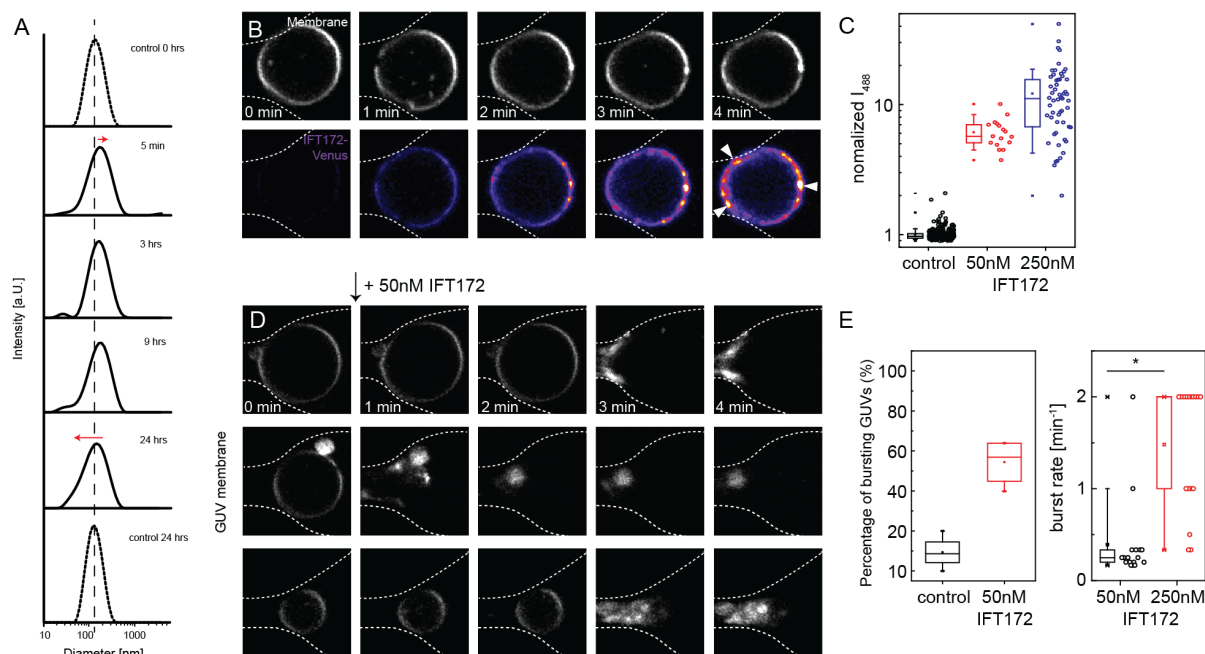
Figure 4 - IFT172 binds and destabilized LUVs/GUVs.

A. DLS measurement of IFT172 with LUVs of 200 nm in diameter. Within first few minutes, the size of LUVs increase due to the binding of IFT172. Afterwards, the peak broadens, indicating remodeling of vesicles. **B.** IFT172-venus binds to GUVs (labeled with DOPE ATTO655) and form clusters on the membrane surface. 50 nM of IFT172 was loaded to GUVs and the data was recorded every 20s. The membrane was shown in grays and IFT172-venus was shown in "fire" color-code from FIJI. Dotted lines show the trace of the micro-fabricated trap used to hold GUVs. **C** Intensity of IFT172 on GUVs. Raw data points are shown in scattered dot plot (right). In the box plots (left), the box denotes the 25th and 75th percentile, the whiskers denote the 10th and 90th percentile, the square denotes the mean and the mid line the median. The x denotes the 1st and 99th percentile. **D.** Collapse of the GUVs by the binding of IFT172. The membrane was shown in grays. 50 nM of IFT172 was loaded to GUVs and the data was recorded every minute. **E.** Statistics of GUVs collapse with IFT172. The definitions of the box plots follow the same as (C).
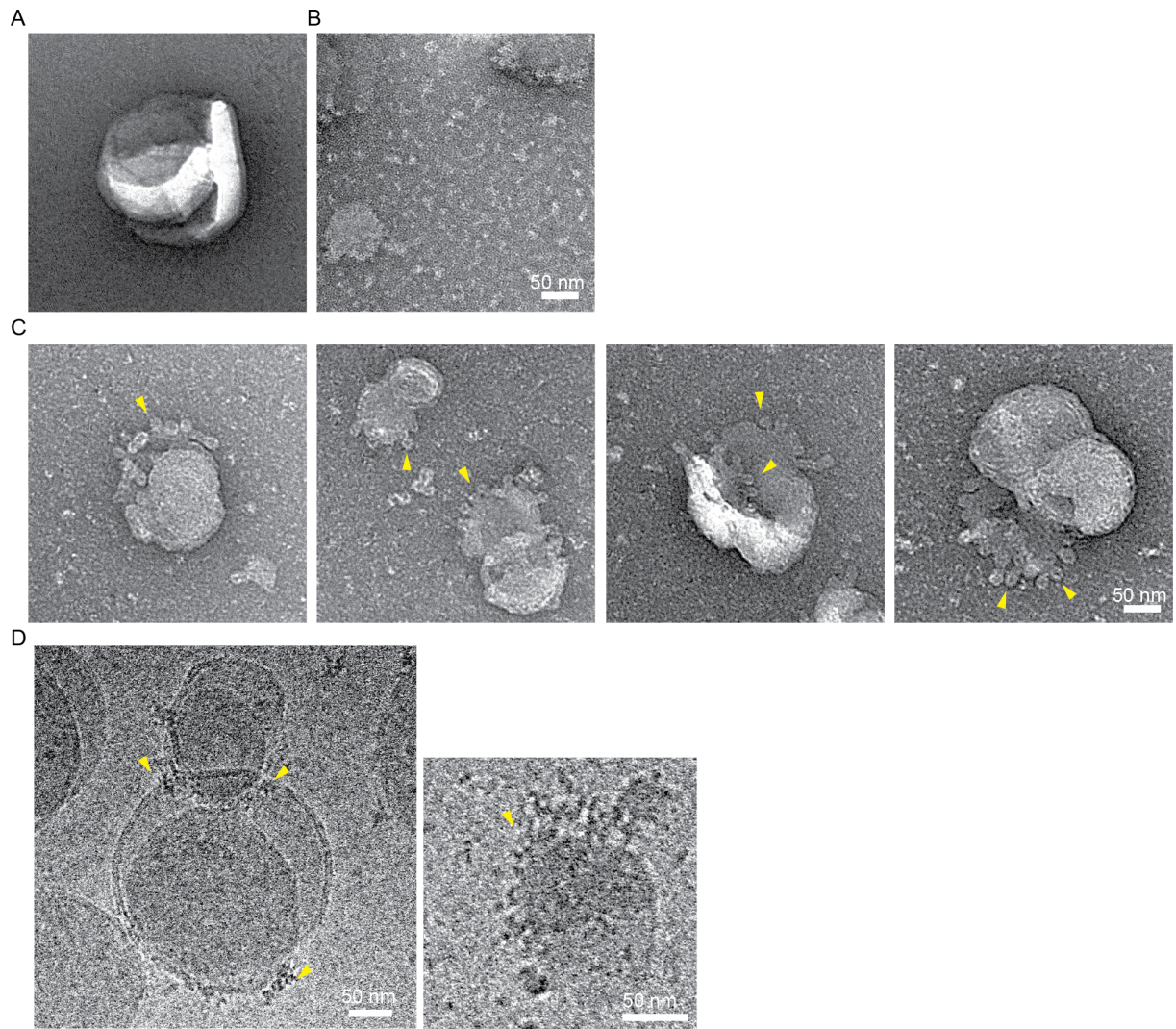
Figure 5 - EM observation of IFT172 with Folch fraction liposomes.

A. Negative-stain EM image of Folch fraction I liposomes as control. **B.** Negative-stain EM image of IFT172 (1 µM) with Folch fraction I liposomes (0.2 mM). The membrane got deformed into small pieces. **C.** Negative-stain EM images of IFT172 (250 nM) with Folch fraction I liposomes (0.2 mM) showing the remodeling of the membrane surface by IFT172. Small vesicles in ~20 nm (Yellow arrowheads) get pinched off from membrane surface. **D.** Cryo-EM images of IFT172 (500 nM) with Folch fraction I liposomes (0.4 mM).
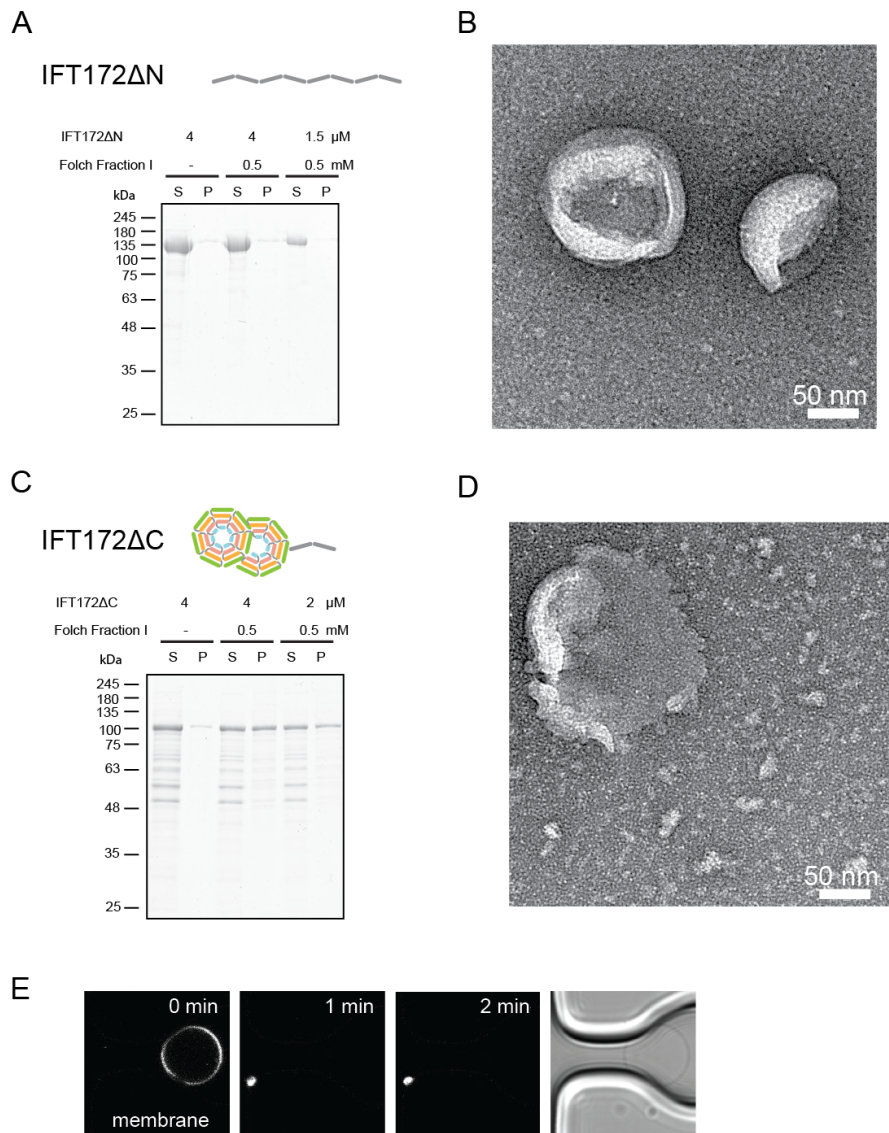
Figure 6 - IFT172 N-terminal beta propeller binds to membranes.

A. Co-sedimentation assay of IFT172ΔN with Folch fraction I MLV. IFT172ΔN shows no affinity to membranes. **B.** Negative-stain EM images of IFT172ΔN with Folch fraction I liposomes do not show remodeling of the membrane surface. **C.** Co-sedimentation assay of IFT172ΔC with Folch fraction I MLV. IFT172ΔC shows affinity to membrane. **D.** Negative-stain EM images of IFT172ΔC with Folch fraction I liposomes show the remodeling of the membrane surface. **E.** GUV observation of IFT172ΔC. GUV collapsed by adding IFT172ΔC.
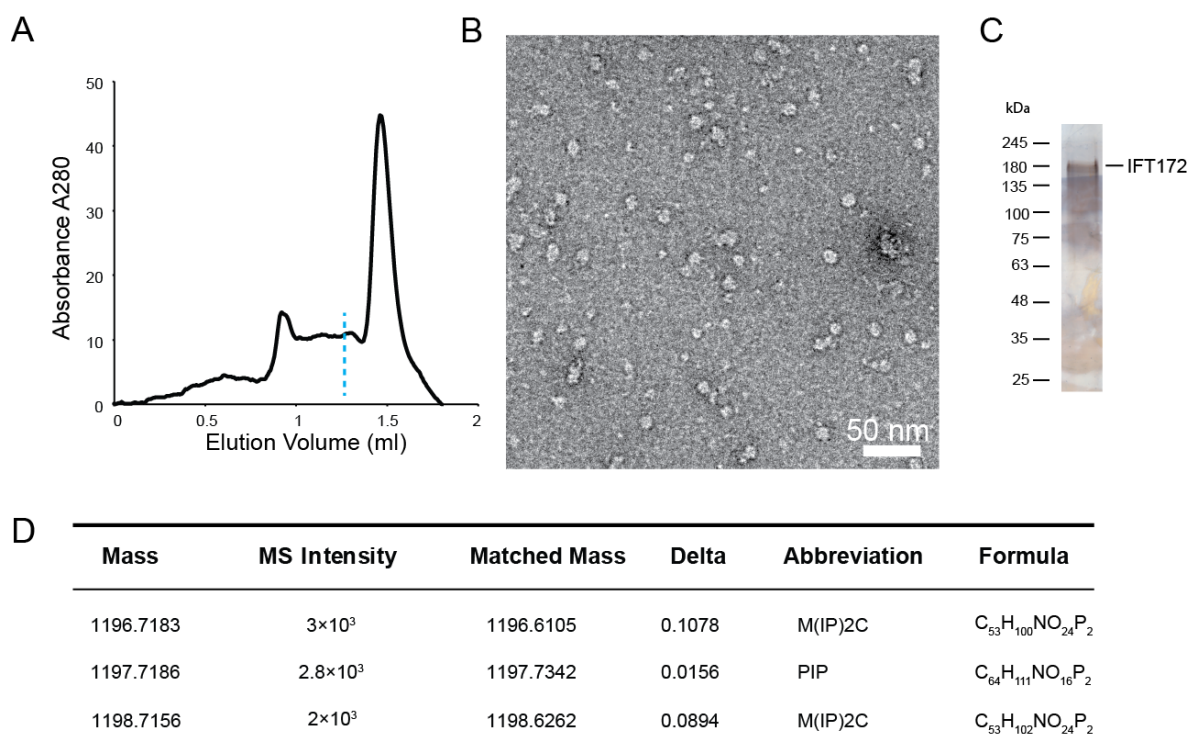
Figure 7 - IFT57 competes the binding of IFT172 to membrane.

A, B. Co-sedimentation assay of IFT172 with Folch fraction I MLV in presence of IFT57. The quantification (B) shows the amount of IFT172 decreased in presence of IFT57. **C.** Scheme representation of IFT172 interacting with IFT57 or membranes.

Mass	MS Intensity (×10^4)	Matched Mass	Delta	Abbreviation	Formula
786.5990	4	786.6008	0.0018	PC, PE	$C_{44}H_{85}NO_8P$
758.5694	4	758.5695	0.0001	PC, PE	$C_{42}H_{81}NO_8P$
788.6149	3	788.6164	0.0015	PC, PE	$C_{44}H_{87}NO_8P$
760.5825	2	760.5851	0.0026	PC, PE	$C_{42}H_{83}NO_8P$
744.5524	2	744.5538	0.0014	PC, PE	$C_{41}H_{79}NO_8P$

Supplementary Table - Mass spectrometry result of the purified IFT172 shows existence of lipids. Five most intense peaks are shown with molecular mass (Mass), and the intensity value (MS Intensity) detected by the mass spectrometry measurement. The mass was compared to known lipid masses using the online tool: http://www.lipidmaps.org/tools/index.html. "Delta" shows the difference between the input mass and the calculated mass. Abbreviation and Formula show the possible lipid species based on the molecule weight.

A

B

100 nm

C

100 nm

20 nm
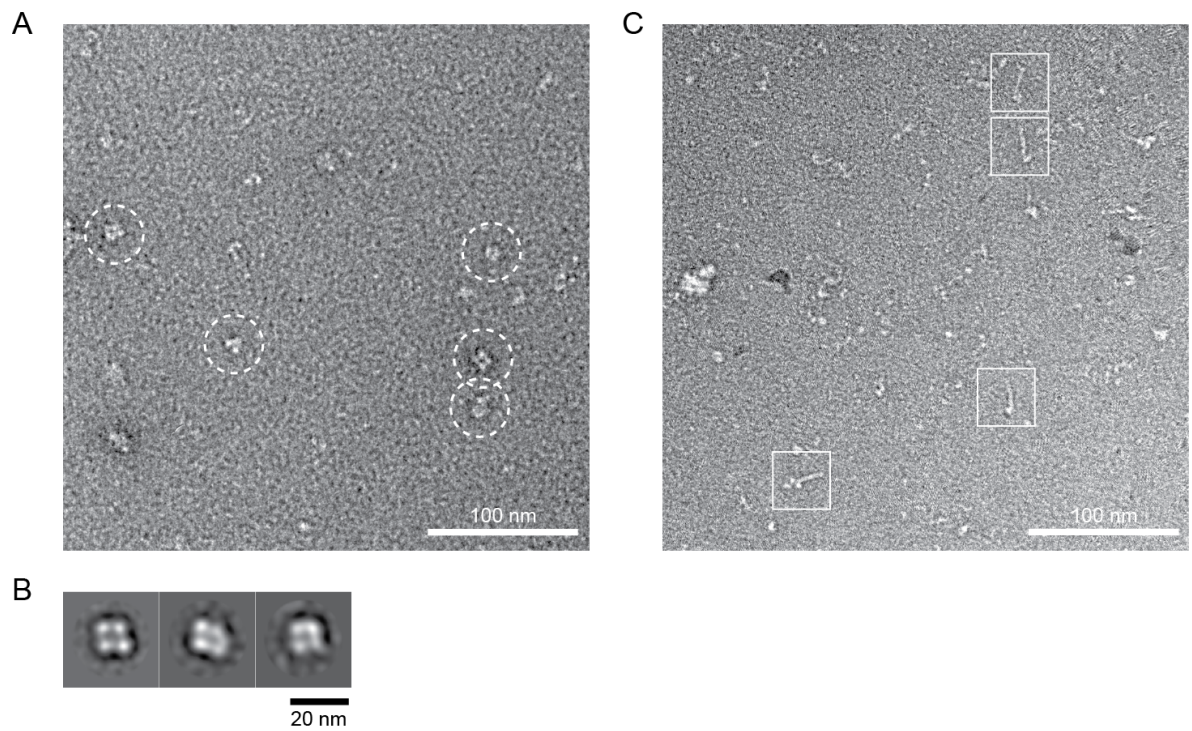
Supplementary Figure 1 - IFT172 monomer purified with additional aninon-exchange chromatography.

A and B. Negative-stain EM image (A) and 2D reference free class average of IFT172 monomer shows close conformation without DDM during purification. **C.** IFT172 employs the open conformation (marked with square) in the presence of DDM.

A. SEC profile

B. Negative staining micrograph

C. Silver-staining gel

D. Mass spectrometry table

Mass	MS Intensity	Matched Mass	Delta	Abbreviation	Formula
1196.7183	3×10^3	1196.6105	0.1078	M(IP)2C	$C_{53}H_{100}NO_{24}P_2$
1197.7186	2.8×10^3	1197.7342	0.0156	PIP	$C_{64}H_{111}NO_{16}P_2$
1198.7156	2×10^3	1198.6262	0.0894	M(IP)2C	$C_{53}H_{102}NO_{24}P_2$

Supplementary Figure 2 - Membrane remodeling products by IFT172 contain both IFT172 and lipids.

A. SEC profile of IFT172 with Folch Fraction I mixture. 10 µM of IFT172 was mixed with 2 mM Folch Fraction I and incubated for 10 min. The large lipid aggregation was removed by centrifugation before loading to the column. **B.** Negative staining micrograph of the fraction marked in A. **C.** Silver-staining gel of the fraction marked in A, indicating IFT172 is present in the fraction. **D.** Mass spectrometry result of the fraction shows existence of lipids.
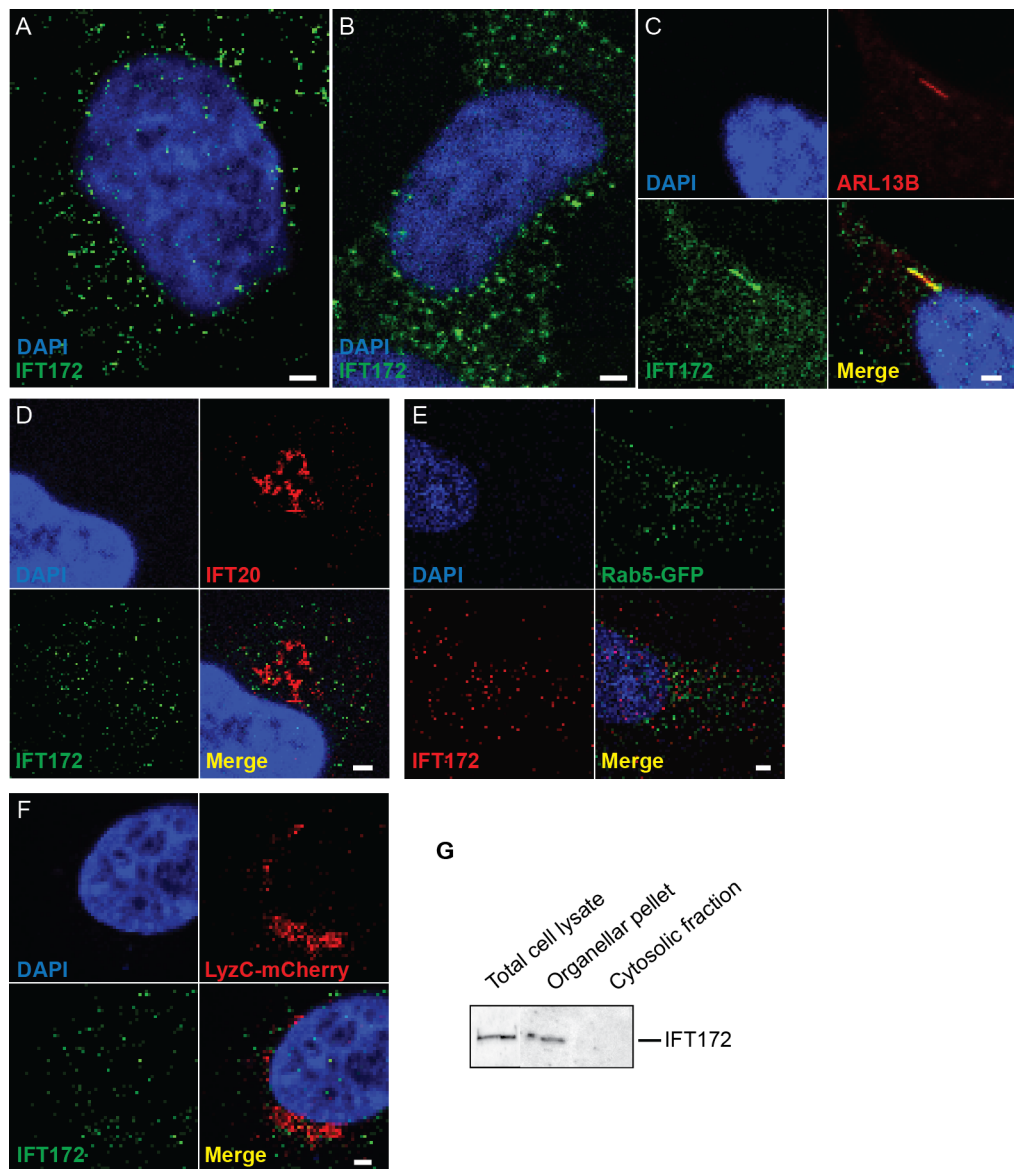
Supplementary Figure 3 - Subcellular localization of endogenous IFT172.

A and B. Antibody staining of IFT172 in Hela cell and RPE-1 cell, respectively. **C.** IFT172 and Arl13b showed co-localization in axoneme in 24 h-starved RPE-1 cells. **D, E and F.** No colocalization of IFT172 with IFT20 (D), overexpressed Rab5-GFP (E), and overexpressed LyzC-mCherry (F) in Hela cell. **G.** Western blotting of total cell lysate, organellar pellet, cytosolic fraction of RPE-1 cell. Antibody was used with dilution of 1:200. Scale bar: 2 μm

REFERENCES

Absalon S, Blisnick T, Kohl L, Toutirais G, Doré G, Julkowska D, Tavenet A & Bastin P (2008) Intraflagellar transport and functional analysis of genes required for flagellum formation in trypanosomes. *Mol Biol Cell* **19:** 929–944

Akashi K, Miyata H, Itoh H & Kinosita K (1996) Preparation of giant liposomes in physiological conditions and their characterization under an optical microscope. *Biophys. J.* **71:** 3242–3250

Avidor-Reiss T, Maer AM, Koundakjian E, Polyanovsky A, Keil T, Subramaniam S & Zuker CS (2004) Decoding cilia function: defining specialized genes required for compartmentalized cilia biogenesis. *Cell* **117:** 527–539

Beck R, Sun Z, Adolf F, Rutz C, Bassler J, Wild K, Sinning I, Hurt E, Brügger B, Béthune J & Wieland F (2008) Membrane curvature induced by Arf1-GTP is essential for vesicle formation. *Proc Natl Acad Sci USA* **105:** 11731–11736

Benmerah A (2013) The ciliary pocket. *Curr. Opin. Cell Biol.* **25:** 78–84

Braun DA & Hildebrandt F (2017) Ciliopathies. *Cold Spring Harb Perspect Biol* **9:**

Cole DG (2003) The intraflagellar transport machinery of Chlamydomonas reinhardtii. *Traffic* **4:** 435–442

Cole DG, Diener DR, Himelblau AL, Beech PL, Fuster JC & Rosenbaum JL (1998) Chlamydomonas kinesin-II-dependent intraflagellar transport (IFT): IFT particles contain proteins required for ciliary assembly in Caenorhabditis elegans sensory neurons. *J Cell Biol* **141:** 993–1008

Ding J, Shao L, Yao Y, Tong X, Liu H, Yue S, Xie L & Cheng SY (2017) DGKδ triggers endoplasmic reticulum release of IFT88-containing vesicles destined for the assembly of primary cilia. *Sci Rep* **7:** 5296

Dodonova SO, Diestelkoetter-Bachert P, Appen von A, Hagen WJH, Beck R, Beck M, Wieland F & Briggs JAG (2015) VESICULAR TRANSPORT. A structure of the COPI coat and the role of coat proteins in membrane vesicle assembly. *Science (New York, NY)* **349:** 195–198

Faini M, Beck R, Wieland FT & Briggs JAG (2013) Vesicle coats: structure, function, and general principles of assembly. *Trends Cell Biol* **23:** 279–288

Follit JA, Tuft RA, Fogarty KE & Pazour GJ (2006) The intraflagellar transport protein IFT20 is associated with the Golgi complex and is required for cilia assembly. *Mol Biol Cell* **17:** 3781–3792

Halbritter J, Bizet AA, Schmidts M, Porath JD, Braun DA, Gee HY, McInerney-Leo AM, Krug P, Filhol E, Davis EE, Airik R, Czarnecki PG, Lehman AM, Trnka P, Nitschké P, Bole-Feysot C, Schueler M, Knebelmann B, Burtey S, Szabó AJ, et al (2013) Defects in the IFT-B component IFT172 cause Jeune and Mainzer-Saldino syndromes in humans. *Am. J. Hum. Genet.* **93:** 915–925

Heymann JB & Belnap DM (2007) Bsoft: image processing and molecular modeling for electron microscopy. *J Struct Biol* **157:** 3–18

Huangfu D, Liu A, Rakeman AS, Murcia NS, Niswander L & Anderson KV (2003) Hedgehog signalling in the mouse requires intraflagellar transport proteins. *Nature* **426:** 83–87

Ishikawa H & Marshall WF (2011) Ciliogenesis: building the cell's antenna. *Nat Rev Mol Cell Biol* **12:** 222–234

Itzhak DN, Tyanova S, Cox J & Borner GH (2016) Global, quantitative and dynamic mapping of protein subcellular localization. *Elife* **5:**

Jékely G & Arendt D (2006) Evolution of intraflagellar transport from coated vesicles and autogenous origin of the eukaryotic cilium. *Bioessays* **28:** 191–198

Johnson KA & Rosenbaum JL (1992) Polarity of flagellar assembly in Chlamydomonas. *J Cell Biol* **119:** 1605–1611

Kelley LA, Mezulis S, Yates CM, Wass MN & Sternberg MJE (2015) The Phyre2 web portal for protein modeling, prediction and analysis. *Nat Protoc* **10:** 845–858

Kowal TJ & Falk MM (2015) Primary cilia found on HeLa and other cancer cells. *Cell Biol. Int.* **39:** 1341–1347

Kozminski KG, Beech PL & Rosenbaum JL (1995) The Chlamydomonas kinesin-like protein FLA10 is involved in motility associated with the flagellar membrane. *J Cell Biol* **131:** 1517–1527

Kozminski KG, Johnson KA, Forscher P & Rosenbaum JL (1993) A motility in the eukaryotic flagellum unrelated to flagellar beating. *Proc Natl Acad Sci USA* **90:** 5519–5523

Lee C & Goldberg J (2010) Structure of coatomer cage proteins and the relationship among COPI, COPII, and clathrin vesicle coats. *Cell* **142:** 123–132

Marshall WF & Rosenbaum JL (2001) Intraflagellar transport balances continuous turnover of outer doublet microtubules: implications for flagellar length control. *J Cell Biol* **155:** 405–414

McMahon HT & Mills IG (2004) COP and clathrin-coated vesicle budding: different pathways, common approaches. *Curr. Opin. Cell Biol.* **16:** 379–391

Morga B & Bastin P (2013) Getting to the heart of intraflagellar transport using Trypanosoma and Chlamydomonas models: the strength is in their differences. *Cilia* **2:** 16

Nager AR, Goldstein JS, Herranz-Pérez V, Portran D, Ye F, Garcia-Verdugo JM & Nachury MV (2017) An Actin Network Dispatches Ciliary GPCRs into Extracellular Vesicles to Modulate Signaling. *Cell* **168:** 252–263.e14

Nigg EA & Raff JW (2009) Centrioles, centrosomes, and cilia in health and disease.

Cell **139:** 663–678

Pazour GJ, Agrin N, Leszyk J & Witman GB (2005) Proteomic analysis of a eukaryotic cilium. *J Cell Biol* **170:** 103–113

Pedersen LB & Rosenbaum JL (2008) Intraflagellar transport (IFT) role in ciliary assembly, resorption and signalling. *Curr. Top. Dev. Biol.* **85:** 23–61

Pedersen LB, Miller MS, Geimer S, Leitch JM, Rosenbaum JL & Cole DG (2005) Chlamydomonas IFT172 is encoded by FLA11, interacts with CrEB1, and regulates IFT at the flagellar tip. *Curr Biol* **15:** 262–266

Pigino G, Geimer S, Lanzavecchia S, Paccagnini E, Cantele F, Diener DR, Rosenbaum JL & Lupetti P (2009) Electron-tomographic analysis of intraflagellar transport particle trains in situ. *J Cell Biol* **187:** 135–148

Piperno G & Mead K (1997) Transport of a novel complex in the cytoplasmic matrix of Chlamydomonas flagella. *Proc Natl Acad Sci USA* **94:** 4457–4462

Proteins of the ciliary axoneme are found on cytoplasmic membrane vesicles during growth of cilia. (2014) Proteins of the ciliary axoneme are found on cytoplasmic membrane vesicles during growth of cilia. **24:** 1114–1120 Available at: http://eutils.ncbi.nlm.nih.gov/entrez/eutils/elink.fcgi?dbfrom=pubmed&id=24814 148&retmode=ref&cmd=prlinks

Robinson T, Kuhn P, Eyer K & Dittrich PS (2013) Microfluidic trapping of giant unilamellar vesicles to study transport through a membrane pore. *Biomicrofluidics* **7:** 44105

Rosenbaum JL & Witman GB (2002) Intraflagellar transport. *Nat Rev Mol Cell Biol* **3:** 813–825

Rosenbaum JL, Moulder JE & Ringo DL (1969) Flagellar elongation and shortening in Chlamydomonas. The use of cycloheximide and colchicine to study the synthesis and assembly of flagellar proteins. *J Cell Biol* **41:** 600–619

Rout MP & Field MC (2017) The Evolution of Organellar Coat Complexes and Organization of the Eukaryotic Cell. *Annu. Rev. Biochem.* **86:** 637–657

Scheres SHW (2012) RELION: implementation of a Bayesian approach to cryo-EM structure determination. *J Struct Biol* **180:** 519–530

Schindelin J, Arganda-Carreras I, Frise E, Kaynig V, Longair M, Pietzsch T, Preibisch S, Rueden C, Saalfeld S, Schmid B, Tinevez J-Y, White DJ, Hartenstein V, Eliceiri K, Tomancak P & Cardona A (2012) Fiji: an open-source platform for biological-image analysis. *Nat. Methods* **9:** 676–682

Sedmak T & Wolfrum U (2010) Intraflagellar transport molecules in ciliary and nonciliary cells of the retina. *J Cell Biol* **189:** 171–186

Snead WT, Hayden CC, Gadok AK, Zhao C, Lafer EM, Rangamani P & Stachowiak JC (2017) Membrane fission by protein crowding. *Proc Natl Acad Sci USA* **114:**

E3258–E3267

Söding J, Biegert A & Lupas AN (2005) The HHpred interactive server for protein homology detection and structure prediction. *Nucleic Acids Res.* **33:** W244–8

Tang G, Peng L, Baldwin PR, Mann DS, Jiang W, Rees I & Ludtke SJ (2007) EMAN2: an extensible image processing suite for electron microscopy. *J Struct Biol* **157:** 38–46

Taschner M, Bhogaraju S & Lorentzen E (2012) Architecture and function of IFT complex proteins in ciliogenesis. *Differentiation* **83:** S12–22

Taschner M, Weber K, Mourão A, Vetter M, Awasthi M, Stiegler M, Bhogaraju S & Lorentzen E (2016) Intraflagellar transport proteins 172, 80, 57, 54, 38, and 20 form a stable tubulin-binding IFT-B2 complex. *EMBO J* **35:** 773–790

Tsao C-C & Gorovsky MA (2008) Different effects of Tetrahymena IFT172 domains on anterograde and retrograde intraflagellar transport. *Mol Biol Cell* **19:** 1450–1461

Veland IR, Awan A, Pedersen LB, Yoder BK & Christensen ST (2009) Primary cilia and signaling pathways in mammalian development, health and disease. *Nephron Physiol* **111:** p39–53

Wang J & Deretic D (2014) Molecular complexes that direct rhodopsin transport to primary cilia. *Prog Retin Eye Res* **38:** 1–19

Wang J, Silva M, Haas LA, Morsci NS, Nguyen KCQ, Hall DH & Barr MM (2014) C. elegans ciliated sensory neurons release extracellular vesicles that function in animal communication. *Curr Biol* **24:** 519–525

Wheatley DN (2005) Landmarks in the first hundred years of primary (9+0) cilium research. *Cell Biol. Int.* **29:** 333–339

Wood CR & Rosenbaum JL (2014) Proteins of the ciliary axoneme are found on cytoplasmic membrane vesicles during growth of cilia. *Curr Biol* **24:** 1114–1120

Wood CR & Rosenbaum JL (2015) Ciliary ectosomes: transmissions from the cell's antenna. *Trends Cell Biol* **25:** 276–285

Wood CR, Wang Z, Diener D, Zones JM, Rosenbaum J & Umen JG (2012) IFT proteins accumulate during cell division and localize to the cleavage furrow in Chlamydomonas. *PLoS ONE* **7:** e30729

2.2.2 Extended discussion

2.2.2.1 Involvement of IFT172 in membrane vesicles trafficking *in vivo*

Biochemical and biophysical experiments performed in this article indicate IFT172 has strong binding affinity for membranes and has the propensity to remodel membrane surfaces into small vesicles, which imply IFT172 might be involved in one of the vesicle trafficking pathways in cells. We sought to investigate functions of IFT172 in terms of its membrane binding property. Based on the observation that IFT20 is localized on the Golgi membrane in addition to the basal body and cilia, together with the proposed model that IFT proteins associate with outer surface of cytoplasmic vesicles and get delivered to cell membranes, we carried out experiments in cell to detect if IFT172 is involved in vesicles trafficking between Golgi membrane and cell membrane (Follit et al., 2006, Wood and Rosenbaum, 2014). First, we performed immunofluorescence microscopy experiments using Retina Pigmented Epithelium-1 (RPE-1) cells and Hela cells for subcellular location study. IFT172 was shown cytosolic puncta in wild type RPE-1 and Hela cells. To further identify if these cytosolic puncta are membrane vesicles trafficking between different membrane compartments, we carried out co-localization experiments of IFT172 and vesicle markers. IFT20 is an ideal marker since it has been known that IFT20 localizes to the Golgi complex. However, there was no co-localization observed between IFT20 and IFT172. Apart from IFT20, we also assessed if IFT172 co-localize with other cytoplasmic vesicles markers, including Rab5 and lysozyme C. Rab5 is a small GTPase and a key regulator in early endosomal trafficking, while lysozyme C is present in the vesicles from trans-Golgi network to the cell surface. Overexpressing Rab5 and lysozyme C in Hela cell followed by co-staining with IFT172 antibody, we did not see any co-localization between Rab5 and IFT172 or between lysozyme C and IFT172. Thus, IFT172 does not seem to be involved in these vesicle transport pathway. Recently it was found that IFT88 is associated with vesicles transporting from ER to cilia (Ding et al., 2017). Therefore, IFT proteins are required for multiple vesicle transport pathways. It would be exciting to detect where and how IFT172 perform the membrane binding property from functional point of view *in vivo* in the future.

IFT172 is not only expressed in ciliated cell, it is also present in some of the non-ciliated cell lines. The immunostaining of IFT172 antibody in U-2 OS, a non-ciliated cell line, showed the vesicle patterns according to the website 'THE HUMAN PROTEIN ATLAS'. We confirmed the results in our study with U-2 OS cells (Figure 10). However, it is still not clear yet the functions of IFT172 in these non-ciliated cell lines.
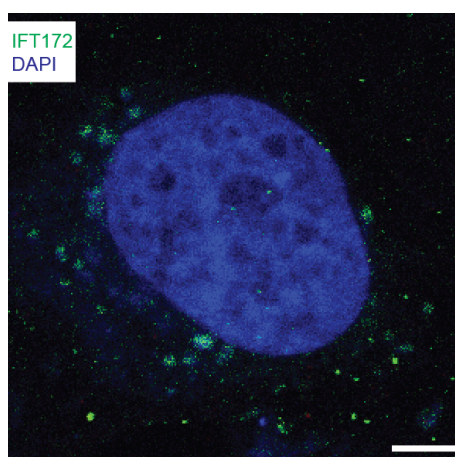

Figure 10. Subcellular localization of IFT172 in U-2 OS cells. Scale bar: 5 μm.

2.2.2.2 WD40 domain in IFT172 is a membrane-binding domain

To understand how IFT172 binds to the membrane, we performed truncation studies and we found that the N-terminal WD40 domains but not the C-terminal TPR repeats showed membrane-binding properties. WD40 domains are abundant in eukaryotic proteomes and play diverse cellular roles in signal transduction, RNA processing, and cell division. The WD40 domain is large with about 300 amino acids, which form β-propellers. β-propellers have three surfaces available for interactions: the top region, the bottom region and the circumference (Stirnimann et al., 2010). In this article we proposed that IFT172 binds to membrane due to the basic surface at the inner lumen based on homology modeling, but the exact mechanisms of membrane binding remain unclear. However, IFT172 is not the only WD40 containing protein showing membrane association. The yeast polarity protein Sro7, an allosteric regulator functions in fusion of secretory vesicles on the plasma membrane. Sro7 possesses two WD40 domains and a previous study showed Sro7 is associated with the plasma

membrane at the bud site. However, the mechanism of Sro7 membrane association is unknown (Lehman et al., 1999). One possibility is that the β-propellers of Sro7 contribute to the membrane association similar to IFT172 as described in this article.

IFT172 shares the same domain architectures with membrane-coated vesicle subunits and it has been proposed that IFT proteins and vesicle coat proteins share a common origin in an ancestral protocoatomer, as mentioned in the introduction. However, unlike IFT172, there is no direct evidence to show β-propeller and α-solenoid containing vesicle coat proteins associate with membrane compartments. Clathrin, COPI and COPII vesicles are initiated by small GTPases, which bind to membrane and in turn recruit coatomer through a direct interaction. For example, clathrin and COPI vesicle budding are initiated by Arf proteins; COPII vesicles are initiated by membrane-bound Sar1; and membrane coating by BBSome proteins are initiated by BBS3/Arl6 (Faini et al., 2013, Jin et al., 2010). Within IFT proteins, there are also two small GTPases present: IFT22 and IFT27. However, IFT22 and IFT27 have not been detected on any membrane compartment yet. Although there is no direct interaction reported between coatomer and membrane, the cryo-electron tomography of the COPI coat showed N-terminal β-propeller domains of β' subunits are positioned against the membrane (Dodonova et al., 2015). This observation suggests that there may be direct interaction between β-propeller domains and membrane, like the interaction of IFT172 with membrane.

IFT57 is the direct binding partner of IFT172 within IFT protein according to the biochemistry assay, probably via the β-propeller domains of IFT172 (Taschner et al., 2016). Our data showed that IFT172 has strong affinity to membrane, and IFT57 competes with membranes for the binding site on IFT172. One possibility is that IFT57 and lipids use the same binding site on IFT172, so IFT172 could not bind to both at the same time. The other possibility is IFT57 and membrane bind to two different positions on β-propeller domains, however, IFT172 has higher affinity to membrane and membrane association cause spatially hindrance for further IFT57 binding. Our result provides a framework for further dissection of multiple functions of IFT172.

3. Outlook

Microtubule dynamics are highly regulated with numerous microtubule-binding proteins spatially and temporally, to achieve its functions involving in multiple cellular activities. As a microtubule-stabilizing factor, p150^{glued} binds not only to acidic tails of tubulins through its CAP-Gly domain and basic patch, but also to microtubule plus-end tracking proteins CLIP170 and EB proteins. The interaction network between these proteins is important for recruiting dynein to microtubule plus ends in presence of the proteins that compete with p150^{glued} for EB binding. To better understand EB-dependent plus end tracking of dynein, it would be exciting to get high-resolution structures of p150^{glued} and EB proteins complex on microtubules, as well as EB proteins, CLIP170 and p150^{glued} complex on microtubules by reconstitution *in vitro*. Moreover, a recent cryo-EM structure of dynactin complex suggested dynactin adopting an autoinhibited state with its p150^{glued} CAP-Gly domain and the first coiled-coil buried in the groove of the dynactin shoulder, which inhibits the interaction with EB proteins (Urnavicius et al., 2015). This raised questions of how p150^{glued} in the dynactin complex mediate EB-dependent plus end tracking of dynein, whether other regulators are needed in this process.

IFT172 C-terminus was found to be required for IFT protein turnaround at the ciliary tip (Tsao and Gorovsky, 2008). In this article, it was found that IFT172 shows both an open conformation and a close conformation, most likely by closing up of the long C-terminus. It will be interesting to determine whether the conformation changing of IFT172 is involved in rearrangement and turnaround of the IFT proteins at ciliary tip. Regarding the membrane binding properties of IFT172, functional studies are needed to address the importance of IFT172 *in vivo*. It has been observed that there is a close association between IFT particles and ciliary membrane. Is it possible that IFT172 mediate the association of IFT complex with ciliary membrane? Furthermore, it was found IFT172 has a loose interaction with other IFT proteins, which implies that IFT172 may have distinct functions out of the IFT system. All these questions require dealing with functions and mechanisms of IFT172.

4. Abbreviations

^oC	Degree celsius
Δ	Deletion
a.a.	Amino acid (s)
APC	Adenomatous polyposis coil
BBS	Bardet-Biedl syndrome
C. elegans	Caenorhabditis elegans
CAP-Gly	Cytoskeleton-associated protein Gly-rich
CH domain	Calponin homology domain
CHO	Chinese hamster ovary
CLASP	CLIP170 associated protein
CLIPs	Cytoplasmic linker proteins
Cryo-EM	Cryo electron microscopy
Da	Dalton
DGKδ	Diacylglycerol kinase δ
DLS	Dynamic light scattering
DMSO	Dimethyl sulfoxide
DTT	Dithiothreitol
EBs	End-binding proteins
E. coil	*Escherichia coil*
ER	Endoplasmic reticulum
g	Gram or gravitational acceleration on earth's surface
GTP	Guanosine triphosphate
GUV	Giant unilamellar vesicles
HEPES	2-[4-(2-hydroxyethyl)-1-piperazinyl]-ethanesulfonic acid
JBTS	Joubert syndrome
IDA	Inner dynein arm

IFT	Intraflagellar transport
IPTG	Isopropyl ß-D-1-thiogalactopyranoside
LUV	Large unilamellar vesicle
M	Molar
MACF	Microtubule-actin crosslinking factor
MT	Microtubule
MTOC	Microtubule-organization center
MW	Molecular weight
NPC	Nuclear pore complex
NPHP	Nephronophthisis
ODA	Outer dynein arm
PE	Phosphatidylethanolamine
PKD	Polycystic kidney disease
PTMs	Posttranslational modifications
SDS	Sodium dodecyl sulfate
SEM	Scanning electron micrograph
SxIP	Ser-any amino acid-Ile-Pro
TBCB/TBCE	Tubulin-folding cofactor B/E
+TIPs	Microtubule plus-end tracking proteins
TOG	Tumour overexpressed gene
TPR	Tetratricopeptide repeat
XMAP215	Xenopus microtubule-associated protein

5. References

AHMED, N. T. & MITCHELL, D. R. 2005. ODA16p, a Chlamydomonas flagellar protein needed for dynein assembly. *Mol Biol Cell,* 16**,** 5004-12.

AKHMANOVA, A., HOOGENRAAD, C. C., DRABEK, K., STEPANOVA, T., DORTLAND, B., VERKERK, T., VERMEULEN, W., BURGERING, B. M., DE ZEEUW, C. I., GROSVELD, F. & GALJART, N. 2001. Clasps are CLIP-115 and -170 associating proteins involved in the regional regulation of microtubule dynamics in motile fibroblasts. *Cell,* 104, 923-35.

AHMED, N. T. & MITCHELL, D. R. 2005. ODA16p, a Chlamydomonas flagellar protein needed for dynein assembly. *Mol Biol Cell,* 16**,** 5004-12.

AKHMANOVA, A. & STEINMETZ, M. O. 2008. Tracking the ends: a dynamic protein network controls the fate of microtubule tips. *Nat Rev Mol Cell Biol,* 9, 309-22.

AKHMANOVA, A. & STEINMETZ, M. O. 2010. Microtubule plus TIPs at a glance. *Journal of Cell Science,* 123, 3415-3419.

AKHMANOVA, A. & STEINMETZ, M. O. 2015. Control of microtubule organization and dynamics: two ends in the limelight. *Nat Rev Mol Cell Biol,* 16, 711-26.

ARCE, C. A., RODRIGUEZ, J. A., BARRA, H. S. & CAPUTTO, R. 1975. Incorporation of L-Tyrosine, L-Phenylalanine and L-3,4-Dihydroxyphenylalanine as Single Units into Rat-Brain Tubulin. *European Journal of Biochemistry*, 59, 145-149.

ARNAL, I., HEICHETTE, C., DIAMANTOPOULOS, G. S. & CHRETIEN, D. 2004. CLIP-170/tubulin-curved oligomers coassemble at microtubule ends and promote rescues. *Curr Biol,* 14, 2086-95.

ASKHAM, J. M. & MORRISON, E. E. 2002. Evidence that an interaction between EB1 and p150(Glued) is required for the formation and maintenance of a radial microtubule array anchored at the centrosome. *Molecular Biology of the Cell,* 13, 186A-186A.

AYAZ, P., YE, X. C., HUDDLESTON, P., BRAUTIGAM, C. A. & RICE, L. M. 2012. A TOG:alpha beta-tubulin Complex Structure Reveals Conformation-Based Mechanisms for a Microtubule Polymerase. *Science,* 337, 857-860.

BADANO, J. L., MITSUMA, N., BEALES, P. L. & KATSANIS, N. 2006. The ciliopathies: an emerging class of human genetic disorders. *Annu Rev Genomics Hum Genet,* 7, 125-48.

BADIN-LARCON, A. C., BOSCHERON, C., SOLEILHAC, J. M., PIEL, M., MANN, C., DENARIER, E., FOUREST-LIEUVIN, A., LAFANECHERE, L., BORNENS, M. & JOB, D. 2004. Suppression of nuclear oscillations in Saccharomyces cerevisiae expressing Glu tubulin. *Proc Natl Acad Sci U S A,* 101, 5577-82.

BARBOSA, D. J., DURO, J., PREVO, B., CHEERAMBATHUR, D. K., CARVALHO, A. X. & GASSMANN, R. 2017. Dynactin binding to tyrosinated microtubules promotes centrosome centration in C. elegans by enhancing dynein-mediated organelle transport. *PLoS Genet,* 13, e1006941.

BENMERAH, A. 2013. The ciliary pocket. *Curr Opin Cell Biol,* 25, 78-84.

BHOGARAJU, S., CAJANEK, L., FORT, C., BLISNICK, T., WEBER, K., TASCHNER, M., MIZUNO, N., LAMLA, S., BASTIN, P., NIGG, E. A. & LORENTZEN, E. 2013. Molecular Basis of Tubulin Transport Within the Cilium by IFT74 and IFT81. *Science,* 341, 1009-1012.

BIELING, P., KANDELS-LEWIS, S., TELLEY, I. A., VAN DIJK, J., JANKE, C. & SURREY, T. 2008. CLIP-170 tracks growing microtubule ends by dynamically recognizing composite EB1/tubulin-binding sites. *Journal of Cell Biology,* 183, 1223-1233.

BIELING, P., LAAN, L., SCHEK, H., MUNTEANU, E. L., SANDBLAD, L., DOGTEROM, M., BRUNNER, D. & SURREY, T. 2007. Reconstitution of a microtubule plus-end tracking system in vitro. *Nature,* 450, 1100-5.

BLACQUE, O. E., LI, C., INGLIS, P. N., ESMAIL, M. A., OU, G., MAH, A. K., BAILLIE, D. L., SCHOLEY, J. M. & LEROUX, M. R. 2006. The WD repeat-containing protein IFTA-1 is required for retrograde intraflagellar transport. *Mol Biol Cell,* 17, 5053-62.

BLACQUE, O. E., REARDON, M. J., LI, C., MCCARTHY, J., MAHJOUB, M. R., ANSLEY, S. J., BADANO, J. L., MAH, A. K., BEALES, P. L., DAVIDSON, W. S., JOHNSEN, R. C., AUDEH, M., PLASTERK, R. H., BAILLIE, D. L.,

KATSANIS, N., QUARMBY, L. M., WICKS, S. R. & LEROUX, M. R. 2004. Loss of C. elegans BBS-7 and BBS-8 protein function results in cilia defects and compromised intraflagellar transport. *Genes Dev,* 18, 1630-42.

BRAUN, D. A. & HILDEBRANDT, F. 2017. Ciliopathies. *Cold Spring Harb Perspect Biol,* 9.

BROOKS, E. R. & WALLINGFORD, J. B. 2014. Multiciliated Cells. *Current Biology,* 24**,** R973-R982.

BROUHARD, G. J., STEAR, J. H., NOETZEL, T. L., AL-BASSAM, J., KINOSHITA, K., HARRISON, S. C., HOWARD, J. & HYMAN, A. A. 2008. XMAP215 is a processive microtubule polymerase. *Cell,* 132, 79-88.

CEMERSKI, S. & SHAW, A. 2006. Immune synapses in T-cell activation. *Curr Opin Immunol,* 18**,** 298-304.

CHU, C. W., HOU, F., ZHANG, J., PHU, L., LOKTEV, A. V., KIRKPATRICK, D. S., JACKSON, P. K., ZHAO, Y. & ZOU, H. 2011. A novel acetylation of beta-tubulin by San modulates microtubule polymerization via down-regulating tubulin incorporation. *Mol Biol Cell,* 22**,** 448-56.

COLE, D. G., DIENER, D. R., HIMELBLAU, A. L., BEECH, P. L., FUSTER, J. C. & ROSENBAUM, J. L. 1998. Chlamydomonas kinesin-II-dependent intraflagellar transport (IFT): IFT particles contain proteins required for ciliary assembly in Caenorhabditis elegans sensory neurons. *J Cell Biol,* 141, 993-1008.

CRAFT, J. M., HARRIS, J. A., HYMAN, S., KNER, P. & LECHTRECK, K. F. 2015. Tubulin transport by IFT is upregulated during ciliary growth by a cilium-autonomous mechanism. *Journal of Cell Biology,* 208, 223-237.

CULVER-HANLON, T. L., LEX, S. A., STEPHENS, A. D., QUINTYNE, N. J. & KING, S. J. 2006. A microtubule-binding domain in dynactin increases dynein processivity by skating along microtubules. *Nat Cell Biol,* 8, 264-70.

DEACON, S. W., SERPINSKAYA, A. S., VAUGHAN, P. S., FANARRAGA, M. L., VERNOS, I., VAUGHAN, K. T. & GELFAND, V. I. 2003. Dynactin is required for bidirectional organelle transport. *Journal of Cell Biology,* 160, 297-301.

DESAI, A. & MITCHISON, T. J. 1997. Microtubule polymerization dynamics. *Annu Rev Cell Dev Biol,* 13, 83-117.

DEVOS, D., DOKUDOVSKAYA, S., ALBER, F., WILLIAMS, R., CHAIT, B. T., SALI, A. & ROUT, M. P. 2004. Components of coated vesicles and nuclear pore complexes share a common molecular architecture. *PLoS Biol,* 2, e380.

DIKOVSKAYA, D., ZUMBRUNN, J., PENMAN, G. A. & NATHKE, I. S. 2001. The adenomatous polyposis coli protein: in the limelight out at the edge. *Trends in Cell Biology,* 11, 378-384.

DING, J., SHAO, L., YAO, Y., TONG, X., LIU, H., YUE, S., XIE, L. & CHENG, S. Y. 2017. DGKdelta triggers endoplasmic reticulum release of IFT88-containing vesicles destined for the assembly of primary cilia. *Sci Rep,* 7, 5296.

DODONOVA, S. O., DIESTELKOETTER-BACHERT, P., VON APPEN, A., HAGEN, W. J., BECK, R., BECK, M., WIELAND, F. & BRIGGS, J. A. 2015. VESICULAR TRANSPORT. A structure of the COPI coat and the role of coat proteins in membrane vesicle assembly. *Science,* 349, 195-8.

DRUMMOND, I. A. 2012. Cilia functions in development. *Current Opinion in Cell Biology,* 24, 24-30.

DUELLBERG, C., TROKTER, M., JHA, R., SEN, I., STEINMETZ, M. O. & SURREY, T. 2014. Reconstitution of a hierarchical +TIP interaction network controlling microtubule end tracking of dynein. *Nat Cell Biol,* 16, 804-11.

EFIMENKO, E., BLACQUE, O. E., OU, G., HAYCRAFT, C. J., YODER, B. K., SCHOLEY, J. M., LEROUX, M. R. & SWOBODA, P. 2006. Caenorhabditis elegans DYF-2, an orthologue of human WDR19, is a component of the intraflagellar transport machinery in sensory cilia. *Mol Biol Cell,* 17, 4801-11.

EGGENSCHWILER, J. T. & ANDERSON, K. V. 2007. Cilia and developmental signaling. *Annu Rev Cell Dev Biol,* 23, 345-73.

EGUETHER, T., SAN AGUSTIN, J. T., KEADY, B. T., JONASSEN, J. A., LIANG, Y., FRANCIS, R., TOBITA, K., JOHNSON, C. A., ABDELHAMED, Z. A., LO, C. W. & PAZOUR, G. J. 2014. IFT27 links the BBSome to IFT for maintenance of the ciliary signaling compartment. *Dev Cell,* 31, 279-90.

ERSFELD, K., WEHLAND, J., PLESSMANN, U., DODEMONT, H., GERKE, V. & WEBER, K. 1993. Characterization of the tubulin-tyrosine ligase. *J Cell Biol,* 120**,** 725-32.

FAINI, M., BECK, R., WIELAND, F. T. & BRIGGS, J. A. G. 2013. Vesicle coats: structure, function, and general principles of assembly. *Trends in Cell Biology,* 23, 279-288.

FAN, Z. C., BEHAL, R. H., GEIMER, S., WANG, Z., WILLIAMSON, S. M., ZHANG, H., COLE, D. G. & QIN, H. 2010. Chlamydomonas IFT70/CrDYF-1 is a core component of IFT particle complex B and is required for flagellar assembly. *Mol Biol Cell,* 21, 2696-706.

FINETTI, F., PACCANI, S. R., RIPARBELLI, M. G., GIACOMELLO, E., PERINETTI, G., PAZOUR, G. J., ROSENBAUM, J. L. & BALDARI, C. T. 2009. Intraflagellar transport is required for polarized recycling of the TCR/CD3 complex to the immune synapse. *Nature Cell Biology,* 11, 1332-U163.

FLIEGAUF, M., BENZING, T. & OMRAN, H. 2007. Mechanisms of disease - When cilia go bad: cilia defects and ciliopathies. *Nature Reviews Molecular Cell Biology,* 8, 880-893.

FOLKER, E. S., BAKER, B. M. & GOODSON, H. V. 2005. Interactions between CLIP-170, tubulin, and microtubules: Implications for the mechanism of CLIP-170 plus-end tracking behavior. *Molecular Biology of the Cell,* 16, 5373-5384.

FOLLIT, J. A., SAN AGUSTIN, J. T., XU, F., JONASSEN, J. A., SAMTANI, R., LO, C. W. & PAZOUR, G. J. 2008. The Golgin GMAP210/TRIP11 anchors IFT20 to the Golgi complex. *PLoS Genet,* 4, e1000315.

FOLLIT, J. A., TUFT, R. A., FOGARTY, K. E. & PAZOUR, G. J. 2006. The intraflagellar transport protein IFT20 is associated with the Golgi complex and is required for cilia assembly. *Mol Biol Cell,* 17, 3781-92.

FOLLIT, J. A., XU, F., KEADY, B. T. & PAZOUR, G. J. 2009. Characterization of mouse IFT complex B. *Cell Motil Cytoskeleton,* 66, 457-68.

FU, M. M. & HOLZBAUR, E. L. 2014. Integrated regulation of motor-driven organelle transport by scaffolding proteins. *Trends Cell Biol,* 24, 564-74.

FUJIWARA, M., ISHIHARA, T. & KATSURA, I. 1999. A novel WD40 protein, CHE-2, acts cell-autonomously in the formation of C. elegans sensory cilia. *Development,* 126, 4839-48.

GADADHAR, S., BODAKUNTLA, S., NATARAJAN, K. & JANKE, C. 2017. The tubulin code at a glance. *Journal of Cell Science,* 130, 1347-1353.

GIBBONS, B. H., ASAI, D. J., TANG, W. J., HAYS, T. S. & GIBBONS, I. R. 1994. Phylogeny and expression of axonemal and cytoplasmic dynein genes in sea urchins. *Mol Biol Cell,* 5, 57-70.

GIBBONS, I. R. 1981. Cilia and flagella of eukaryotes. *J Cell Biol,* 91, 107s-124s.

GILULA, N. B. & SATIR, P. 1972. The ciliary necklace. A ciliary membrane specialization. *J Cell Biol,* 53, 494-509.

GOETZ, S. C. & ANDERSON, K. V. 2010. The primary cilium: a signalling centre during vertebrate development. *Nature Reviews Genetics,* 11, 331-344.

HAO, L., THEIN, M., BRUST-MASCHER, I., CIVELEKOGLU-SCHOLEY, G., LU, Y., ACAR, S., PREVO, B., SHAHAM, S. & SCHOLEY, J. M. 2011. Intraflagellar transport delivers tubulin isotypes to sensory cilium middle and distal segments. *Nat Cell Biol,* 13, 790-8.

HAYCRAFT, C. J., SCHAFER, J. C., ZHANG, Q., TAULMAN, P. D. & YODER, B. K. 2003. Identification of CHE-13, a novel intraflagellar transport protein required for cilia formation. *Exp Cell Res,* 284, 251-63.

HAYCRAFT, C. J., SWOBODA, P., TAULMAN, P. D., THOMAS, J. H. & YODER, B. K. 2001. The C. elegans homolog of the murine cystic kidney disease gene Tg737 functions in a ciliogenic pathway and is disrupted in osm-5 mutant worms. *Development,* 128, 1493-505.

HEUSER, T., RAYTCHEV, M., KRELL, J., PORTER, M. E. & NICASTRO, D. 2009. The dynein regulatory complex is the nexin link and a major regulatory node in cilia and flagella. *Journal of Cell Biology,* 187, 921-933.

HILDEBRANDT, F., BENZING, T. & KATSANIS, N. 2011. Ciliopathies. *N Engl J Med,* 364, 1533-43.

HONNAPPA, S., JOHN, C. M., KOSTREWA, D., WINKLER, F. K. & STEINMETZ, M. O. 2005. Structural insights into the EB1-APC interaction (vol 24, pg 261, 2005). *Embo Journal,* 24, 872-872.

HONNAPPA, S., OKHRIMENKO, O., JAUSSI, R., JAWHARI, H., JELESAROV, I., WINKLER, F. K. & STEINMETZ, M. O. 2006. Key interaction modes of dynamic +TIP networks. *Mol Cell,* 23, 663-71.

HOU, Y. Q., QIN, H. M., FOLLIT, J. A., PAZOUR, G. J., ROSENBAUM, J. L. & WITMAN, G. B. 2007. Functional analysis of an individual IFT protein: IFT46 is required for transport of outer dynein arms into flagella. *Journal of Cell Biology,* 176**,** 653-665.

HOWES, S. C., ALUSHIN, G. M., SHIDA, T., NACHURY, M. V. & NOGALES, E. 2014. Effects of tubulin acetylation and tubulin acetyltransferase binding on microtubule structure. *Mol Biol Cell,* 25**,** 257-66.

HOYLE, H. D., TURNER, F. R. & RAFF, E. C. 2008. Axoneme-dependent tubulin modifications in singlet microtubules of the Drosophila sperm tail. *Cell Motil Cytoskeleton,* 65, 295-313.

HU, Q. & NELSON, W. J. 2011. Ciliary diffusion barrier: the gatekeeper for the primary cilium compartment. *Cytoskeleton (Hoboken),* 68, 313-24.

HUANGFU, D., LIU, A., RAKEMAN, A. S., MURCIA, N. S., NISWANDER, L. & ANDERSON, K. V. 2003. Hedgehog signalling in the mouse requires intraflagellar transport proteins. *Nature,* 426, 83-7.

HYMAN, A. A., SALSER, S., DRECHSEL, D. N., UNWIN, N. & MITCHISON, T. J. 1992. Role of GTP hydrolysis in microtubule dynamics: information from a slowly hydrolyzable analogue, GMPCPP. *Mol Biol Cell,* 3, 1155-67.

IOMINI, C., BABAEV-KHAIMOV, V., SASSAROLI, M. & PIPERNO, G. 2001. Protein particles in Chlamydomonas flagella undergo a transport cycle consisting of four phases. *J Cell Biol,* 153**,** 13-24.

ISHIKAWA, H., IDE, T., YAGI, T., JIANG, X., HIRONO, M., SASAKI, H., YANAGISAWA, H., WEMMER, K. A., STAINIER, D. Y., QIN, H., KAMIYA, R. & MARSHALL, W. F. 2014. TTC26/DYF13 is an intraflagellar transport protein required for transport of motility-related proteins into flagella. *Elife,* 3, e01566.

ISHIKAWA, H. & MARSHALL, W. F. 2011. Ciliogenesis: building the cell's antenna. *Nat Rev Mol Cell Biol,* 12, 222-34.

ISHIKAWA, H. & MARSHALL, W. F. 2017. Intraflagellar Transport and Ciliary Dynamics. *Cold Spring Harb Perspect Biol,* 9.

ISHIKAWA, T. 2017. Axoneme Structure from Motile Cilia. *Cold Spring Harb Perspect Biol,* 9.

JANKE, C. 2014. The tubulin code: molecular components, readout mechanisms, and functions. *J Cell Biol,* 206, 461-72.

JEKELY, G. & ARENDT, D. 2006. Evolution of intraflagellar transport from coated vesicles and autogenous origin of the eukaryotic cilium. *Bioessays,* 28, 191-198.

JIANG, K. & AKHMANOVA, A. 2011. Microtubule tip-interacting proteins: a view from both ends. *Current Opinion in Cell Biology,* 23, 94-101.

JIANG, K., WANG, J. Y., LIU, J., WARD, T., WORDEMAN, L., DAVIDSON, A., WANG, F. S. & YAO, X. B. 2009. TIP150 interacts with and targets MCAK at the microtubule plus ends. *Embo Reports,* 10, 857-865.

JIN, H., WHITE, S. R., SHIDA, T., SCHULZ, S., AGUIAR, M., GYGI, S. P., BAZAN, J. F. & NACHURY, M. V. 2010. The Conserved Bardet-Biedl Syndrome Proteins Assemble a Coat that Traffics Membrane Proteins to Cilia. *Cell,* 141, 1208-U198.

JOHNSON, K. A. 1998. The axonemal microtubules of the Chlamydomonas flagellum differ in tubulin isoform content. *J Cell Sci,* 111 (Pt 3), 313-20.

JOHNSON, K. A. & ROSENBAUM, J. L. 1992. Polarity of flagellar assembly in Chlamydomonas. *J Cell Biol,* 119, 1605-11.

KARDON, J. R., RECK-PETERSON, S. L. & VALE, R. D. 2009. Regulation of the processivity and intracellular localization of Saccharomyces cerevisiae dynein by dynactin. *Proc Natl Acad Sci U S A,* 106, 5669-74.

KERSSEMAKERS, J. W. J., MUNTEANU, E. L., LAAN, L., NOETZEL, T. L., JANSON, M. E. & DOGTEROM, M. 2006. Assembly dynamics of microtubules at molecular resolution. *Nature,* 442, 709-712.

KIM, H., LING, S. C., ROGERS, G. C., KURAL, C., SELVIN, P. R., ROGERS, S. L. & GELFAND, V. I. 2007. Microtubule binding by dynactin is required for microtubule organization but not cargo transport. *Journal of Cell Biology,* 176, 641-651.

KING, S. J., BROWN, C. L., MAIER, K. C., QUINTYNE, N. J. & SCHROER, T. A. 2003. Analysis of the dynein-dynactin interaction in vitro and in vivo. *Molecular Biology of the Cell,* 14, 5089-5097.

KING, S. J. & SCHROER, T. A. 2000. Dynactin increases the processivity of the cytoplasmic dynein motor. *Nat Cell Biol,* 2, 20-4.

KITA, K., WITTMANN, T., NATHKE, I. S. & WATERMAN-STORER, C. M. 2006. Adenomatous polyposis coli in cell extensions can promote with or without EB1. *Molecular Biology of the Cell,* 17, 2331-2345.

KUBO, T., BROWN, J. M., BELLVE, K., CRAIGE, B., CRAFT, J. M., FOGARTY, K., LECHTRECK, K. F. & WITMAN, G. B. 2016. Together, the IFT81 and IFT74 N-termini form the main module for intraflagellar transport of tubulin. *J Cell Sci,* 129**,** 2106-19.

KODAMA, A., KARAKESISOGLOU, I., WONG, E., VAEZI, A. & FUCHS, E. 2003. ACF7: an essential integrator of microtubule dynamics. *Cell,* 115, 343-54.

KOMAROVA, Y. A., AKHMANOVA, A. S., KOJIMA, S., GALJART, N. & BORISY, G. G. 2002. Cytoplasmic linker proteins promote microtubule rescue in vivo. *J Cell Biol,* 159, 589-99.

KOZMINSKI, K. G., BEECH, P. L. & ROSENBAUM, J. L. 1995. The Chlamydomonas kinesin-like protein FLA10 is involved in motility associated with the flagellar membrane. *J Cell Biol,* 131, 1517-27.

KOZMINSKI, K. G., JOHNSON, K. A., FORSCHER, P. & ROSENBAUM, J. L. 1993. A motility in the eukaryotic flagellum unrelated to flagellar beating. *Proc Natl Acad Sci U S A,* 90, 5519-23.

LAMPERT, F., HORNUNG, P. & WESTERMANN, S. 2010. The Dam1 complex confers microtubule plus end-tracking activity to the Ndc80 kinetochore complex. *J Cell Biol,* 189, 641-9.

LANSBERGEN, G., KOMAROVA, Y., MODESTI, M., WYMAN, C., HOOGENRAAD, C. C., GOODSON, H. V., LEMAITRE, R. P., DRECHSEL, D. N., VAN MUNSTER, E., GADELLA, T. W., JR., GROSVELD, F., GALJART, N., BORISY, G. G. & AKHMANOVA, A. 2004. Conformational changes in CLIP-170 regulate its binding to microtubules and dynactin localization. *J Cell Biol,* 166, 1003-14.

LAZARUS, J. E., MOUGHAMIAN, A. J., TOKITO, M. K. & HOLZBAUR, E. L. F. 2013. Dynactin Subunit p150(Glued) Is a Neuron-Specific Anti-Catastrophe Factor. *Plos Biology,* 11.

LECHTRECK, K. F., JOHNSON, E. C., SAKAI, T., COCHRAN, D., BALLIF, B. A., RUSH, J., PAZOUR, G. J., IKEBE, M. & WITMAN, G. B. 2009. The Chlamydomonas reinhardtii BBSome is an IFT cargo required for export of specific signaling proteins from flagella. *Journal of Cell Biology,* 187**,** 1117-1132.

LEHMAN, K., ROSSI, G., ADAMO, J. E. & BRENNWALD, P. 1999. Yeast homologues of tomosyn and lethal giant larvae function in exocytosis and are associated with the plasma membrane SNARE, Sec9. *J Cell Biol,* 146, 125-40.

LHERNAULT, S. W. & ROSENBAUM, J. L. 1985. Chlamydomonas Alpha-Tubulin Is Posttranslationally Modified by Acetylation on the Epsilon-Amino Group of a Lysine. *Biochemistry,* 24**,** 473-478.

LI, S., FERNANDEZ, J. J., MARSHALL, W. F. & AGARD, D. A. 2012. Three-dimensional structure of basal body triplet revealed by electron cryo-tomography. *EMBO J,* 31**,** 552-62.

LI, S., FINLEY, J., LIU, Z. J., QIU, S. H., CHEN, H., LUAN, C. H., CARSON, M., TSAO, J., JOHNSON, D., LIN, G., ZHAO, J., THOMAS, W., NAGY, L. A., SHA, B., DELUCAS, L. J., WANG, B. C. & LUO, M. 2002. Crystal structure of the cytoskeleton-associated protein glycine-rich (CAP-Gly) domain. *J Biol Chem,* 277, 48596-601.

LI, S. H., GUTEKUNST, C. A., HERSCH, S. M. & LI, X. J. 1998. Interaction of huntingtin-associated protein with dynactin P150 (Glued). *J Neurosci,* 18, 1261-9.

LI, W. J., MORIWAKI, T., TANI, T., WATANABE, T., KAIBUCHI, K. & GOSHIMA, G. 2012. Reconstitution of dynamic microtubules with Drosophila XMAP215, EB1, and Sentin. *Journal of Cell Biology,* 199, 849-862.

LIEW, G. M., YE, F., NAGER, A. R., MURPHY, J. P., LEE, J. S., AGUIAR, M., BRESLOW, D. K., GYGI, S. P. & NACHURY, M. V. 2014. The intraflagellar transport protein IFT27 promotes BBSome exit from cilia through the GTPase ARL6/BBS3. *Dev Cell,* 31, 265-78.

LIGON, L. A., SHELLY, S. S., TOKITO, M. & HOLZBAUR, E. L. F. 2003. The microtubule plus-end proteins EB1 and dynactin have differential effects on microtubule polymerization. *Molecular Biology of the Cell,* 14, 1405-1417.

LINCK, R. W., AMOS, L. A. & AMOS, W. B. 1985. Localization of tektin filaments in microtubules of sea urchin sperm flagella by immunoelectron microscopy. *J Cell Biol,* 100, 126-35.

LOKTEV, A. V., ZHANG, Q., BECK, J. S., SEARBY, C. C., SCHEETZ, T. E., BAZAN, J. F., SLUSARSKI, D. C., SHEFFIELD, V. C., JACKSON, P. K. & NACHURY, M. V. 2008. A BBSome subunit links ciliogenesis, microtubule stability, and acetylation. *Dev Cell,* 15, 854-65.

LUCKER, B. F., BEHAL, R. H., QIN, H., SIRON, L. C., TAGGART, W. D., ROSENBAUM, J. L. & COLE, D. G. 2005. Characterization of the

intraflagellar transport complex B core: direct interaction of the IFT81 and IFT74/72 subunits. *J Biol Chem,* 280, 27688-96.

MAIATO, H., DELUCA, J., SALMON, E. D. & EARNSHAW, W. C. 2004. The dynamic kinetochore-microtubule interface. *J Cell Sci,* 117, 5461-77.

MANDELKOW, E. M., MANDELKOW, E. & MILLIGAN, R. A. 1991. Microtubule dynamics and microtubule caps: a time-resolved cryo-electron microscopy study. *J Cell Biol,* 114, 977-91.

MAURER, S. P., CADE, N. I., BOHNER, G., GUSTAFSSON, N., BOUTANT, E. & SURREY, T. 2014. EB1 Accelerates Two Conformational Transitions Important for Microtubule Maturation and Dynamics. *Current Biology,* 24, 372-384.

MAURER, S. P., FOURNIOL, F. J., BOHNER, G., MOORES, C. A. & SURREY, T. 2012. EBs recognize a nucleotide-dependent structural cap at growing microtubule ends. *Cell,* 149, 371-82.

MCKENNEY, R. J., HUYNH, W., VALE, R. D. & SIRAJUDDIN, M. 2016. Tyrosination of alpha-tubulin controls the initiation of processive dynein-dynactin motility. *EMBO J,* 35, 1175-85.

MIMORI-KIYOSUE, Y., GRIGORIEV, I., LANSBERGEN, G., SASAKI, H., MATSUI, C., SEVERIN, F., GALJART, N., GROSVELD, F., VOROBJEV, I., TSUKITA, S. & AKHMANOVA, A. 2005. CLASP1 and CLASP2 bind to EB1 and regulate microtubule plus-end dynamics at the cell cortex. *Journal of Cell Biology,* 168, 141-153.

MISHIMA, M., MAESAKI, R., KASA, M., WATANABE, T., FUKATA, M., KAIBUCHI, K. & HAKOSHIMA, T. 2007. Structural basis for tubulin recognition by cytoplasmic linker protein 170 and its autoinhibition. *Proc Natl Acad Sci U S A,* 104, 10346-51.

MITCHISON, T. & KIRSCHNER, M. 1984. Dynamic instability of microtubule growth. *Nature,* 312, 237-42.

MOORES, C. A. & MILLIGAN, R. A. 2006. Lucky 13-microtubule depolymerisation by kinesin-13 motors. *J Cell Sci,* 119, 3905-13.

MUNEMITSU, S., SOUZA, B., MULLER, O., ALBERT, I., RUBINFELD, B. & POLAKIS, P. 1994. The APC gene product associates with microtubules in vivo and promotes their assembly in vitro. *Cancer Res,* 54, 3676-81.

NACHURY, M. V., LOKTEV, A. V., ZHANG, Q., WESTLAKE, C. J., PERANEN, J., MERDES, A., SLUSARSKI, D. C., SCHELLER, R. H., BAZAN, J. F., SHEFFIELD, V. C. & JACKSON, P. K. 2007. A core complex of BBS proteins cooperates with the GTPase Rab8 to promote ciliary membrane biogenesis. *Cell,* 129, 1201-13.

NAKAMURA, S., GRIGORIEV, I., NOGI, T., HAMAJI, T., CASSIMERIS, L. & MIMORI-KIYOSUE, Y. 2012. Dissecting the nanoscale distributions and functions of microtubule-end-binding proteins EB1 and ch-TOG in interphase HeLa cells. *PLoS One,* 7, e51442.

NEHLIG, A., MOLINA, A., RODRIGUES-FERREIRA, S., HONORE, S. & NAHMIAS, C. 2017. Regulation of end-binding protein EB1 in the control of microtubule dynamics. *Cell Mol Life Sci,* 74, 2381-2393.

NICASTRO, D., MCINTOSH, J. R. & BAUMEISTER, W. 2005. 3D structure of eukaryotic flagella in a quiescent state revealed by cryo-electron tomography. *Proc Natl Acad Sci U S A,* 102, 15889-94.

NONAKA, S., TANAKA, Y., OKADA, Y., TAKEDA, S., HARADA, A., KANAI, Y., KIDO, M. & HIROKAWA, N. 1998a. Randomization of left-right asymmetry due to loss of nodal cilia generating leftward flow of extraembryonic fluid in mice lacking KIF3B motor protein. *Cell,* 95, 829-37.

NONAKA, S., TANAKA, Y., OKADA, Y., TAKEDA, S., HARADA, A., KANAI, Y., KIDO, M. & HIROKAWA, N. 1998b. Randomization of left-right asymmetry due to loss of nodal cilia generating leftward flow of extraembryonic fluid in mice lacking KIF3B motor protein. *Cell,* 95, 829-837.

O'TOOLE, E. T., GIDDINGS, T. H., JR. & DUTCHER, S. K. 2007. Understanding microtubule organizing centers by comparing mutant and wild-type structures with electron tomography. *Methods Cell Biol,* 79, 125-43.

PATURLELAFANECHERE, L., MANIER, M., TRIGAULT, N., PIROLLET, F., MAZARGUIL, H. & JOB, D. 1994. Accumulation of Delta-2-Tubulin, a Major Tubulin Variant That Cannot Be Tyrosinated, in Neuronal Tissues and in Stable Microtubule Assemblies. *Journal of Cell Science,* 107, 1529-1543.

PAZOUR, G. J., AGRIN, N., LESZYK, J. & WITMAN, G. B. 2005. Proteomic analysis of a eukaryotic cilium. *J Cell Biol,* 170, 103-13.

PAZOUR, G. J., DICKERT, B. L., VUCICA, Y., SEELEY, E. S., ROSENBAUM, J. L., WITMAN, G. B. & COLE, D. G. 2000. Chlamydomonas IFT88 and its

mouse homologue, polycystic kidney disease gene tg737, are required for assembly of cilia and flagella. *J Cell Biol,* 151, 709-18.

PAZOUR, G. J., WILKERSON, C. G. & WITMAN, G. B. 1998. A dynein light chain is essential for the retrograde particle movement of intraflagellar transport (IFT). *Journal of Cell Biology,* 141, 979-992.

PEDERSEN, L. B., GEIMER, S. & ROSENBAUM, J. L. 2006. Dissecting the molecular mechanisms of intraflagellar transport in chlamydomonas. *Curr Biol,* 16, 450-9.

PEREZ, F., DIAMANTOPOULOS, G. S., STALDER, R. & KREIS, T. E. 1999. CLIP-170 highlights growing microtubule ends in vivo. *Cell,* 96, 517-27.

PERIS, L., THERY, M., FAURE, J., SAOUDI, Y., LAFANECHERE, L., CHILTON, J. K., GORDON-WEEKS, P., GALJART, N., BORNENS, M., WORDEMAN, L., WEHLAND, J., ANDRIEUX, A. & JOB, D. 2006. Tubulin tyrosination is a major factor affecting the recruitment of CAP-Gly proteins at microtubule plus ends. *Journal of Cell Biology,* 174, 839-849.

PERIS, L., WAGENBACH, M., LAFANECHERE, L., BROCARD, J., MOORE, A. T., KOZIELSKI, F., JOB, D., WORDEMAN, L. & ANDRIEUX, A. 2009. Motor-dependent microtubule disassembly driven by tubulin tyrosination. *J Cell Biol,* 185, 1159-66.

PHUA, S. C., CHIBA, S., SUZUKI, M., SU, E., ROBERSON, E. C., PUSAPATI, G. V., SETOU, M., ROHATGI, R., REITER, J. F., IKEGAMI, K. & INOUE, T. 2017. Dynamic Remodeling of Membrane Composition Drives Cell Cycle through Primary Cilia Excision. *Cell,* 168, 264-+.

PIGINO, G., GEIMER, S., LANZAVECCHIA, S., PACCAGNINI, E., CANTELE, F., DIENER, D. R., ROSENBAUM, J. L. & LUPETTI, P. 2009. Electron-tomographic analysis of intraflagellar transport particle trains in situ. *Journal of Cell Biology,* 187, 135-148.

PIPERNO, G. & FULLER, M. T. 1985. Monoclonal-Antibodies Specific for an Acetylated Form of Alpha-Tubulin Recognize the Antigen in Cilia and Flagella from a Variety of Organisms. *Journal of Cell Biology,* 101, 2085-2094.

PIPERNO, G. & MEAD, K. 1997. Transport of a novel complex in the cytoplasmic matrix of Chlamydomonas flagella. *Proc Natl Acad Sci U S A,* 94, 4457-62.

PREVO, B., MANGEOL, P., OSWALD, F., SCHOLEY, J. M. & PETERMAN, E. J. 2015. Functional differentiation of cooperating kinesin-2 motors orchestrates cargo import and transport in C. elegans cilia. *Nat Cell Biol,* 17, 1536-45.

PREVO, B., SCHOLEY, J. M. & PETERMAN, E. J. G. 2017. Intraflagellar transport: mechanisms of motor action, cooperation, and cargo delivery. *FEBS J.*

QUINTYNE, N. J., GILL, S. R., ECKLEY, D. M., CREGO, C. L., COMPTON, D. A. & SCHROER, T. A. 1999. Dynactin is required for microtubule anchoring at centrosomes. *Journal of Cell Biology,* 147, 321-334.

REDEKER, V., LEVILLIERS, N., SCHMITTER, J. M., LE CAER, J. P., ROSSIER, J., ADOUTTE, A. & BRE, M. H. 1994. Polyglycylation of tubulin: a posttranslational modification in axonemal microtubules. *Science,* 266, 1688-91.

REITER, J. F., BLACQUE, O. E. & LEROUX, M. R. 2012. The base of the cilium: roles for transition fibres and the transition zone in ciliary formation, maintenance and compartmentalization. *EMBO Rep,* 13, 608-18.

ROHATGI, R. & SNELL, W. J. 2010. The ciliary membrane. *Curr Opin Cell Biol,* 22, 541-6.

ROSENBAUM, J. L. & WITMAN, G. B. 2002. Intraflagellar transport. *Nat Rev Mol Cell Biol,* 3, 813-25.

ROUT, M. P. & FIELD, M. C. 2017. The Evolution of Organellar Coat Complexes and Organization of the Eukaryotic Cell. *Annu Rev Biochem,* 86, 637-657.

SATIR, P. & CHRISTENSEN, S. T. 2008. Structure and function of mammalian cilia. *Histochem Cell Biol,* 129, 687-93.

SCHROER, T. A. 2004. Dynactin. *Annu Rev Cell Dev Biol,* 20, 759-79.

SEDMAK, T. & WOLFRUM, U. 2010. Intraflagellar transport molecules in ciliary and nonciliary cells of the retina. *J Cell Biol,* 189, 171-86.

SEETAPUN, D., CASTLE, B. T., MCINTYRE, A. J., TRAN, P. T. & ODDE, D. J. 2012. Estimating the microtubule GTP cap size in vivo. *Curr Biol,* 22, 1681-7.

SERRICCHIO, M., SCHMID, A. W., STEINMANN, M. E., SIGEL, E., RAUCH, M., JULKOWSKA, D., BONNEFOY, S., FORT, C., BASTIN, P. & BUTIKOFER, P. 2015. Flagellar membranes are rich in raft-forming phospholipids. *Biology Open,* 4, 1143-1153.

SHEEMAN, B., CARVALHO, P., SAGOT, I., GEISER, J., KHO, D., HOYT, M. A. & PELLMAN, D. 2003. Determinants of S. cerevisiae dynein localization and

activation: implications for the mechanism of spindle positioning. *Curr Biol,* 13, 364-72.

SLEP, K. C. 2009. The role of TOG domains in microtubule plus end dynamics. *Biochem Soc Trans,* 37, 1002-6.

SLEP, K. C., ROGERS, S. L., ELLIOTT, S. L., OHKURA, H., KOLODZIEJ, P. A. & VALE, R. D. 2005. Structural determinants for EB1-mediated recruitment of APC and spectraplakins to the microtubule plus end. *J Cell Biol,* 168, 587-98.

SOUSA, A., REIS, R., SAMPAIO, P. & SUNKEL, C. E. 2007. The Drosophila CLASP homologue, Mast/Orbit regulates the dynamic behaviour of interphase microtubules by promoting the pause state. *Cell Motility and the Cytoskeleton,* 64, 605-620.

SOPPINA, V., HERBSTMAN, J. F., SKINIOTIS, G. & VERHEY, K. J. 2012. Luminal localization of alpha-tubulin K40 acetylation by cryo-EM analysis of fab-labeled microtubules. *PLoS One,* 7**,** e48204.

STEPANEK, L. & PIGINO, G. 2016. Microtubule doublets are double-track railways for intraflagellar transport trains. *Science,* 352, 721-4.

STIRNIMANN, C. U., PETSALAKI, E., RUSSELL, R. B. & MULLER, C. W. 2010. WD40 proteins propel cellular networks. *Trends Biochem Sci,* 35, 565-74.

SU, L. K., BURRELL, M., HILL, D. E., GYURIS, J., BRENT, R., WILTSHIRE, R., TRENT, J., VOGELSTEIN, B. & KINZLER, K. W. 1995. APC binds to the novel protein EB1. *Cancer Res,* 55, 2972-7.

SUBOTA, I., JULKOWSKA, D., VINCENSINI, L., REEG, N., BUISSON, J., BLISNICK, T., HUET, D., PERROT, S., SANTI-ROCCA, J., DUCHATEAU, M., HOURDEL, V., ROUSSELLE, J. C., CAYET, N., NAMANE, A., CHAMOT-ROOKE, J. & BASTIN, P. 2014. Proteomic analysis of intact flagella of procyclic Trypanosoma brucei cells identifies novel flagellar proteins with unique sub-localization and dynamics. *Mol Cell Proteomics,* 13, 1769-86.

SURYAVANSHI, S., EDDE, B., FOX, L. A., GUERRERO, S., HARD, R., HENNESSEY, T., KABI, A., MALISON, D., PENNOCK, D., SALE, W. S., WLOGA, D. & GAERTIG, J. 2010. Tubulin glutamylation regulates ciliary motility by altering inner dynein arm activity. *Curr Biol,* 20, 435-40.

TASCHNER, M., BHOGARAJU, S. & LORENTZEN, E. 2012. Architecture and function of IFT complex proteins in ciliogenesis. *Differentiation,* 83, S12-22.

TASCHNER, M., KOTSIS, F., BRAEUER, P., KUEHN, E. W. & LORENTZEN, E. 2014. Crystal structures of IFT70/52 and IFT52/46 provide insight into intraflagellar transport B core complex assembly. *J Cell Biol,* 207, 269-82.

TASCHNER, M. & LORENTZEN, E. 2016. The Intraflagellar Transport Machinery. *Cold Spring Harb Perspect Biol,* 8.

TASCHNER, M., MOURAO, A., AWASTHI, M., BASQUIN, J. & LORENTZEN, E. 2017. Structural basis of outer dynein arm intraflagellar transport by the transport adaptor protein ODA16 and the intraflagellar transport protein IFT46. *J Biol Chem,* 292, 7462-7473.

TASCHNER, M., WEBER, K., MOURAO, A., VETTER, M., AWASTHI, M., STIEGLER, M., BHOGARAJU, S. & LORENTZEN, E. 2016. Intraflagellar transport proteins 172, 80, 57, 54, 38, and 20 form a stable tubulin-binding IFT-B2 complex. *EMBO J,* 35, 773-90.

TAULMAN, P. D., HAYCRAFT, C. J., BALKOVETZ, D. F. & YODER, B. K. 2001. Polaris, a protein involved in left-right axis patterning, localizes to basal bodies and cilia. *Molecular Biology of the Cell,* 12, 589-599.

TSAO, C. C. & GOROVSKY, M. A. 2008. Tetrahymena IFT122A is not essential for cilia assembly but plays a role in returning IFT proteins from the ciliary tip to the cell body. *J Cell Sci,* 121, 428-36.

TSAO, C. C. & GOROVSKY, M. A. 2008. Different effects of Tetrahymena IFT172 domains on anterograde and retrograde intraflagellar transport. Mol Biol Cell, 19, 1450-61.

URNAVICIUS, L., ZHANG, K., DIAMANT, A. G., MOTZ, C., SCHLAGER, M. A., YU, M., PATEL, N. A., ROBINSON, C. V. & CARTER, A. P. 2015. The structure of the dynactin complex and its interaction with dynein. Science, 347, 1441-1446.

VAN DAM, T. J., TOWNSEND, M. J., TURK, M., SCHLESSINGER, A., SALI, A., FIELD, M. C. & HUYNEN, M. A. 2013. Evolution of modular intraflagellar transport from a coatomer-like progenitor. *Proc Natl Acad Sci U S A,* 110, 6943-8.

VAN DER VAART, B., MANATSCHAL, C., GRIGORIEV, I., OLIERIC, V., GOUVEIA, S. M., BJELIC, S., DEMMERS, J., VOROBJEV, I.,

HOOGENRAAD, C. C., STEINMETZ, M. O. & AKHMANOVA, A. 2011. SLAIN2 links microtubule plus end-tracking proteins and controls microtubule growth in interphase. *J Cell Biol,* 193, 1083-99.

VANNUCCINI, E., PACCAGNINI, E., CANTELE, F., GENTILE, M., DINI, D., FINO, F., DIENER, D., MENCARELLI, C. & LUPETTI, P. 2016. Two classes of short intraflagellar transport train with different 3D structures are present in Chlamydomonas flagella. *J Cell Sci,* 129**,** 2064-74.

VAUGHAN, K. T., TYNAN, S. H., FAULKNER, N. E., ECHEVERRI, C. J. & VALLEE, R. B. 1999. Colocalization of cytoplasmic dynein with dynactin and CLIP-170 at microtubule distal ends. *Journal of Cell Science,* 112, 1437-1447.

VISWANADHA, R., SALE, W. S. & PORTER, M. E. 2017. Ciliary Motility: Regulation of Axonemal Dynein Motors. *Cold Spring Harb Perspect Biol,* 9.

WARNER, F. D. & SATIR, P. 1973. The substructure of ciliary microtubules. *J Cell Sci,* 12**,** 313-26.

WEI, Q., ZHANG, Y., LI, Y., ZHANG, Q., LING, K. & HU, J. 2012. The BBSome controls IFT assembly and turnaround in cilia. *Nat Cell Biol,* 14, 950-7.

WEISBRICH, A., HONNAPPA, S., JAUSSI, R., OKHRIMENKO, O., FREY, D., JELESAROV, I., AKHMANOVA, A. & STEINMETZ, M. O. 2007. Structure-function relationship of CAP-Gly domains. *Nat Struct Mol Biol,* 14, 959-67.

WEN, Y., ENG, C. H., SCHMORANZER, J., CABRERA-POCH, N., MORRIS, E. J., CHEN, M., WALLAR, B. J., ALBERTS, A. S. & GUNDERSEN, G. G. 2004. EB1 and APC bind to mDia to stabilize microtubules downstream of Rho and promote cell migration. *Nat Cell Biol,* 6, 820-30.

WLOGA, D., JOACHIMIAK, E., LOUKA, P. & GAERTIG, J. 2017. Posttranslational Modifications of Tubulin and Cilia. *Cold Spring Harb Perspect Biol,* 9.

WOOD, C. R. & ROSENBAUM, J. L. 2014. Proteins of the Ciliary Axoneme Are Found on Cytoplasmic Membrane Vesicles during Growth of Cilia. *Current Biology,* 24, 1114-1120.

WOOD, C. R. & ROSENBAUM, J. L. 2015. Ciliary ectosomes: transmissions from the cell's antenna. *Trends Cell Biol,* 25, 276-85.

WOOD, C. R., WANG, Z., DIENER, D., ZONES, J. M., ROSENBAUM, J. & UMEN, J. G. 2012. IFT proteins accumulate during cell division and localize to the cleavage furrow in Chlamydomonas. *PLoS One,* 7, e30729.

WU, X. F., XIANG, X. & HAMMER, J. A. 2006. Motor proteins at the microtubule plus-end. *Trends in Cell Biology,* 16, 135-143.

ZANIC, M., STEAR, J. H., HYMAN, A. A. & HOWARD, J. 2009. EB1 recognizes the nucleotide state of tubulin in the microtubule lattice. *PLoS One,* 4, e7585.

ZHANG, J., LI, S. H., FISCHER, R. & XIANG, X. 2003. Accumulation of cytoplasmic dynein and dynactin at microtubule plus ends in Aspergillus nidulans is kinesin dependent. *Molecular Biology of the Cell,* 14, 1479-1488.

6. Acknowledgements

When I started to write this thesis, I realized how time flies. I still remember the moment that I stepped into MPI-B four years ago, filling with nervousness and curiosity. Now it is the time to leave, I am feeling sad and reluctant to leave. During the time here, much advice is given by my supervisor as well as fellow colleagues so that I am supported by them all the time. Here I would like to thank all the people who helped me during these years.

Firstly, I need to thank my supervisor Dr. Naoko Mizuno for giving me the opportunity to work in her lab and her excellent supervision. I feel so lucky that I can learn electron microscopy technique from her. When I started my PhD, I had no experience about the electron microscopy and data processing. Naoko was so patient to teach me and provided much-needed support. When I encountered any difficulty, she offered me valuable advice and encouraged me nicely. I learned a lot from Naoko, not only in terms of professional research but also from her values of life such as her optimistic attitudes and high efficiency of work. All of these will influence my life in future.

I am grateful to Dr. Esben Lorentzen. He gave me opportunity to work on IFT project. I really enjoy this project, although it made me frustrated sometimes. I learned much than I expected from the project. He is always supportive and gives me a lot of good ideas. His general attitude towards science contributed to shaping my own ideas.

I want to thank Prof. Dr. Elena Conti for offering me the chance to work in the department. I really enjoy the atmosphere here. Thanks also for giving me advice in my group meeting and Thesis Advisory Committee meeting.

My thanks go out to my colleagues in Mizuno group, Dirk Dedden, Nirakar Basnet, Stephanie Schumacher and Charlotte Kelley for the discussion and suggestions. Especially Dirk and Nirakar for sharing their experiences in microscope. Thank Alexandra Neagoe for working together with me about the IFT project. Thank our previous technicians Ines Kunze and Wolfgang Fink. Ineas helped me a lot at the initial stage of my PhD. Thank my pervious colleagues in Lorentzen group. In

particular, Dr. Taschner Michael for teaching me the IFT protein purifications and keeping supplying protein samples for my EM studies.

I want to thank Dr. Christian Biertuempfel and his group, especially Shun-Hsiao Lee, Carina Vraschek, and Giulia Chiapparini. I was stimulated by shining ideas in our lunch meeting. I thank my biophysical collaborators, Dr. Kristina Ganzinger and Prof. Dr. Petra Schwille for helping and teaching me to do biophysical analysis. I also want thank Dr. Tanvir Shaikh from Central European Institute of Technology in Brno for giving me the opportunity to use their microscope and also teaching me the Spider software for data processing.

I thank the Biochemistry Core Facility, Imaging Facility and Cryo-EM Facility for providing instruction and opportunities for the usage of the excellent infrastructure, particularly mass spectrometry measurement, light microscopy observation and Cryo-EM data collections during my study. I thank the members in my Thesis Advisory Committee: Prof. Dr. Elena Conti, Dr. Daniel Wilson, Dr. Naoko Mizuno and Dr. Esben Lorentzen. I thank Molecular structural biology department directed by Prof. Dr. Wolfgang Baumeister, where I can use all microscopes and getting technical support.

I must thank all my friends who made my weekend relax with a lot of fun.

In the end, I need to thank all my family members, especially my grandparents and parents. I would not manage my PhD without their encouragement and spiritual support. They are always standing behind me. Thank my husband, Dr. Youwei Xu for his continuing support. Thank him for the scientific discussion, sharing unforgettable moments, love, and life.